Proposal for a Large Area Time of Flight System for STAR

The STAR TOF Collaboration

October 27, 2003

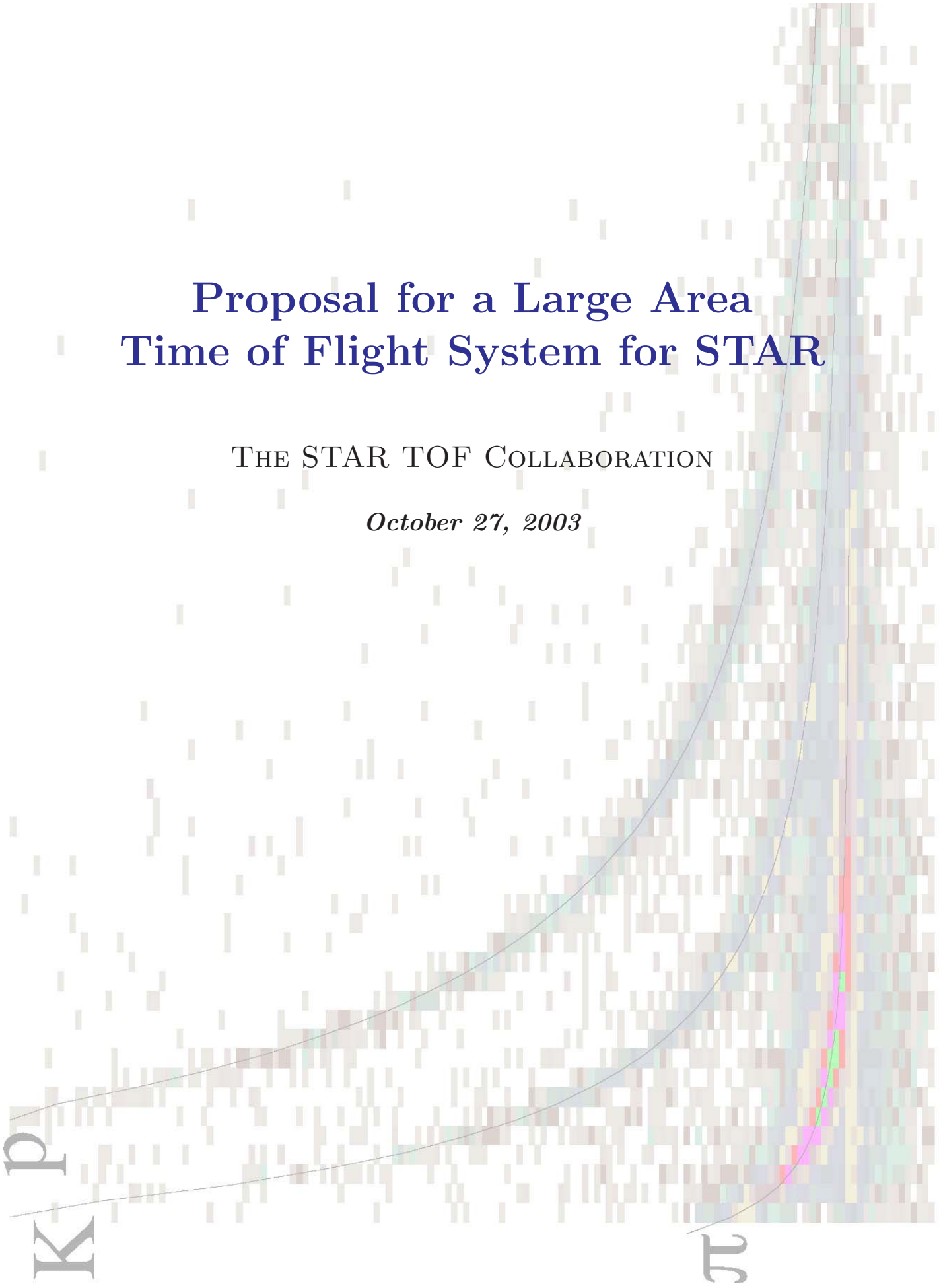

Proposal for a Large Area Time of Flight System for STAR

STAR-TOF

(The STAR TOF Collaboration)

P. Fachini, Zhangbu Xu
Brookhaven National Laboratory, Upton, NY 11973

Feng Liu, Lianshou Liu, Zhixu Liu, Jinghua Fu,
Yuan Hu, Zhiming Li, Yuanfang Wu, Yan Lu
HuaZhong Normal University, Wuhan, China

Jin Li, Junguang Lu, Bingyun Zhang
Institute of High Energy Physics (IHEP), Beijing, China

Wenlong Zhan, Zhiyu Sun
Institute of Modern Physics (IMP), LanZhou, China

D. Hardtke, F. Retiere, N. Xu
Lawrence Berkeley National Laboratory, Berkeley, CA 94720

L. Kotchenda
Moscow Engineering Physics Institute, Moscow, Russia

J.W. Mitchell
NASA - Goddard Space Flight Center, Greenbelt, MD 20771

G. Paic, E. Cuautle, A. Martinez, G. Calderon
UNAM & CINVESTAV, Mexico City, Mexico

B. Bonner, G. Eppley, F. Geurts, W.J. Llope,
G. Mutchler, T. Nussbaum, J. Roberts, P. Yepes
Rice University, Houston, TX 77005

Wenging Shen, Yugang Ma, Xiangzhou Cai
Shanghai Institute of Nuclear Research (SINR), Shanghai, China

Kejun Kang, Jianping Cheng, Yuanjing Li, Yulan Li, Yi Wang
Tsinghua University, Beijing, China

C. Whitten, H. Huang, G. Igo, V. Ghazikhanian,
S. Trentalange, A. Tai, H. Long
University of California - Los Angeles, Los Angeles, CA 90095

Hongfang Chen, Xin Dong, Xiaolian Wang, Ziping Zhang, Cheng Li,
Lijuan Ruan, Shuwei Ye, Jian Wu, Ming Shao, Shengli Huang
University of Science and Technology of China (USTC), Hefei, China

G. Hoffmann, A. Ishihara, C.F. Moore, L. Ray, J. Schambach, H. Ward
University of Texas, Austin, TX 78712

T. Trainor
University of Washington, Seattle, WA 98195

C. Markert
Yale University, New Haven, CT 06520

Acknowledgement

The STAR Collaboration gratefully acknowledges the pioneering research and development work performed by the LAA project, and especially C. Williams, under A. Zichichi on MRPC Time Of Flight Technology.

Contents

1 Executive Summary

The STAR Collaboration proposes to build a barrel Time of Flight (TOF) detector based on recently developed Multi-gap Resistive Plate Chamber (MRPC) technology. This detector will significantly extend the reach of the STAR scientific program, doubling the percentage of kaons and protons for which particle identification is possible to more than 95% of all those produced within the MRPC-TOF acceptance. Combined with existing STAR detectors, the barrel TOF detector will allow STAR to extract the maximum amount of information available from soft physics measures on an event-by-event basis. It will:

- allow the detailed unfolding of large and small scale correlations and fluctuations to map, in detail, the dynamics and evolution of the produced matter;
- significantly reduce the integrated luminosity needed for key measures such as multiply-strange baryon (Ω) elliptic flow (v2); such measures are needed to identify possible partonic collectivity and to explore in detail the early time bulk physics properties of the produced matter;
- extend the p_T reach for accurate measurement of the mass and width of resonances to ∼1-2 GeV/c, affording a precision tool for model comparison and essential information concerning the importance of re-scattering versus regeneration during the period between chemical and thermal freeze-out.

When combined with a possible future vertex detector upgrade, the proposed TOF detector will also reduce the integrated luminosity needed to measure a statistically robust sample of D°, D^+, D_S^+ mesons by approximately an order of magnitude on average, enabling STAR to make systematic studies of charm thermalization and D° meson flow.

The development of new, low-cost MRPC technology for the ALICE experiment combined with the parallel development of new high precision TDC chips at CERN provides a cost effective means to fulfill the physics-driven requirements of this proposal: to extract the maximum information available from soft (up to ∼2-3 GeV/c) hadronic spectra. After extensive testing of MRPC technology at CERN and BNL and its successful implementation in the HARP experiment, this technology is mature. A 168 channel MRPC prototype tray was installed in STAR for in-situ testing during the 2003 RHIC run. It demonstrated stable performance, meeting all key performance requirements and producing important physics results (not possible with particle identification from the TPC alone) on the Cronin effect for identified particles. This result was submitted to the Physical Review Letters on September 15, 2003 (nucl-ex/030912) demonstrating the ability and importance of this new technology for producing new physics results in STAR.

By providing nearly complete particle identification within the large solid angle acceptance subtended by the STAR Time Projection Chamber (TPC), Silicon Vertex Tracker (SVT), and Barrel Electromagnetic Calorimeter (BEMC), the proposed barrel

Time of Flight detector will uniquely position STAR to provide definitive measures, unavailable otherwise without extremely large amounts of beam time, to establish whether or not the relevant degrees of freedom for the new matter being produced at RHIC are equilibrated and partonic in nature.

The research and development of the electronic components of this detector is expected to continue in FY2004. The construction project is proposed to begin in FY2005, and to continue through FY2007. The cost of the U.S. contribution to this construction is projected to be \$4.1M in FY2004 dollars. Subject to approval by the Chinese funding agencies, the Chinese institutions involved in this project are committed to the construction and testing of $\sim$4000 MRPC chambers, the full amount required for this detector. This represents a projected in-kind contribution of approximately \$2.3M by the participating Chinese institutions.

2 Overview

2.1 Introduction

A unique strength of the STAR detector at RHIC is its large, uniform acceptance capable of measuring and identifying a substantial fraction of the particles produced in heavy ion collisions. This large acceptance is central to STAR's scientific capability and has already resulted in new and intriguing physics results such as the recent measurement of the suppression of back-to-back jets in central Au+Au collisions. Large acceptance detectors central to the STAR heavy ion physics program are the Silicon Vertex Tracker (SVT), the Time-Projection Chamber (TPC), and the Barrel Electromagnetic Calorimeter (BEMC) all having an acceptance covering 2π in azimuthal angle and $|\eta| \lesssim 1.5$ in pseudo-rapidity. We propose a barrel Time-of-Flight (TOF) detector matching the acceptance of these detectors. This upgrade will provide essential particle identification capability. Specifically, it will double the percentage of kaons and protons for which particle identification is possible to more that 95% of all those produced within the acceptance of the TOF barrel ($|\eta| \lesssim 1$), greatly enhancing the discovery potential of STAR. This increase in particle identification efficiency over a large solid angle is especially important for measurements of multi-particle correlations since the feasibility of such measurements depends (on average) on the single particle efficiency raised to the power of the number of particles used in the correlation. The extended momentum range for particle identified spectra provided by the MRPC barrel TOF detector is crucial to understand the information contained in the large scale correlations and fluctuations being observed in Au+Au collisions at RHIC. This can not be done without the proposed TOF system.

Large acceptance TOF coverage is integral to the STAR detector design. The importance of the capability provided by large acceptance TOF was underscored in the 1996 review by NSAC of STAR's proposal for Additional Experimental Equipment. At that time, the TOF detector technology proposed was based on mesh-dynode phototubes and was deemed to be too expensive. In its conclusions, the NSAC [8] subcommittee noted:

> "STAR should aim at a [TOF] coverage which is sufficient for event-by-event kaon (and possibly proton) identification, which in other observables is the prominent feature and strength of STAR. If fiscal constraints are such that this cannot be realized, ...further R&D should be encouraged to search for a viable solution for large area coverage."

STAR has found a viable solution. The proposed TOF detector is based on a new detector technology called the Multi-gap Resistive Plate Chamber (MRPC), which has been developed at CERN for the LHC. In particular, the LHC heavy ion experiment, ALICE, has adopted MRPC technology for its TOF detector [5]. This technology has also been used successfully in the HARP experiment at CERN for a period of approximately 2 years. It has now been used successfully in the STAR experiment for one year. The sections of this chapter which follow will provide an overview of

the physics justification, technical construction, and installation plan for a proposed STAR Barrel MRPC TOF detector.

2.2 STAR Heavy Ion Physics and the TOF Upgrade

The main goal of the relativistic heavy ion program at RHIC is to produce a new form of matter, the Quark-Gluon Plasma (QGP), and to study Quantum Chromo-Dynamics (QCD) at high temperature. Initial experimental measurements of particle multiplicity and transverse momentum (energy) distributions indicate that the high energy density being reached in nucleus-nucleus collisions at RHIC is unprecedented. Recent RHIC results have offered a new view into nucleus-nucleus collisions with respect to studying the gluon dominated initial phase, partonic and hadronic evolution dynamics, and hadronic freeze-out scenarios. The following is a selected list of key physics topics in STAR where the proposed barrel TOF detector will have a major impact on enhancing STAR's future physics capability. The large acceptance of the proposed STAR TOF is essential for these physics achievements.

The proposed barrel TOF detector will significantly extend STAR's physics reach for the following topics:

1. Unfolding the origin of non-statistical fluctuations and correlations as well as the conditions at the phase boundary for hadronization through measurement of event-by-event pion, kaon and proton $\langle p_T \rangle$, multiplicity fluctuations, and two particle correlations in η-ϕ . The proposed TOF detector is essential to provide the required p_T coverage and overall particle identification (PID) acceptance necessary for such measurements.

2. Determining the nature of the strongly interacting dense matter produced in the early stage of nucleus-nucleus collisions at RHIC and whether the relevant degrees of freedom are partonic; studying parton dynamics in the early stage of the collision and searching for possible partonic collectivity; placing constraints on the initial conditions in terms of the parton structure function of the colliding nuclei. These topics will be studied by measuring the yields and p_T spectra of Ω baryons and D mesons to determine important constraints on the initial parton flux and the magnitude of the elliptic flow and transverse radial flow of heavy quarks. Elliptic flow of the Ω is of particular importance to search for partonic collectivity. The added capability of the barrel TOF detector is essential to increase the efficiency for detection of these particles so that precision measurements are possible within the beam time projected to be available.

3. Exploring possible new physics domains at RHIC such as a possible critical point in the QCD phase diagram and searches for exotic di-Omega particles. Recent theoretical conjecture has raised the possibility of a critical point in the phase diagram relating temperature and baryon density. If a critical point

exists one way it might be observed is through QCD critical phenomenon manifest through unusually large fluctuations of particle ratios such as K/π and K/p. With respect to possible exotic states the Di-Omega is predicted to be one of the most stable di-baryon candidates based on recent QCD inspired chiral SU(3) phenomenological calculations. RHIC is the first accelerator where multiple Omegas are produced per collision with sufficiently high probability that a sensitive search for a possible di-Omega particle is possible. Without the PID capability of the full TOF these studies are not possible since the detection efficiency for a possible Di-Omega particle is too low.

Fluctuations and Large Scale Correlations

With the proposed barrel TOF detector, STAR will investigate the nature of non-statistical fluctuations and will study medium induced modification of multiparticle correlations. Specifically, by using the TOF to measure particle identified spectra in the full range of p_T relevant for soft physics measures, STAR will investigate the transport and possible correlation of quantum numbers such as strangeness and baryon number in various regions of phase space. Possible fluctuations in these distributions as a function of centrality will be studied as well. Such fluctuations are expected to be sensitive to important underlying physics like the possible existence of a critical point and/or the order of the quark-hadron phase transition. Possible modification of the correlation length due to the presence of a strongly interacting QCD medium will probe the nature of the medium over a time scale long compared to that for the initial non-equilibrium phase probed by high p_T particles, providing important complementary information. The proposed full TOF detector is essential to provide detailed information on flavor composition and particle dynamics in order to search for and study these types of fluctuations and correlations.

In the analysis of event-wise $\langle p_T \rangle$ fluctuations from the top 15% most central Au+Au collisions at 130 GeV, STAR has already observed fluctuations significantly beyond what can be accounted for by statistics [26]. Figure 1 shows a distribution of event-wise mean-p_T with respect to $\hat{p}_T$ in units of $\sigma_{\hat{p}_T}/\sqrt{n}$. This distribution is compared to a gamma distribution which is the reference appropriate in the absence of non-statistical fluctuations ($\hat{p}_T$ and $\sigma^2_{\hat{p}_T}$ are the mean and variance of the inclusive p_T distribution respectively.) To match the gamma distribution with the data, an increase in the *rms* width by $\sim$14% is required which is attributed to dynamical (non-statistical) fluctuations.

This observation is just one example of why a large acceptance TOF detector is necessary. This effect results from a large scale fluctuation over the full STAR acceptance ($|\eta| \lesssim 1.0$, 2π in ϕ). Its origin can not be unambiguously determined without additional particle identification. Possible divergent origins of the excess fluctuations in Fig.1 include large event-by-event temperature variations for the selected centrality class and/or large fluctuations in the relative numbers of pions, kaons, and protons since the observed mean p_T is known to be strongly particle dependent. In order to disentangle different dynamical explanations and understand the underlying physics leading to these fluctuations it is essential to measure event-by-event mean p_T and

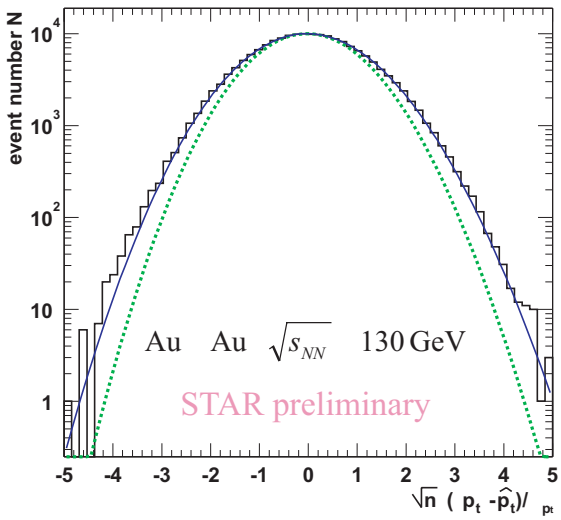

Figure 1: Distributions of $\sqrt{n}(\langle p_T \rangle - \hat{p}_T)/\sigma_{\hat{p}_T}$ for all primary hadrons from central (top 15%) events (upper histogram) compared to two gamma distributions: reference in the absence of non-statistical fluctuations (dotted line) and with a 14% increased rms width (solid curve).

particle number fluctuations for pions, kaons and protons, respectively. The limited PID capability in the low p_T region from the TPC+SVT alone does not provide adequate coverage in acceptance or transverse momentum to determine the mean p_T for identified particles event by event. For example, the average p_T of protons is approximately 0.9 GeV/c, while the PID from TPC dE/dx covers only up to $p_T < 1.0$ GeV/c. The extended p_T coverage of proton PID above 2.0 GeV/c from the barrel TOF system is essential to determine the event mean p_T for protons in this instance.

First observations of large-scale charge correlations in Au+Au collisions at RHIC already show strong variation with collision centrality, exhibiting features similar to those expected from correlations in p-p interactions in peripheral heavy ion collisions, but very different structure for the most central heavy ion events. This suggests the correlations observed in central collisions may be influenced by strong medium effects; the study of possible medium-induced modifications to local quantum number conservation at hadronization is just beginning.

Conserved quantum numbers such as electric charge, baryon number, and strangeness are expected to be locally conserved in pair production in nuclear collisions. An interesting possibility is that local quantum number conservation could be modified due to the presence of a strongly interacting QCD medium surrounding the produced particle pair. While a first observation of charge correlations of particles in large $\Delta\eta$ and $\Delta\phi$ appears to exhibit gross features qualitatively similar to those observed in elementary p-p collisions, the study of possible medium induced modifications is just beginning. The large acceptance of the TPC ($|\eta| \lesssim 1.5$ and 2π in ϕ) will be essential to achieve the necessary sensitivity to large-scale structure of the expected correlations.

In addition, the proposed barrel TOF detector is essential to measure the correlation length for local baryon number and strangeness conservation, to search for possible medium effects, and to extend the p_T acceptance to cover the transition region between soft and semi-hard particle production. Baryon number and strangeness are generally considered more sensitive probes of the QCD medium than charge conservation, which may be heavily influenced by the decays of resonances in the final state.

Event-by-event fluctuation analysis in heavy ion collisions has been advocated as a unique tool in searches for a phase transition and possible critical phenomena near the QCD phase boundary. Strong dependence of non-statistical fluctuations on centrality, beam energy, and nucleus size could provide direct indication of a phase transition to a quark-gluon plasma [24, 25]. The large acceptance of the TPC combined with the proposed barrel TOF detector will reduce the statistical error to 10-15% for the measurement of event-by-event kaon and proton yields in central Au+Au collisions. With the addition the proposed barrel TOF detector, STAR will have unprecedented sensitivity to explore event-by-event physics in this domain.

Collective Flow Observables

Collective flow measurements have been very important for studying relativistic nucleus-nucleus collisions at all beam energies [17, 18] because the magnitude and pattern of the collective motion is closely related to the equation of state (EOS) of the produced matter. Assuming local equilibrium, the EOS will be driven by the degrees of freedom relevant for the basic constituents which make up the matter. It is therefore possible by studying collective flow to determine important information about the nature of the matter when it is produced, *e.g.* whether it is partonic or hadronic in nature.

STAR has measured both elliptic and transverse radial flow observables systematically for several particle species up to the moderate-to-high p_T region. These measurements have already yielded important information as shown in Figure 2(a) which shows an example of the STAR measurement for the anisotropy parameter (elliptic flow) $v_2 = \langle cos(2\psi) \rangle$ vs. transverse momentum for K^0_S and Λ from 200 GeV Au + Au minimum bias collisions. Two intriguing features are noted: (i) in the low p_T region, the predictions of a hydrodynamic calculation [19] match the data rather well in contrast to results at the SPS where it over-predicted the observed anisotropy significantly; (ii) in the region $p_T \geq 2$ GeV/c, the magnitude of the elliptic flow reaches saturation, the amount of elliptic flow (v_2) at saturation being mass dependent. The saturation seems constant up to $p_T \sim 6$ GeV/c.

Figure 2 (b) shows the $\langle p_T \rangle$ versus particle mass for central Au+Au and minimum bias p+p collisions. Thermal fit results are shown as curves. Two important observations are noted: (i) for Au+Au collisions, the bulk of the particles fall along the curve with the freeze-out temperature and velocity parameters $[T_{fo}, \beta]_{AuAu}$ = [110 (MeV), 0.55 (c)] indicating a substantial degree of transverse radial flow. The results for p+p collisions indicate a behavior closer to the curve for $[T_{fo}, \beta]_{pp}$ = [170 (MeV),0.0 (c)]. The apparent conclusion is that particles freeze-out at hadronization

in p+p collisions when the temperature is very close to that of the chemical freeze-out temperature [22, 23]. In the Au+Au collisions, multi-strange baryons Ξ and Ω clearly deviate from the bulk freeze-out curve showing somewhat smaller collective velocity and a higher temperature.

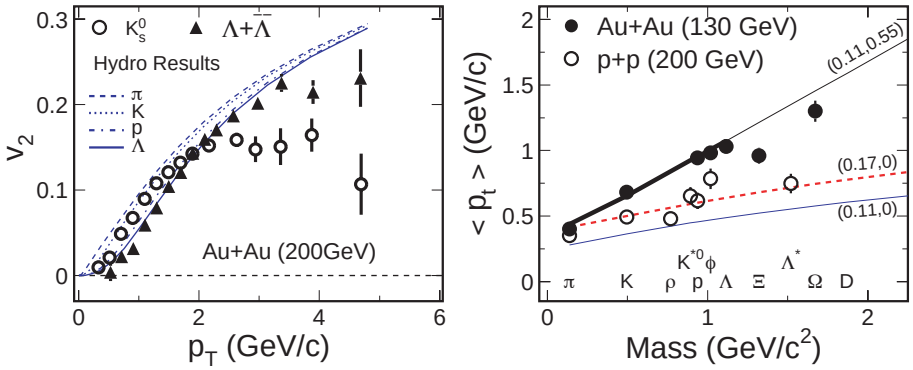

Figure 2: (Left) Azimuthal anisotropy parameters v_2 as a function of p_T for strange particles K^0_S (open circle) and $\overline{\Lambda}/\Lambda$ (closed triangles) from minimum bias 200 GeV Au+Au collisions. Lines are from hydrodynamic model calculations [19] for (from top to bottom) pions, kaons, protons, and $\overline{\Lambda}/\Lambda$. (Right) The $\langle p_T \rangle$ vs. particle mass. The lines represent the thermal results with given temperature and velocity (T_{fo},β).

These studies, carried out for particles for which topological identification is possible, demonstrate the importance of studying elliptic flow as a function of particle species. They also point to a potentially definitive signature of partonic collectivity in relativistic nucleus-nucleus collisions.

Due to the fact that at late times, the expansion of the produced matter tends to reduce the effects of spatial anisotropy in the initial collision, elliptic flow is expected to be self-quenching. If observed, elliptic flow is therefore likely developed in the early stage of the collision when partonic degrees of freedom are most relevant. Due to the small elastic hadronic cross sections for multi-strange baryons (Ξ, Ω) and charm hadrons ($D, J/\Psi$), those particles are expected to couple weakly to hadronic matter in the later stages of the collision (as evidenced by the departure of the behavior of the omega and cascade baryons from the trend for lighter particles). A finite value of v_2 for those particles should therefore carry partonic information. A non-zero value of v_2 and possible v_2 saturation for those particles would serve as a very strong signature of partonic collectivity in nuclear collisions at RHIC.

The barrel TOF detector will allow measurement of the elliptic flow for Ω baryons up to moderately high p_T, well into the region of possible saturation. Specifically, it will increase the Ω detection efficiency over the existing TPC+SVT configuration in STAR by a factor of 3 to 8 for the p_T region from 1.5 GeV/c to >4 GeV/c. Such an enhancement in the detection efficiency is necessary in order to unambiguously

establish possible collective phenomenon for the Ω within reasonable amount of running time. Without the proposed barrel TOF system, due to the reduced detection efficiency and increased combinatorial background, the beam time needed to make this measurement is prohibitive. A precise measurement of the Ω yield at moderately high p_T as a function of collision centrality and beam species will also allow STAR to study possible suppression of the Ω baryon yield relative to the yield in p+p interactions scaled appropriately. This intriguing phenomenon has already been studied in STAR for unidentified charged hadrons, K^0_s, and Λ^0. The transverse momentum at which the yield saturates and decreases relative to p+p is mass-dependent. The Ω baryon is particularly interesting because it is a three-strange quark cluster.

D Meson Production

For moderate p_T of D mesons, particle identification of the daughter kaon and pion is possible, although these are separated by large gaps in rapidity and ϕ angle. Therefore the large acceptance of the proposed barrel TOF is essential to measure the D meson spectrum from the $D \rightarrow K+\pi$ decay, where the decay kinematics of the D meson decay can be fully reconstructed.

With the proposed barrel TOF detector, the combinatorial background for $D \rightarrow K+\pi$ candidates can be reduced by a factor of 3 due to the identification of the decay daughters. This will allow STAR to make a D meson yield measurement with an error approximately 15% for central Au+Au collisions with one-year of data-taking. Without the barrel TOF, a multi-year run and analysis period would be required for a single beam energy and species, and a systematic study of the yield and spectra of open charm would thus not be feasible. The determination of the D meson yield and the shape of the p_T distribution will provide constraints on the incoming gluon flux in the colliding nuclei and provide important information on the magnitude of the transverse radial flow of charm quarks. In order to further reduce the background and extend the p_T reach, a STAR micro-vertex detector upgrade will be required to precisely measure the displaced D meson decay vertices. Both the barrel TOF and the micro-vertex detector upgrades are required in order to complete the STAR D meson physics program aimed at constraining the gluon structure function of the nuclei, determining open charm yields for the normalization of charmonium measurements, studying the energy loss of charm quark jets in the QCD medium, and searching for possible charm quark thermalization. Together, the barrel TOF detector and future micro-vertex detector will reduce the amount of beam time required for charm measurements by more than an order of magnitude.

Hadronic Dynamics

In order to develop transport models to describe nucleus-nucleus collisions, it is imperative that the hadronic evolution and dynamics be understood. These play a dominant role in determining the total charged particle yield, momentum correlations and space-time geometry of the final state. The precise measurement of resonances with a range of lifetimes can trace the evolution between the hadron formation stage and the final decoupling of the system, since resonances continue to decay, scatter, and regenerate during this period, and their yield is therefore sensitive to the

medium. Short lived resonances such as the ρ, Δ, and $\Lambda(1520)$ are particularly interesting in-medium probes because of their short lifetime. However, the large width of these resonances makes their measurement very susceptible to large combinatorial backgrounds and distortion of the background invariant mass distribution due to particle misidentification. This is precisely the reason there are difficulties measuring the yield of ρ and $\Lambda(1520)$ from the central Au+Au collisions in the ongoing STAR scientific program. As most charged particles are believed to come from resonance decays, a precise determination of resonance contributions will constrain models of hadronization such as thermal/statistical models and string fragmentation models.

STAR has already observed a list of resonances including the ρ, $K^*(892)$, $f^0(980)$, $\phi(1020)$, Δ, $\Sigma(1385)$, and $\Lambda(1520)$, some of which have been observed for the first time in heavy ion collisions. Despite this exciting development however, the crucial information which could be provided by these studies is not fully available. This is because the signal to noise and p_T range accessible using the TPC alone are not adequate for resonance studies to be a precision tool. In STAR, the proposed TOF upgrade will 1) significantly reduce the combinatorial background by identifying the decay daughters so that precise yields can be measured up to moderately high p_T ($\sim$2 GeV), and 2) remove the residual background structure underneath the resonance peaks due to misidentification of particles from the decays of other resonances. Precise measurements of resonances are important to determine the evolution dynamics during the time interval from hadron formation to kinetic freeze-out.

The barrel TOF detector will also allow us to measure non-identical two-particle correlations. Non-identical two-particle correlations are sensitive to the temporal emission pattern of different particles at the kinetic freeze-out stage. These correlation functions are constructed at the same velocity for different particle species. Because of their different masses, these particles have different momenta in the correlation function. Presently STAR does not have sufficient p_T coverage to allow non-identical particle correlations to place significant constraints on models of hadronic evolution. A large area TOF detector is necessary to extend the p_T reach and provide sufficient data rate.

2.3 TOF MRPC Detector Technology

The Multi-gap Resistive Plate Chamber (MRPC) is a new detector capable of sub-one hundred picosecond time resolution and high detection efficiency (>95%) for minimum ionizing particles. The mechanical and electric structure of the MRPC is different from that of previous Resistive Plate Chambers (RPC). The STAR MRPC TOF proposal is based on a successful MRPC R&D program involving collaborators from Rice University and the Chinese institutions in STAR in collaboration with the ALICE TOF group at CERN. This team has constructed a number of MRPC detectors and tested them in the CERN T10 beam line during the period from 2000 - 2001. The MRPC detectors tested have demonstrated the timing resolution, detection efficiency, and operational stability necessary to meets STAR's requirements. In addition, a full scale STAR MRPC prototype tray (1/120 of the full barrel TOF

detector) has been tested at the AGS, installed in the STAR detector during the fall of 2002, and operated successfully in the FY2003 run. Details of the prototype results will be presented in section 5. As a brief summary, the MRPC TOFr prototype tray installed in STAR for Run III demonstrated stable performance, meeting all key performance parameters and producing important physics results. The conclusion from these studies is that MRPC technology is mature for use in large scale detector applications. Further evidence for this fact is provided by the HARP experiment at CERN which successfully operated a ∼400 channel system for approximately two years.

The proposed detector is a full acceptance time-of-flight system matching the acceptance of the SVT, TPC, and BEMC. Coverage of the entire sixty square meter area of STAR will be accomplished by placing approximately 3800 MRPC modules in an overlapping geometry within 120 aluminum trays that fit inside the integration envelope of the present STAR Central Trigger Barrel (CTB). Since each MRPC module has 6 electrodes, the envisioned detector would comprise approximately 23,000 channels, each having an active area of 3.3 cm × 6.1 cm. With this degree of of granularity, the expected occupancy and multiple hit percentage is approximately 12% and 1% respectively for a central Au+Au collision at $\sqrt{s_{\rm NN}}$=200 GeV. The full barrel TOF detector will extend STAR's present capability for kaon separation from ∼0.6 to ∼1.7 GeV/c; the range for proton separation would be increased from approximately ∼1 GeV/c to ∼3.0 GeV/c. This extension of the momentum range for particle identification is crucial to enable a number of key measurements that can not be achieved otherwise.

Prototypes of the proposed electronics for front end signal amplification and discrimination have been in use for two years. The digitization is based on a time-to-digital integrated circuit now in final development at CERN.

2.4 Project Cost-Schedule and Resources

The cost of the MRPC TOF barrel construction is proposed to be shared jointly by the U.S. and Chinese institutions collaborating on the project. The U.S. part of the construction project is projected to be $4.1M in FY2004 dollars. The proposed Chinese contribution in equivalent U.S. dollars is valued at $2.3M dollars. The average level of contingency for all project components is 27%.

The project schedule is summarized in Figure 3. The schedule anticipates that research and development of the electronic components will continue in FY2004. The construction schedule begins in October 2004. MRPC module construction in China would begin at this time and continue until the second quarter of calendar year 2006. The construction of the mechanical and electronic components would also begin in early FY2005, allowing for installation of a substantial portion of the system in time for the run beginning in the fall of 2005. Detector construction and commissioning would be completed in 2006-2007.

The team within STAR proposing to construct and integrate this detector system consists of 47 scientists, engineers, and students from 10 institutions in the United

ID	Task Name	Duration	Start	Finish
1	Funding	0d	10/1/04	10/1/04
2	Four (4) Tray System Installed	0d	10/1/04	10/1/04
3	Four (4) Tray System Commissioning	88d	10/15/04	2/15/05
4	**Module Assy and Test**	390d	10/1/04	3/30/06
6	**Tray Assy and Test**	448d	10/1/04	6/20/06
8	**Electronics Engineering**	620d	10/1/04	2/15/07
9	Final Design Completed	0d	10/1/04	10/1/04
10	Prototyping & Test Completed	0d	10/1/04	10/1/04
11	System Testing & Integration	610d	10/15/04	2/15/07
12	**Install Gas System**	45d	5/17/05	7/18/05
14	**Thirty (30) Tray System**	262d	2/15/05	2/15/06
15	Fabricate & Test Electronics	130d	2/15/05	8/15/05
16	Installation	110d	5/2/05	10/1/05
17	Commissioning	90d	10/13/05	2/15/06
18	**Ninety (90) Tray System**	262d	2/15/06	2/15/07
19	Fabricate & Test Electronics	130d	2/15/06	8/15/06
20	Installation	72d	6/23/06	10/2/06
21	Commissioning	90d	10/13/06	2/15/07

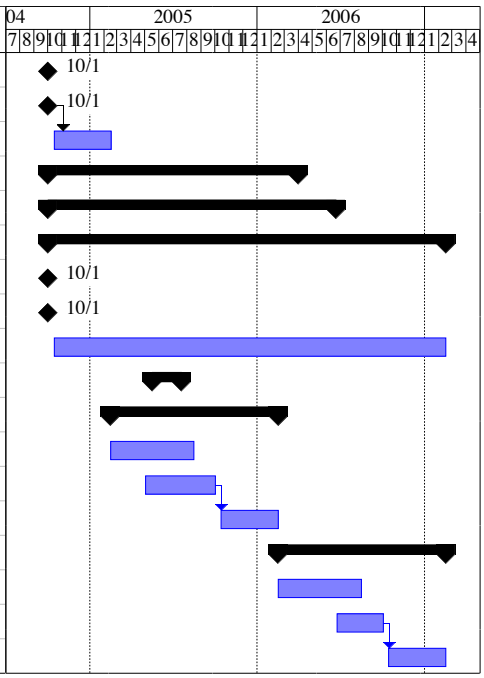

Figure 3: The summary schedule for the construction project.

States (4) and China (6).

In addition to contributing to the scientific measurements afforded by this detector system, the Chinese institutions will be responsible for providing high quality MRPC modules, built and tested in China, for integration into the barrel TOF system. These groups have extensive experience with this technology from test beam work at CERN, as well as module construction and testing in China. Twenty MRPC modules constructed in China were installed in the prototype TOFr tray and were tested at the AGS in the spring of 2002, and operated successfully in STAR in the FY2003 run. The results of these tests indicate the MRPC TOF detectors tested meet all STAR specifications.

The U.S. institutions participating in this project are responsible for the design, fabrication, testing, and integration of the front end and readout electronics as well as the mechanical assemblies required for this detector. They are responsible as well for overall project management and coordination.

The proposed TOF upgrade is a major STAR construction project involving international cooperation, with the STAR groups from China contributing significantly to the project both financially and technically. This project has been discussed in concept with the Directorate of the National Natural Science Foundation of China, which looks forward to reviewing a corresponding Chinese proposal once the review process for this proposal is begun by the U.S. Department of Energy. The team proposing to construct this detector has considerable experience in TOF techniques, and MPRC construction and testing as well as in high energy and nuclear physics experimentation in general.

2.5 Summary

A full acceptance time of flight system based on multi-gap resistive plate chamber technology is proposed. This detector is essential to upgrade STAR's particle identification capability to afford precision soft physics studies out to transverse momenta of approximately 2-3 GeV/c (depending on particle species) to help address the question of whether the relevant degrees of freedom in the initial stage of heavy ion collisions at RHIC are partonic, and whether they are equilibrated. With the proposed MRPC TOF barrel, essential information on the evolution of the produced matter will be afforded by examining, in detail, large scale correlation structures, non-identical two-particle correlations, and short-lived hadronic resonances. Without a full acceptance TOF barrel, these studies are significantly compromised or impossible. In addition, the proposed TOF barrel upgrade will reduce the time required for data acquisition and analysis of D mesons and the elliptic flow of multiply-strange baryons (e.g. the Ω) to the extent that these studies will become possible without multiple RHIC runs and production analysis runs extending more than 1 year. These studies are essential to study the degree of thermalization of the produced matter and to search for possible partonic collectivity. A search for a possible di-Omega di-baryon state is also made possible with the addition of the proposed system.

3 TOF Physics Discussion

3.1 Introduction

Figure 4 shows a schematic description of a central nucleus-nucleus collision as a function of time. Two Lorentz contracted nuclei collide, presumably creating non-equilibrated partonic matter which is initially comprised mainly of gluons. The high density partonic matter evolves towards equilibrium and expands under high pressure. During the later stages of the evolution, hadrons are formed until chemical freeze-out. The resulting high density hadronic system continues to expand until the particle density is sufficiently dilute that elastic collisions stop and kinetic freeze-out is reached.

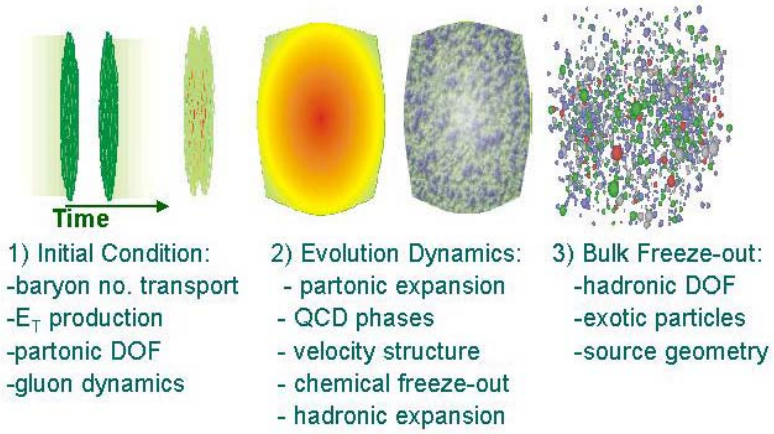

Figure 4: A schematic description of nucleus-nucleus collisions at RHIC from Ref. [11].

The proposed MRPC barrel TOF detector will provide crucial information, unavailable otherwise, to determine whether this type of physical picture is fundamentally correct. For the earliest gluon dominated stage, the barrel TOF will enable a systematic study of open charm to place important constraints on the gluon structure function of the colliding nuclei and establish a baseline for studies of quarkonium (J/ψ) suppression (enhancement) in a deconfined color medium. It will allow STAR to make definitive measurements of elliptic flow for multiply-strange baryons and heavy mesons (Ω, D mesons and possibly J/ψ) to study the pressure in the early stage of the collision and to search for possible partonic collectivity. Concerning the later stages of the collision, the proposed barrel TOF detector will provide detailed information on particle production in the hadronic stage as well as the evolution of the matter between chemical and kinetic freeze-out through systematic studies of large scale correlation structures, resonance production, and non-identical particle correlations. It will also enable sensitive searches for rare and exotic particles, which will test the boundaries of what is presently known about possible stable multi-quark (antiquark) configurations.

Key scientific measurements that will be made possible or will be significantly enhanced by the proposed barrel TOF detector are discussed in the sections which follow.

3.2 Partonic Collective Dynamics at RHIC

The proposed barrel TOF detector will enhance or make available a number of observables that are sensitive to collective dynamics in nucleus-nucleus collisions at RHIC, both in the early stage of the evolution when the degrees of freedom are presumed to be partonic (quarks and gluons), and in the later stage when they are hadronic.

Collective flow measurements have been very important for studying relativistic nucleus-nucleus collisions at all beam energies [17, 18] because the magnitude and pattern of the collective motion is closely related to the equation of state (EOS) of the produced matter. Assuming, local equilibrium, the EOS will be driven by the degrees of freedom relevant for the basic constituents which make up the matter. It is therefore possible by studying collective flow to determine important information about the nature of the matter when it is produced, *e.g.* whether it is partonic or hadronic in nature.

In order to access information about the early partonic stage, one possibility is to make measurements using particles that have small interaction cross sections during the hadronic stage, such as the $\phi, \Xi, \Omega, D, J/\psi$, and ψ'. For these particles, collective behavior observed in the lab is expected to be strongly correlated with pressure, equation of state, etc. in the early partonic stage of the evolution. An example of such an observable is the azimuthal anisotropy parameter v_2 (where v_2=$\langle\cos[2(\phi-\psi_{RP})]\rangle$, and ϕ is the azimuthal angle of the particle of interest and ψ_{RP} is the azimuthal angle of the reaction plane). By measuring v_2 for these particles, important information can be accessed about the early stage evolution. A specific example discussed below is the information afforded by measurements of transverse anisotropic flow (elliptic flow) and transverse radial flow for the Ω.

The focus of the STAR physics measurements of collective dynamics includes:

1. measurement of collective flow for rarely produced particles;
2. studying collective flow as a function of centrality;
3. systematic investigations of collective flow as a function of the colliding beam species.

The additional PID capability provided by the proposed barrel TOF detector is essential for these studies. Specifically, it will:

- increase the detection efficiencies for rarely produced particles such as the Ω and D meson making it possible to measure flow observables for these particles with an amount of beam time and analysis time that is not prohibitive;

- extend the range for p_T spectra to 5-6 GeV/c for these particles where the transition between soft physics and hard scattering becomes important and must be studied;
- allow STAR to make a systematic investigation of collective flow as a function of centrality and colliding system (A)

3.2.1 Transverse anisotropic flow

The transverse momentum distribution of particles produced in relativistic heavy ion collisions can be described by the following relation:

$$\frac{d^3N}{dp_T^2 d\phi dy} = \frac{dN}{2\pi dp_T^2 dy}[1 + 2\sum_n v_n cos(n\phi)]. \quad (1)$$

In this expression, p_T is the transverse momentum of a given particle, ϕ is its azimuthal angle with respect to the reaction plane (the plane containing the impact parameter and the z axis) [28, 29], and y is the particle's rapidity. The v_n harmonic coefficients in this decomposition are termed anisotropy parameters. The coefficients v_1 and v_2 are called *directed flow* and *elliptic flow*, respectively. Here the word "flow" is used to denote collective behavior in general, without necessarily implying a hydrodynamic description. Directed flow v_1 and elliptic flow v_2 are sensitive to the initial gluon density, the degree of thermalization of the constituents, and the conditions of the system at freeze-out. They are therefore important indicators of the properties of the matter during various stages of its evolution.

First experimental results from RHIC [17] included measurements of v_2 as a function of collision centrality for charged hadrons, and v_2 as a function of p_T for charged hadrons, as well as identified charged pions, charged kaons, and protons ($p_T < 0.9$ GeV/c). These initial results were of great interest because the degree to which the initial geometrical anisotropy of the nuclear matter mutually swept out by the colliding nuclei is converted to an anisotropy in the momentum distribution of produced particles is indicative of the density of the system and the mean free path for scattering of particles (parton and/or hadron). These properties are related to the equation of state of the matter.

Further results[17, 32] from RHIC have shown that in the low momentum region, $p_T \leq 2$ GeV/c, hydrodynamic model calculations provide a good description of v_2 as a function of p_T for π, K, p, Λ [33, 34, 19]. Alternatively, in the region where $p_T \geq 2.5$ GeV/c, the hard scattering of partons becomes prominent and the hydrodynamic model predictions fail. Recent theoretical work has attempted to explain these observations by assuming various values for the initial gluon density (and energy loss) in an early partonic stage [30], and by assuming an equation of state described by a hydrodynamic model [19, 31]. In general, flow that is observed may be hadronic or partonic in origin [30, 36, 37].

These studies have been very important in their own right and have yielded very important clues as to the condition of the matter produced in Au+Au collisions at

RHIC in the early stages of the collision. More importantly however, they have shown that, combined with observations of transverse radial flow, the measurement of elliptic flow for multiply strange baryons may provide a key and potentially definitive insight into the state of the matter and possible partonic collectivity in the early stage of the collision. Specifically, significant elliptic flow observed for the Ξ and Ω, would be a strong indication of partonic collectivity in the initial stages of the collision.

Based on analysis of TPC only Au+Au data at 200 GeV in the nucleon-nucleon center of mass system, approximately 2000 Ω's were reconstructed from 3.5 million central collisions. For flow studies, min bias data is required, which reduces the yield per event of Ω's by approximately a factor of 5. A simple scaling based on the number of Ω's needed for flow studies ($\sim$40,000) indicates a data sample of approximately 350 million events would be required using data from the TPC alone. The additional information provided by the STAR SVT is expected to improve the reconstruction efficiency by a factor of 2-3. However, without the proposed barrel TOF detector, the number of minimum bias Au+Au collisions needed to obtain a statistically significant sample of Ω's for flow studies is still 100 million. Given that the time to analyze $\sim$3 million events from the 2001 RHIC run took 2.5 months, this study is beyond the realm of feasibility for the present STAR detector without the additional PID capability provided by the proposed barrel TOF detector. With the proposed TOF upgrade, the additional particle identification capability for detecting the decay daughters increases the reconstruction efficiency for Ω's by a factor of 3-8, making this measurement possible.

3.2.2 Transverse radial flow

At the SPS, it has been observed that multi-strange baryons like Ξ and Ω [44] do not follow the common flow pattern shown by lighter hadrons π, K, and p [45] (See the open circles in Fig. 5 left plot). This observation was interpreted as a result of the earlier freeze-out of the multi-strange baryons due to their smaller elastic cross sections in a hadron gas [46]. This effect provides a unique possibility for studying the collision properties at the early stage of the collision.

The data in Fig. 5 provide an important insight as to how information on the early stage of the collision can be accessed. Due to the fact that at late times, the expansion of the produced matter tends to reduce the effects of spatial anisotropy in the initial collision, elliptic flow is expected to be self-quenching. If observed, elliptic flow is therefore likely developed in the early stage of the collision when partonic degrees of freedom are most relevant. Due to the small elastic hadronic cross sections for multi-strange baryons (Ξ, Ω) and charm hadrons ($D, J/\Psi$), those particles are expected to couple weakly to hadronic matter in the later stages of the collision (as evidenced by the departure of the behavior of the inverse slope for the omega and cascade from the trend for lighter particles). A finite value of v_2 for those particles therefore should carry partonic information. A non-zero value of v_2 and possible v_2 saturation for those particles would serve as a strong signature of partonic collectivity in nuclear collisions at RHIC.

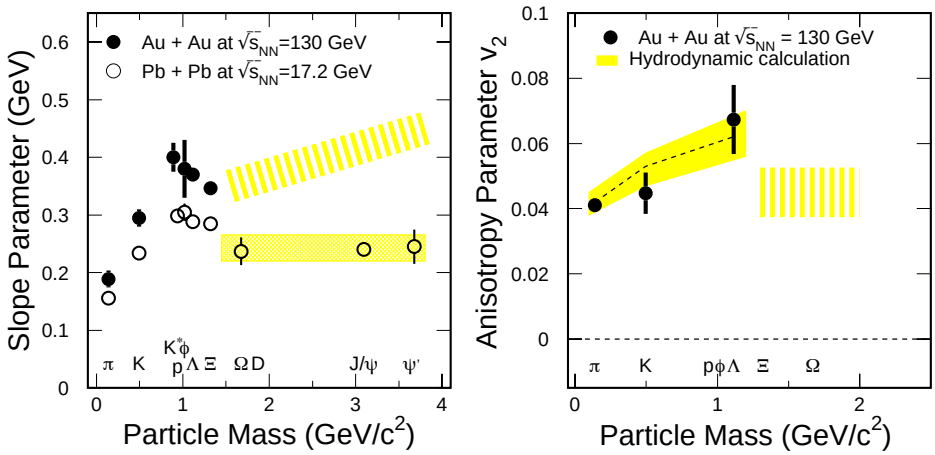

Figure 5: (Left) Measured slope parameter as a function of particle mass. Open symbols are for results from Pb+Pb central collisions at the SPS ($\sqrt{s_{NN}}$ = 17.2 GeV); filled symbols are for central Au+Au collisions at RHIC ($\sqrt{s_{NN}}$ = 130 GeV). (Right) Integrated azimuthal anisotropy parameters v_2 as a function of particle mass. Data points are from minimum bias Au+Au collisions at RHIC ($\sqrt{s_{NN}}$ = 130 GeV). The gray band indicates the predictions of a hydrodynamic model [19]. The expected range if there is significant partonic collectivity is indicated by the dashed band in both plots.

The barrel TOF detector will allow measurement of the elliptic flow for Ω baryons up to moderately high p_T, well into the region of possible saturation. Specifically, as shown in the following section, the Ω detection efficiency is increased over that for the existing TPC+SVT configuration in STAR by a factor of 3 to 8 for the p_T region from 1.5 GeV/c to >4 GeV/c. Such an enhancement in the detection efficiency is essential to make this measurement in order to unambiguously establish possible collective phenomenon for the Ω within a reasonable amount of running time. Without the proposed barrel TOF system, due to the reduced detection efficiency and increased combinatorial background, the beam time needed to make this measurement is prohibitive.

An increase of the slope parameter for the Ω, D, J/Ψ, Ψ', as shown in the dashed band of the left panel of Fig. 5 combined with a non-zero v_2 for those particles as indicated in the dashed band of the right panel would provide a strong signature of partonic collectivity in nucleus- nucleus collisions at RHIC. Due to the acceptance and p_T range needed, only STAR can make this measurement at RHIC. STAR can only make this measurement with the addition of the particle identification capability provided by the proposed barrel TOF detector.

3.2.3 Simulation Results

A TOF detector matching the TPC acceptance in the mid-rapidity region will significantly enhance STAR's hyperon detection efficiency. Figure 6 illustrates the increase in detection efficiencies for the Ω using the PID capability that will be provided by the proposed barrel TOF detector. Compared to the particle identification capability with the TPC only, the addition of the proposed barrel TOF detector results in a dramatic improvement for p_T>2.0 GeV/c; at 4.0 GeV/c it enhances the efficiency by a factor of 8.

The analysis was performed by embedding Ω's having a p_T spectrum similar to that observed in the STAR Au+Au collision data. The increase in the detection efficiency from the proposed TOF barrel is most significant for the higher p_T Ωs, which have daughter kaons (p_T>0.5 GeV/c) and Λ decay protons (p_T>0.9 GeV/c) beyond the PID capability of the present TPC + SVT.

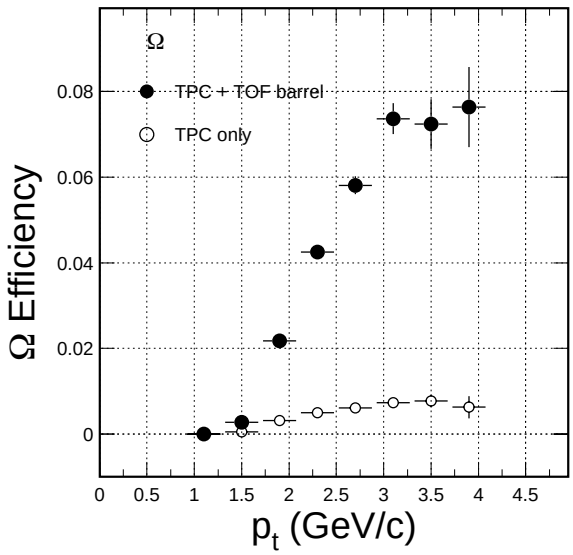

Figure 6: Detection efficiencies with and without TOF PID for Ω decays.

Using the Ω detection efficiency from these simulations, the spectra and corresponding statistical errors were estimated assuming event samples of varying size for 10% central 200 GeV Au+Au collisions. The results are shown in Figure 7. The figure shows the simulated p_T distribution for $\Omega+\overline{\Omega}$ in central collisions (left two frames) and minimum bias collisions (right two frames). What would be measured by the STAR detector assuming TPC PID only (squares) and with the addition of the proposed barrel TOF detector (circles) is also indicated. The right hand panels show the relative statistical error in the spectra assuming event samples of up to 30 million events. These results reflect a value of dN/dy = 0.64 for the $\Omega+\overline{\Omega}$ and an inverse slope parameter of T=450 MeV.

The results in the right panel are for minimum bias Au+Au collisions. For this simulation, the capability of the SVT has also been included in the comparison (TPC

+ SVT versus TPC + SVT + TOF in the upper left panel). The Ω yield per event for minimum bias events is approximately a factor of 10 less than in central collisions. Thus the Ω yield from a sample of 8M central events has roughly same statistical precision as a function of p_T as a sample of 80M minimum bias events. For elliptic flow studies, minimum bias data is needed, since the magnitude of v_2 depends on the initial coordinate space anisotropy of the overlap region, and this is larger for more peripheral collisions.

The lower left panel for minimum bias events (panel b) shows the statistical precision needed for a robust measurement of elliptic flow for $\Omega+\overline{\Omega}$. The statistical errors are plotted on a presumed distribution of v_2 vs p_T to indicate the estimated level of statistical precision with respect to the estimated magnitude of v_2 as a function of p_T. The resolution in determining the reaction plane was taken to be 0.75, consistent with the resolution that has been observed in minimum bias Au+Au collisions in STAR.

This level of statistical precision requires approximately 30 million minimum bias collisions assuming the increased efficiency provided by the particle identification capability of the proposed barrel TOF detector. It requires 5-10 times more events if TPC PID only is assumed. With the barrel TOF detector, this measurement is challenging but feasible. Without the barrel TOF detector it is not possible given the resources and time required to acquire and analyze several hundred million events.

The importance of achieving this level of statistical precision is illustrated by the following example. STAR preliminary results have shown that v_2 for the Λ is approximately 17% at a p_T of 3 GeV/c. Comparing the v_2 expected for the Λ and the Ω, if the relevant degrees of freedom in the early (partonic) stage are those of the constituent quark masses then v_2 would be expected to be proportional to the mass and the v_2 of the Ω would be expected to be $\sim 25\%$. However, if the relevant degrees of freedom when the collective flow is generated are those of massless quarks/gluons, the partonic v_2 of Ω and the Λ would be expected to be approximately the same. To differentiate these scenarios it is necessary that v_2 for the Ω is measured with a relative uncertainty of less than 10%.

The conclusion is that with the additional PID capability provided by the barrel TOF detector, it will be possible to make a definitive measurement of v_2 as a function of p_T for the Ω as well as other multiply-strange baryons and heavy mesons. These measurements will provide crucial information on the relevant degrees of freedom in the early (partonic) stage of the collision and on possible partonic collectivity. Without the proposed barrel TOF detector, these measurements are not possible given the amount of beam time and analysis resources that would be necessary to process the hundreds of millions of events that would be required.

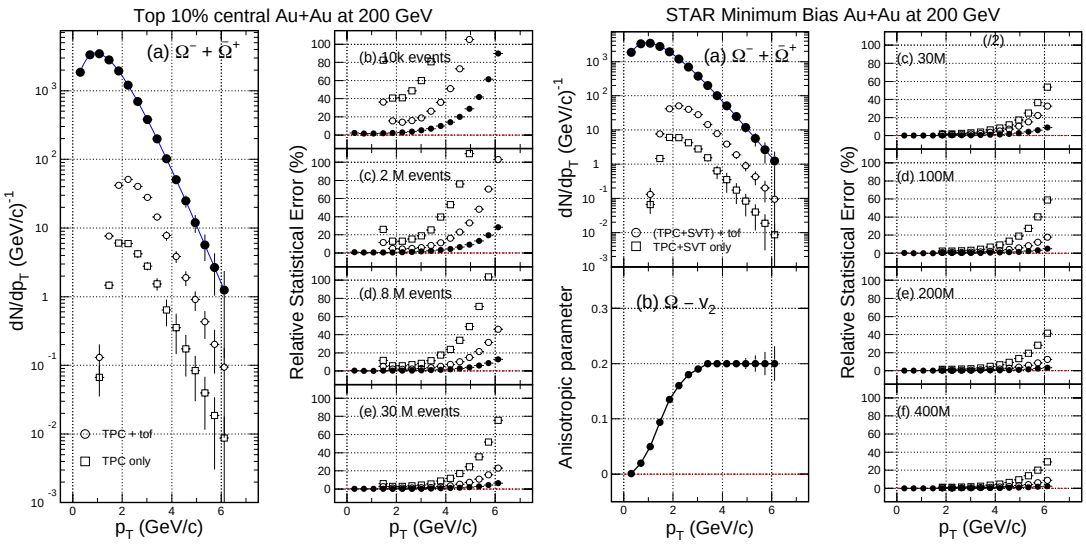

Figure 7: **Left:** Estimate for spectra and statistical errors from 200 GeV Au+Au top 10% central collisions. The value of dN/dy = 0.64 and an inverse slope parameter T = 450 MeV are used, for the sum of Ω and $\overline{\Omega}$. The resulting p_T spectrum, as well as what would be measured in STAR using TPC PID only, and TPC+TOF PID are indicated in left panel (a) and TPC + SVT versus TPC+SVT+TOF in the right panel (a). **Right:** An estimate of the statistical precision needed relative to the projected anisotropy v_2 from minimum bias Au+Au collisions at 200 GeV is shown in panel b. The reaction plane resolution is taken to be 0.75 consistent with previous STAR measurements. This level of statistical precision can be achieved with 30 million minimum bias events with the proposed TOF upgrade. Without the proposed TOF barrel, the number of events needed is 5-10 times greater, and this measurement is not feasible.

3.3 Event-by-Event Fluctuations and the Correlation Structure of Heavy Ion Collision Events

Introduction

Event-by-event analyses of fluctuations and correlations in heavy ion collisions are predicted to provide significant new information on the hot, dense system produced in relativistic heavy ion collisions and the search for color-deconfined matter. Theoretical studies [50]-[60] have concluded that large non-statistical event-wise fluctuations displaying non-monotonic dependence on collision parameters (*e.g.,* energy, ion species, centrality, rapidity range) should be observed if the evolving collision system passes through a QCD phase transition [50] or near a critical endpoint [56]-[58] or evolves hadronizing QGP droplets [50]-[55]. Some recent studies [61] have focused on the time interval from hadronization to kinetic decoupling and its effect on large-scale charge-dependent pseudorapidity correlations.

How are event-by-event fluctuations and correlations in RHIC events related to

collision dynamics and QCD? The system comprised of the two colliding nuclei prior to interaction is initially highly correlated (the entropy is extremely low). The collision process is one of correlation modification and reduction, or equivalently entropy increase. Correlations present during the earliest partonic interactions are expected to be transported from early to late-stage degrees of freedom by several mechanisms, including hydrodynamic response to early pressure in a glue-dominated medium, initial-state multiple scattering, critical correlations associated with a QCD phase transition, and hadronic processes later in the collision. Observation of structure in the hadronic final state depends in part on survival through dissipative processes during system evolution which include nonperturbative-QCD dynamics, the hadronization process itself, and final-state hadronic interactions.

It is precisely because of this that the correlations and fluctuations observed in the final state are important: they carry information on the various stages in the evolution of the matter. This information can be extracted in detail only with particle-identified spectra, since some dynamical/dissipative processes produce final state effects which scale with particle mass, and some do not. The mass dependence of the observed correlations and fluctuations provides clues as to which processes produced them. Based on correlation structures already observed in Au+Au collisions in STAR, large acceptance particle identification capability extending beyond the p_T range covered by dE/dx in the TPC + SVT is crucial for understanding this important and unique source of information.

The QCD medium, velocity fields and dissipation

To unfold correlations and extract the information they carry, it is necessary to separate the effects of various underlying dynamical/ dissipative processes which may result in large scale collective motion (global "structure" in the overall "velocity field" of all the produced particles) or more localized effects such as local temperature (thermal) fluctuations which may affect the motion of smaller groups of particles. These concepts are familiar from heavy ion phenomenology [66]. Examples of large scale velocity fields include radial flow, elliptic flow, and Bjorken expansion. These are specific examples of a more general concept. The structure of the velocity field observed in the final state (the "velocity structure") is expected in general to be complex, since it contains contributions from the entire history of the collision.

Thermal and velocity correlation structures show up in heavy ion collisions as non-statistical fluctuations in event-wise averaged global quantities (*e.g.,* event-wise mean p_T) and in two-particle momentum-space correlations [64]. Little is known at present about the detailed velocity structure of RHIC events. Distinguishing velocity structure and thermal fluctuations from equilibrated thermal energy in the hadron system requires particle identification (mass measurement) of pions, kaons, and protons for transverse momentum substantially beyond $\sim$1 GeV/c. In STAR, this can only be accomplished with the addition of the proposed barrel TOF detector.

Separate determination of velocity and thermal structures in RHIC events is essential because the velocity structure represents an otherwise unknown, fundamental

degree of freedom of the collision system and because velocity and temperature fluctuations are affected differently by QCD dynamics. For example, localized energy perturbations (*e.g.* QGP droplets) could produce 'hot spots' which would be manifest in the data as local temperature fluctuations with respect to a characteristic scale in pseudorapidity and azimuth. Dynamics which produce structured pressure gradients in the early collision should produce event-wise (large scale) fluctuations in the velocity field. Minijets are expected to produce both local temperature and velocity fluctuations. Whether QCD dynamical processes result in thermal or velocity structure, both lead to momentum-space fluctuations and correlations in the unidentified hadron momentum distribution. Unambiguous interpretation of the resulting fluctuation and correlation structure with nonidentified particles simply is not possible.

Analysis of first RHIC data by STAR has revealed that Au+Au collisions have a complex correlation structure, including large-scale two-particle correlations in p_T, η, and ϕ, which provide direct access to a range of QCD phenomena available from no other experimental source. Charge-independent (isoscalar) and charge-dependent (isovector) correlation structures already being observed [63, 67] in distributions of relative two-particle transverse momentum ($m_{t1}\otimes m_{t2}$ up to $\sim$2 GeV/c), pseudo-rapidity ($\eta_1\otimes\eta_2$ up to 2 units), and azimuthal angle ($\phi_1\otimes\phi_2$ up to π radians) are comparable in size to the STAR TPC acceptance. To fully extract the information these correlations carry and use it to understand the role of nonperturbative QCD in Au+Au collisions at RHIC requires particle identification (π, K, p) over the full STAR TPC acceptance, over a momentum range substantially exceeding that for dE/dx PID in the TPC+SVT. This can only be accomplished with the addition of the proposed barrel TOF detector.

Correlations and fluctuations of transverse momentum

Under certain assumptions expected to be valid for central Au+Au collisions at RHIC (validity of the central limit theorem (CLT) [64], absence of internal correlations and fixed parent distribution), the mean and *rms* width of the event-wise $\langle p_T\rangle$ distribution should be equal to $\hat{p}_T$ and $\sigma_{\hat{p}_T}/\sqrt{\bar{N}}$, respectively, where $\hat{p}_T$ and $\sigma^2_{\hat{p}_t}$ are the mean and variance of the inclusive p_T distribution, and $\bar{N}$ is the mean event multiplicity [64, 74]. The frequency distribution of event-wise $\langle p_T\rangle$ for the 15% most central Au+Au collisions at $\sqrt{s_{NN}}$ = 130 GeV from STAR displays a 13.7±0.1(stat)±1.3(sys)% increased width compared to a gamma-distribution reference, which is the appropriate reference assuming finite-number statistics in the absence of non-statistical fluctuations [63, 73, 74]. This reference distribution is indicated as a dotted line in Fig. 8. The distribution in the variable $(\langle p_T\rangle - \hat{p}_T)/(\sigma_{\hat{p}_t}/\sqrt{N})$ minimizes systematic contributions from multiplicity fluctuations and variations of inclusive parameters with centrality.

It is possible to quantify the excess variance of $\langle p_T\rangle$ observed in Fig. 8 using several

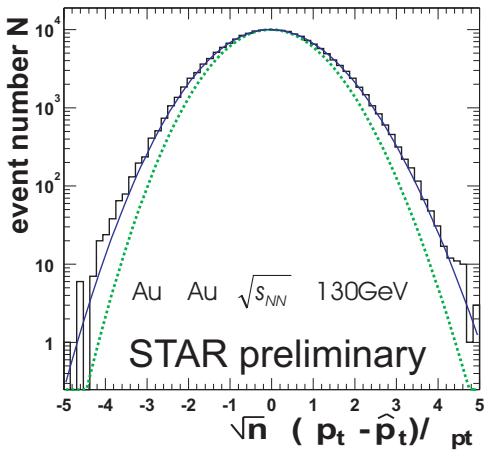

Figure 8: Mean-p_T distribution for $\sqrt{s_{NN}}$ = 130 GeV Au+Au central collisions with respect to $\hat{p}_T$ in units of $\sigma_{\hat{p}_T}/\sqrt{N}$ compared to a gamma distribution reference expected in the absence of non-statistical fluctuations (dotted curve) and a gamma distribution calculated with an *rms* width increased by 14% (solid curve).

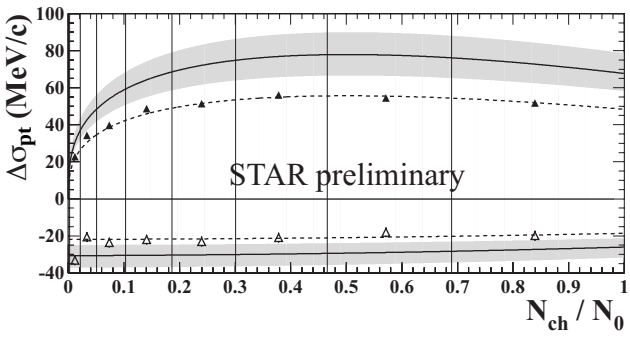

Figure 9: Centrality dependence for Charge Independent (CI) (solid triangles) and Charge Dependent (CD) (open triangles) fluctuation measure $\Delta\sigma_{P_T}$ for 130 GeV minimum bias Au+Au events. The CD values are multiplied by 3 for clarity. The dashed lines are curve fits. Solid lines and bands reflect an extrapolation to 100% for primary charged hadrons in the detector acceptance and include a ±15% systematic error.

quantities [62, 69], for example:

$$\Delta\sigma^2_{p_T} \equiv \frac{1}{\varepsilon}\sum_{j=1}^{\varepsilon} N_j \left(\langle p_T\rangle_j - \hat{p}_T\right)^2 - \sigma^2_{\hat{p}_t} \equiv 2\sigma_{\hat{p}_t}\Delta\sigma_{p_T}, \quad (2)$$

defines the difference variable $\Delta\sigma_{p_T}$. A closely-related differential measure is [69]

$$\Phi_{p_T} \equiv \left[\frac{1}{\varepsilon}\sum_{j=1}^{\varepsilon}\frac{N_j^2}{\bar{N}}(\langle p_T\rangle_j - \hat{p}_T)^2\right]^{1/2} - \sigma_{\hat{p}_t}, \quad (3)$$

where ε is the number of events, j is the event index, N_j is the event multiplicity, and $\bar{N}$ is the ensemble-mean multiplicity. For small fractional variations of N_j within the event ensemble $\Delta\sigma_{p_T} \cong \Phi_{p_T}$.

The centrality dependence of $\Delta\sigma_{p_T}$ is shown in Fig. 9 for 205k $\sqrt{s_{NN}}$=130 GeV Au+Au minimum bias events. The number of charged particles measured per event over the maximum number observed in the sample N_{ch}/N_o is used as a relative measure of event centrality. These data were derived using 70% of all the primary charged particles (this is less than 100% due to tracking inefficiency and track quality requirements) for charge independent and charge dependent fluctuations [63, 73]. Statistical

errors are ±0.5 MeV/c. The dashed lines are polynomial fits to the data, the solid lines are estimated extrapolations to 100% of the primary particles in the acceptance, and the shaded bands indicate a ±15% systematic error.

This analysis provides a quantitative measure of the non-statistical fluctuations visually apparent in Fig. 8 and reveals an intriguing non-monotonic dependence on centrality which may be related to the growing influence of a dissipative (opaque) medium produced in the overlap region in central Au+Au collisions at RHIC. If true, this would represent important independent confirmation of results observed in back-to-back jet studies in STAR. However, to distinguish between thermal fluctuations and velocity structure –to really understand the origin of this newly observed behavior and what it is indicating–requires application of this analysis to identified hadrons. The particle identification capability of the proposed barrel TOF detector is needed to unambiguously interpret the meaning of this potentially definitive result.

Event-wise fluctuations versus two-particle correlations

The enhanced event-wise fluctuations seen in Figs. 8 and 9 result in fact from projections of more general two-particle correlations. An example of the rich structure apparent simply by examining the two-particle correlation in relative transverse mass ($m_{t1}\otimes m_{t2}$) is shown in Figs. 10 and 11. These distributions are simply plots of the ratio of the number of real to mixed-event particle pairs observed in a particular bin of (m_{t1}, m_{t2}). To have more or less uniform statistics in all bins, a transformation has been made which "flattens" the single particle $\mathrm{p_T}$ distribution and maps the m_t interval $[m_0, \infty]$ onto the X interval $[0, 1]$. This minimizes statistical "noise" and allows correlation structure to be clearly seen. Most of the visible structure falls within the $m_t - m_0$ interval $[0.1, 2.0]$ GeV/c^2. Fig. 10 provides a perspective view and Figure 11 a projection onto the $X_{p_{T1}}\otimes X_{p_{T2}}$ plane with bin-by-bin intensity (occupation) indicated by color.[1]

These plots exhibit remarkable richness in the two-particle correlation structure in $m_{t1}\otimes m_{t2}$. The interpretation given the dominant features in the perspective view include quantum-interference (HBT) and Coulomb-interaction correlations which contribute to the diagonal ridge at low m_t. The peak at high m_t is presumably due to hard-QCD processes. The large-scale saddle shape which dominates the distribution is consistent with fluctuations in the effective temperature. All these features have similar amplitudes and represent non-statistical correlations (absence of correlation would be indicated by statistical fluctuations about unity). The event-wise analyses of excess $\langle \mathrm{p_T} \rangle$ fluctuations shown in Fig. 8 and Fig. 9 integrate over all sources of two-particle correlations seen in Fig. 10.

Several conclusions are drawn from these figures. First, two-particle distributions being observed in STAR are rich in structure, and therefore carry a wealth of information on various dynamical/dissipative processes that are important through the evolution of the collision. Secondly, the observed structure is coherent over a large

[1]Measured $\mathrm{P_T}$ was mapped to $X(m_t)$, where $X(m_t) \equiv 1 - [(1 + m_t/T)\exp(-m_t/T)]/[(1 + m_0/T)\exp(-m_0/T)]$, $m_t = \sqrt{\mathrm{P_T^2} + m_0^2}$, and m_0 was assumed equal to the pion mass.

scale. Examining one corner of the phase space in Fig. 10 would provide a very limited perspective on the global features of the full correlation. Third, to fully interpret the information carried by these correlations, particle identification is needed beyond the p_T range afforded by dE/dx in the TPC+SVT. One of the most interesting features is near $m_t \sim 1$ GeV/c^2. This is in a range where the underlying particle composition producing this correlation structure is not known and can not be determined with the existing PID capability of STAR. This structure could be a result of an increasing two-particle correlation in the range of $m_{t1} \otimes m_{t2}$ for a given species, or, it could be due to a change in the relative number of underlying particle species (π, k, p), or both, or neither. If the speculation above is correct that this region is dominated by hard QCD processes, rough charge ordering should be observed, the correlation strength for pairs of same species and opposite sign should be strongest, and a reasonably well-known ratio of meson to baryon pairs would be expected. With the existing PID capability of the STAR TPC + SVT, this information is not available. To realize the full scientific potential of STAR for a robust study of QCD in relativistic heavy ion collisions, it is important to utilize every bit of information available. This is a clear and important example of a major source of unique information that will be lost without the additional PID capability provided by the proposed barrel TOF detector.

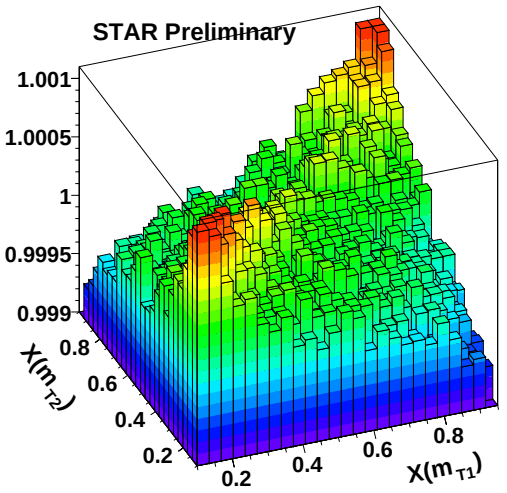

Figure 10: Perspective view of the two-dimensional $X(m_{t1}) \otimes X(m_{t2})$ charge independent correlations for $\sqrt{s_{NN}}$=130 GeV Au+Au collision data.

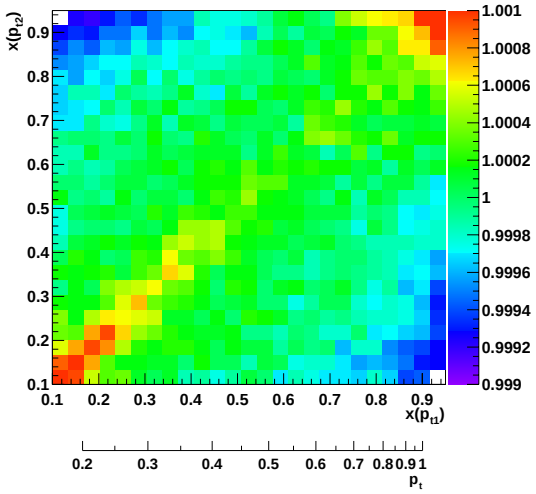

Figure 11: Transverse-mass two-particle $X(p_{t1}) \otimes X(p_{t2})$ correlations for all charged hadrons in the top 15% most central collision events. Corresponding p_T values in GeV/c are shown in the lower horizontal scale.

The conclusions from this section are clear: there is a wealth of correlation structure being observed (some for the first time) in Au+Au collisions at RHIC in several two-particle phase space distributions. These correlation structures are capable of providing crucial information, unavailable otherwise, on important dynami-

cal/dissipative processes central to the evolution of heavy ion collisions at RHIC. Examples include hydrodynamic response to early pressure in a glue-dominated medium, initial-state multiple scattering, critical correlations associated with a possible QCD phase transition, nonperturbative-QCD dynamics, hadronization, and final-state hadronic interactions. To understand these processes, it is necessary to utilize the observed correlations and fluctuations to the fullest. This can not be done in STAR without the addition of the large acceptance particle identification capability that will be provided by the proposed barrel TOF detector. Without this upgrade, STAR will not have access to an important, and perhaps defining source of information to understand the new matter being created at RHIC.

3.3.1 Particle Flavor Dependent Fragmentation at Moderate p_T

At intermediate p_T (>2 GeV/c), a description of the observed correlation structures in terms of jets and mini-jets becomes appropriate. In central heavy-ion collisions, it is impossible to fully reconstruct jets due to the large underlying soft particle production and finite probability of multiple hard interactions in a single Au+Au event. The presence of jets, however, can be inferred by measuring two-particle azimuthal and rapidity correlations [47]. These jet-like correlations are spread over a large region of phase-space ($\Delta\phi\otimes\Delta\eta\approx0.7$). STAR has observed such correlations for charged hadrons [48]. Correlations due to dijets occur over the full available phase-space of the collision. Thus, a large acceptance is vital for studying possible medium induced modifications of jet fragmentation in heavy-ion collisions.

The proposed barrel TOF would allow for two-particle azimuthal correlation studies for several particle species over a large phase-space. Specifically, it would be possible to identify for protons up to 3 GeV/c, and to measure the relative strengths of meson-meson, meson-baryon, and baryon-baryon azimuthal and rapidity correlations. These measurements would allow for a further understanding of particle flavor dependent fragmentation at RHIC energies and a deeper understanding of jet quenching phenomena in heavy-ion collisions.

The particle production mechanism(s) at moderate p_T are poorly understood in central Au+Au collisions. STAR has reported that hadrons above p_T=3 GeV/c show azimuthal correlations characteristic of jet fragmentation [67]. In Figure 12, the analysis described in Ref. [67] is repeated for a trigger particle threshold of 2 GeV/c, which is accessible using the full TOF. The relative strengths of jet-like (squares) and dijet-like (circles) azimuthal correlations are plotted as a function of the number of participants. The jet-like correlations are slightly suppressed in the most peripheral collisions, and show an enhancement above the expectation from proton-proton collisions for the more central collisions.

PHENIX, on the other hand, reports a proton-to-pion ratio near unity in central Au+Au collisions, which is in contrast to the measured value of ≈0.2 in p+p collisions. This enhancement in the proton-to-pion ratio can have several explanations. One possibility is that protons at moderate p_T (≈ 2-3 GeV/c) come primarily from soft processes such as hydrodynamical collective flow. In this case, there will

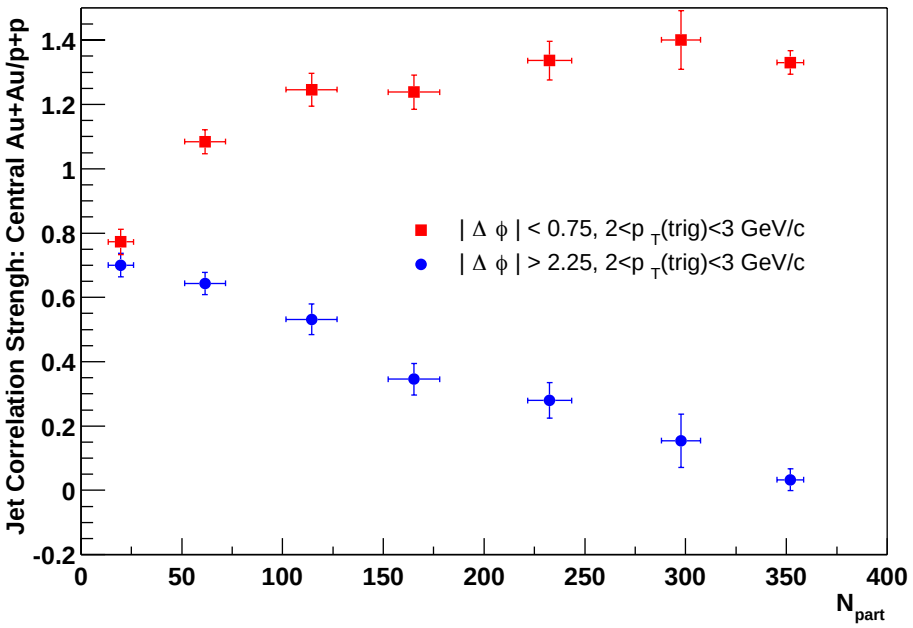

Figure 12: Relative azimuthal correlations for central Au+Au and minimum bias p+p collisions. The squares show the small-angle correlation strength, and the circles show the back-to-back correlation strength.

be no localized jet-like correlations between moderate p_T protons and other hadrons in the event. An alternative explanation for the proton-to-pion ratio is that initial state nuclear effects, including multiple nucleon-nucleon soft interactions, boost the proton-to-pion ratio in jet fragmentation. Identified particle azimuthal correlations can be used to distinguish between these two possibilities. If there is a large contribution to the proton yield from soft processes, azimuthal correlations triggered on a leading proton should show a large suppression. Alternatively, a medium induced particle flavor dependent jet fragmentation would lead to relative enhancements in the azimuthal correlations for leading protons over leading mesons. A systematic comparison between nucleus-nucleus and p+p collisions is also necessary to establish the possible flavor modification of jet fragmentation.

These measurements require large acceptance and the ability to distinguish mesons from baryons into the hard scattering regime. The full TOF coupled with the BEMC, EEMC and possible topological identification will lead to a thorough understanding of the mechanisms of particle production in the moderate p_T region where the transition from soft to hard processes is expected to occur.

Particle identification, correlations and velocity structure

The previous material represents a partial summary of the correlation structures revealed from RHIC data. It is clear that a wealth of structure has emerged and that RHIC collisions may not be viewed as simple equilibrated systems. What role does

large-acceptance particle identification play in this analysis?

In the broadest terms, some of the questions being addressed at RHIC are:

- What evidence is there of hydrodynamic response to pressure gradients?
- Is correlation structure developing in a prehadronic medium with partial transmission through hadronization, or is all the structure observed a consequence of hadronic dynamics?

These types of questions cannot be answered by examining a limited part of the observed correlation structure using unidentified hadrons [65]. Ambiguous and conflicting interpretations can only be resolved by performing a general correlation analysis over a broader p_T interval than is currently accessible to TPC PID, so that detailed information on correlations and fluctuations of identified particles is available in the full acceptance of STAR. This requires the additional PID capability provided by the proposed barrel TOF detector.

An example of how the barrel TOF detector would provide information crucial for deciding between two possible interpretations of observed correlation structure is the following. Analysis of STAR p+p and Au+Au minimum-bias p_T distributions indicates that inclusive mean-p_T ($\hat{p}_T$) is approximately independent of particle mass (pions, kaons, protons) for p+p and peripheral Au+Au collisions and increases monotonically with centrality in proportion to particle mass [82]. Assuming the increase in $\hat{p}_T$ with centrality is caused by increasing transverse expansion it is straightforward to conclude that for more central A+A collisions

- 'temperature' fluctuations in a locally-equilibrated system should produce mass-independent event-wise $\langle p_T \rangle$ fluctuations, and
- transverse-expansion-velocity fluctuations should produce event-wise $\langle p_T \rangle$ fluctuations which increase monotonically with particle mass.

Thus, mass dependence of $\langle p_T \rangle$ fluctuations coupled with centrality dependence would provide a key test of the production mechanism for these fluctuations, the structure of the velocity field, the extent of local equilibration, and the nature of the medium. The observed CD correlation structures for nonidentified hadrons (mainly pions) should thus have counterparts for identified protons/antiprotons and kaons, structures depending on local baryon-number and strangeness conservation. The correlation lengths and amplitudes of these structures are presently unknown. Do different hadron types experience different medium properties, possibly at different times in the collision? Large-acceptance MRPC-TOF is required to answer these questions.

Simulations were done which demonstrate the particle mass dependence of the mean-p_T fluctuation measure, $\Delta\sigma_{p_T}$(CI). This was done for Monte Carlo events which included arbitrary mixtures of random, event-to-event fluctuations in both the temperature and the transverse flow. The events were generated by random sampling a Maxwell-Boltzmann parent distribution with temperature T. In addition to this

random, thermal motion an overall transverse expansion flow field was added to each particle's velocity. This was done by assigning a random coordinate space position to each particle and computing a transverse flow velocity, $\beta_t(r)$=tanh[$\eta_t(r)$], where $\eta_t(r)=\eta_f(r/R_{max})$. This transverse boost velocity was added relativistically to the particle's random thermal velocity to arrive at the total, final state particle velocity. The present model is consistent with other parametrizations of transverse expansion used in so-called "blast-wave" models to describe the p_T distributions and HBT radii in relativistic heavy-ion collision sources.

Twenty thousand (20K) events were generated in this manner for a number of cases in which the particle content consisted entirely of either charged pions (equal numbers of π^+ and π^-), charged kaons (equal numbers of K^+ and K^-), or protons and antiprotons. The local temperature average was T=100 MeV, and the average transverse expansion boost parameter, η_f, was 0.9. The radial density distribution was assumed uniform (a box-like distribution) from r=0 to R_{max}=9.0 fm. The pseudorapidity and azimuthal distributions were assumed to be flat. These parameters are typical of those which describe the measured spectra shape and HBT radii at RHIC. Kinematic acceptances were p_T from 0.1 to 2.0 GeV/c, $|\eta|\leq$1.0, and full 2π azimuthal angle. Results for $\Delta\sigma_{p_T}$(CI) were scaled to an average multiplicity per event of 772 which is typical for charged pions in this acceptance in central Au+Au collisions at $\sqrt{s_{NN}} = 200$ GeV.

Temperature fluctuations were simulated by randomly sampling a Gaussian distribution for the temperature parameter T where the sigma of the distribution was σ_T=0.0032 GeV. Transverse flow fluctuations were similarly studied by event-to-event random sampling of a Gaussian distribution for the boost parameter η_f where σ_{η_f}=0.03. Combined temperature and transverse flow fluctuations were also studied where σ_T=0.0023 GeV and σ_{η_f}=0.021. Each of these three cases results in similar values for $\Delta\sigma_{p_T}$(CI) for charged pions which approximate the measured results for STAR Au+Au collisions at 130 GeV.

Table I: Particle mass dependence of $\Delta\sigma_{p_T}$(CI) for pions, kaons, and protons assuming random event-to-event fluctuations in temperature, transverse flow velocity, or a mixture of both types of fluctuations. Units are in MeV/c.

Particle	σ_T=0.0032 GeV σ_{η_f}=0.0	σ_T=0.0 σ_{η_f}=0.03	σ_T=0.0023 GeV σ_{η_f}=0.021
Pions	96	79	91
Kaons	67	167	123
Protons	27	196	104

The results are listed in Table I and shown in Figure 13 where it is seen that pure temperature fluctuations result in mean-p_T fluctuations which decrease monotonically with particle mass due to the combined effects of fixed temperature fluctuation and

increasing effective temperature, whereas transverse flow velocity fluctuations cause $\Delta\sigma_{p_T}$ (CI) to monotonically increase with particle mass. A mixture of both kinds of fluctuations produces intermediate results.

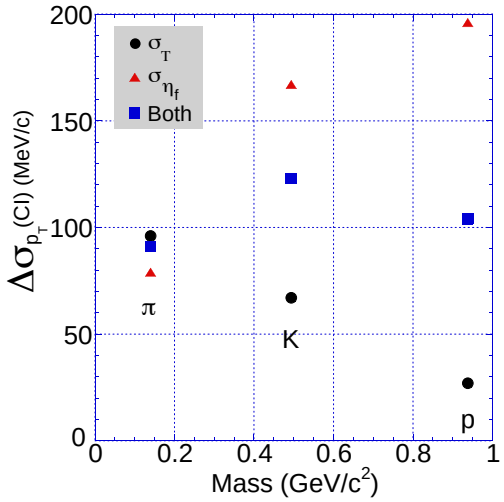

Figure 13: The expected behavior of $\Delta\sigma_{p_T}$ (CI) as a function of particle mass assuming the dominant contribution to it is due to temperature fluctuations (black circles), fluctuations in the transverse flow velocity (red triangles), or a combination of both types of fluctuations (blue squares). Without the additional PID provided by the barrel TOF detector, measurement of $\Delta\sigma_{p_T}$ as a function mass (this plot) *is not possible* over much of the p_T range of interest and essential information to interpret the origin of the observed $\Delta\sigma_{p_T}$ is simply lost.

The simulations reported here were done for transverse velocity fluctuations. Similar studies could also be done for velocity fluctuations along the axial (longitudinal and azimuthal) directions. Mass dependent fluctuation/correlation analyses combined with spectra and HBT radii measurements would enable separate determination of the thermal and velocity fluctuation structure of RHIC events.

This is a clear demonstration of how the additional particle identification capability that would be provided by the barrel TOF detector is absolutely critical to understand the large scale correlations being observed and unambiguously unfold the importance of various essential dynamical/dissipative processes which affect the particle production observed in the final state. Without the proposed barrel TOF detector, these studies will be limited at best, and will serve mainly as a reminder that large acceptance PID up to intermediate p_T is essential to fully understand the history and evolution of the new matter being produced at RHIC.

The two-arm spectrometer

It can be argued that the required reach in momentum difference variables could

be achieved with small acceptance coverage (and cost) by use of a 'two-armed spectrometer' to scan two-particle momentum space in small segments. The two-arm spectrometer alternative does not satisfy the stringent precision requirements for correlation analysis of nucleus-nucleus collisions. In elementary collisions (*e.g.,* e+e, p+p) two-particle correlations have amplitudes of order unity; a two-arm spectrometer may thus suffice for large-scale correlation analysis. The same physics in A+A collisions leads to observed correlations diluted by the event multiplicity which are therefore typically one *permil* in relative amplitude. For STAR's large coverage the reduction of systematic errors below the permil level was achieved with powerful common-mode rejection techniques applied to the entire acceptance [71, 72, 83].

A+A event multiplicities with large-acceptance detectors provide the necessary statistical power to detect these small (permil) effects. Practical considerations of systematic error in precision measurements of large-scale correlations require that the entire acceptance be observed in each event to insure adequate common-mode rejection of systematic 'noise.'

Present and proposed particle identification capabilities

The study of large-scale fluctuations and correlations presented in the preceding sections would not be possible with identified particles using PID based on the present TPC and SVT dE/dx capabilities. Figs. 14 and 15 show simulated transverse momentum and pseudorapidity distributions for accepted and reconstructed protons and kaons respectively for existing methods and full-coverage ToF. The dramatic improvement in coverage on p_T for protons and kaons is evident. Significant improvement is even seen with pions (see Fig. 16). These simulations incorporate distribution parameters from a recent STAR analysis of 200 GeV Au-Au central-collision data, as well as total acceptance and efficiencies from detailed analyses of year-2000 130 GeV Au+Au central and minimum-bias data.

Simulations included fiducial acceptances, particle-decay loss, tracking inefficiencies, two-track merging, and particle-identification efficiencies for the present TPC dE/dx plus kink analysis[2] [84] PID (B - blue), PID with full TOF as proposed here (G - green), and perfect PID (R - red). From these figures we see that $\langle p_T \rangle$ fluctuation studies following the trends described above, especially the requirement to connect the soft part of the two-particle p_T distribution to hard processes through the medium, are not meaningful for identified protons, kaons, and even pions without substantial ToF coverage, since the observed large-scale correlation structure in Figs. 10 and 11 at moderate and higher p_T is not then accessed.

This is more clearly illustrated in Fig. 17 which shows simulated $X(m_t)$ distributions corresponding to Figs. 16 - 14. The values of T for approximately flat $X(m_t)$ distributions for pions, kaons and protons are 175, 310 and 340 MeV, respectively. In Figure 17, the p_T distributions shown previously (Figs. 16, 15, and 14) are replotted

[2]This is a TPC tracking analysis method for charged-kaon identification in which single-prong decays or 'kinks' are identified in the TPC, where kinematic correlations between the parent particle momentum and the decay angle are used to select with minimal background $K \rightarrow \mu + \nu$ and $K \rightarrow \pi + \pi^0$ decays.

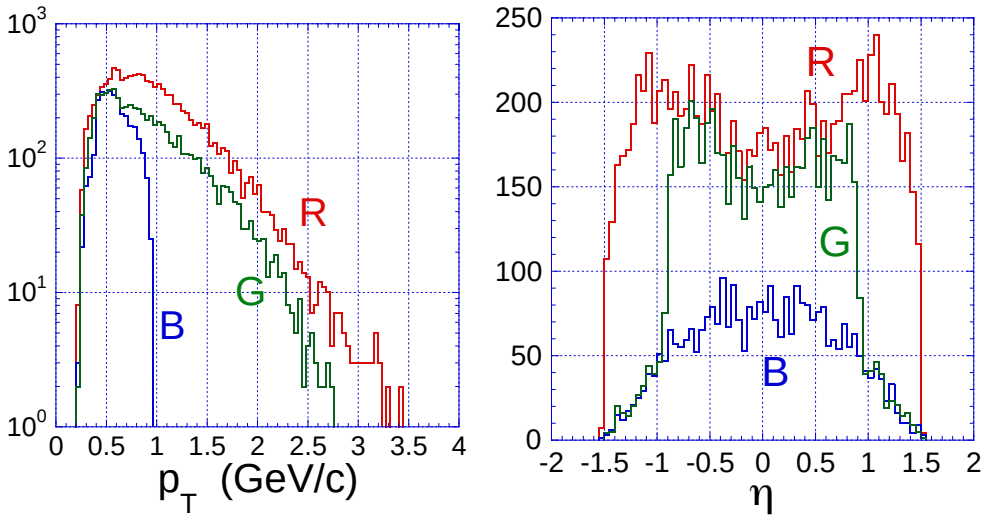

Figure 14: Simulated proton spectra versus transverse momentum (left) and pseudorapidity (right) for 200 GeV Au+Au central collisions for all accepted and reconstructed tracks (R - red), those identified using the TPC only (B - blue), and those identified using both TPC and full TOF (G - green).

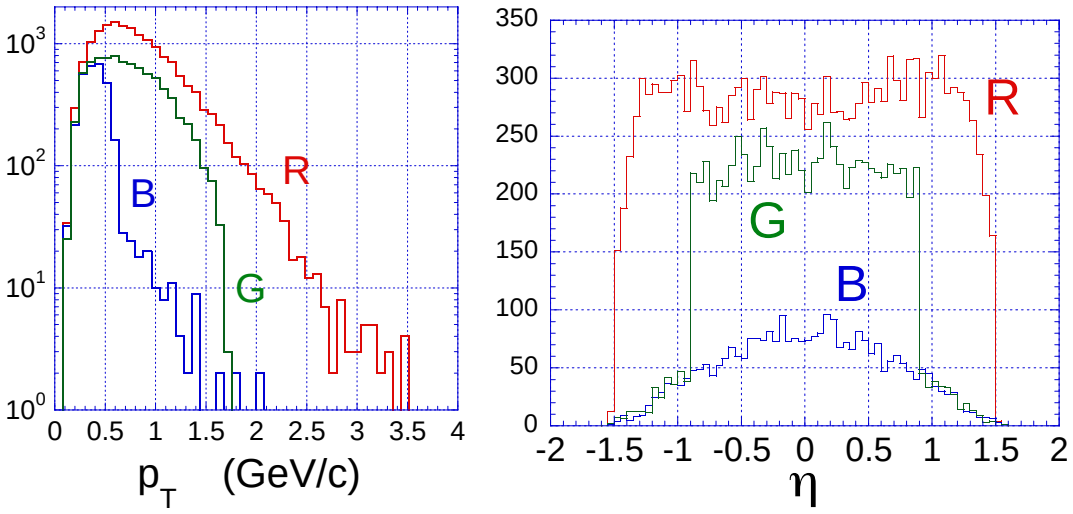

Figure 15: Simulated kaon spectra versus transverse momentum (left) and pseudorapidity (right) for 200 GeV Au+Au central collisions for all accepted and reconstructed tracks (R - red), those identified using the TPC only (B - blue), and those identified using both TPC and full TOF (G - green).

on $X(m_t)$. Shown in Figure 17 are the spectra for pions (left panel), kaons (center panel), and protons (right panel). The red (R), blue (B), and green (G) lines indicate the perfect PID (total reconstructed), TPC dE/dx and kink-analysis PID, and TPC plus full MRPC-TOF PID yields respectively. In the critical region $X(m_t) > 0.7$ which contains the interplay between partially-damped hard-QCD processes and the

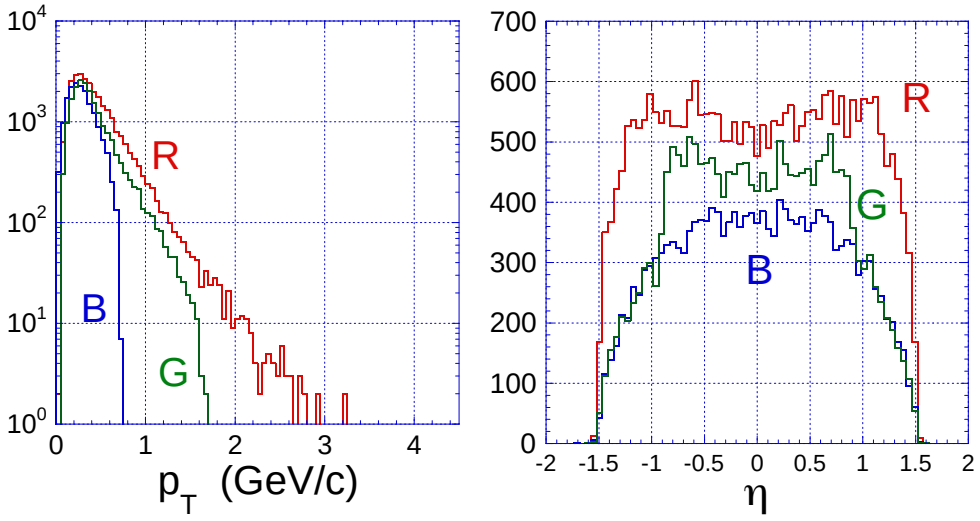

Figure 16: Simulated pion spectra versus transverse momentum (left) and pseudorapidity (right) for 200 GeV Au+Au central collisions for all accepted and reconstructed tracks (R - red), those identified using the TPC only (B - blue), and those identified using both TPC and full TOF (G - green).

structured dissipative medium the identified particle yield from TPC PID alone is virtually non-existent, while a reasonable yield (roughly 50%) of all three particle types is achievable with full MRPC-TOF. These arguments carry over to all aspects of large-scale correlation structure, including number as well as p_T correlations. The basic p_T continuity argument depends on the connection between hard processes at higher p_T and the results of dissipation in the soft p_T spectrum through the intermediary of the QCD medium, which is a primary goal of the STAR program.

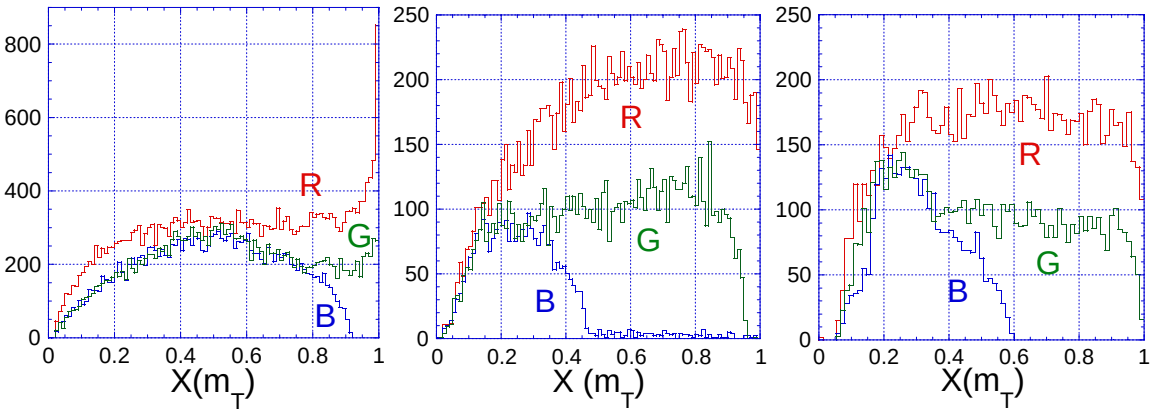

Figure 17: Simulated pion (left), kaon (center), and proton (right) spectra versus $X(m_T)$ for 200 GeV Au+Au central collisions for all accepted and reconstructed tracks (R - red), those identified using the TPC only (B - blue), and those identified using both TPC and full TOF (G - green).

Required data volumes

Unlike a number of the other physics topics discussed in the proposal, the studies discussed here in general do not require extraordinarily large samples of events. Event samples that number in the millions are adequate for most studies, although a systematic study as a function of beam energy, colliding species, *etc.* will require a number of such samples.

The important point for these physics studies is that *they are not possible at all without the addition of the proposed barrel TOF detector.*

That is because *without the extended reach in* p_T *for particle identification over the large acceptance of the proposed TOF upgrade detector, it is simply not possible* to unambiguously relate the structure of the observed correlations and fluctuations to the underlying dynamical/dissipative/QCD processes which have produced them. A crucial source of unique information will simply be lost.

Summary

An initial survey of correlations and fluctuations in first-year RHIC events at $\sqrt{s_{NN}}$ = 130 GeV has revealed particle correlations rich in structure, including isoscalar and isovector correlations of hadron number and mean p_T on the variables (η, ϕ). Some of the physical mechanisms revealed were previously known in heavy ion collisions, some are familiar from elementary collisions but newly observed in heavy ion collisions, and some features are unique to RHIC collisions, giving us the first comprehensive look at the properties of a dynamically evolving QCD medium.

An initial survey has been completed with unidentified hadrons in the STAR TPC acceptance. Some of the novel physical mechanisms which produce these structures are suggested already by studies on collision centrality. Detailed study of thermal and velocity correlation structures can be pursued effectively with STAR using the scale-dependent fluctuation/correlation analyses described here, provided the most abundant hadron masses (π, k, p) are measured. Full interpretation of revealed structure, for instance discrimination between thermal and velocity structures, relies on determination of mass dependence.

A common property of the newly-observed structures is their large characteristic scale relative to the STAR TPC acceptance, which is the largest available at RHIC for precision studies of identified particle momenta. The correlation lengths observed on pseudorapidity (2 units) and azimuthal angle (2 *rad*) in Au+Au collisions with STAR, together with the large range in transverse momentum (up to 1 - 2 GeV/c) required to span the interval from soft-QCD physics to perturbative-QCD hard scattering require the large coverage of a full-barrel MRPC-TOF detector in STAR. No other detector combination at RHIC can access this comprehensive and essential physics program.

3.4 Charm Meson Measurement

RHIC is the first heavy ion facility with a sufficiently high center-of-mass energy that the low Bjorken x behavior of the parton structure functions of the nucleon are directly relevant to the initial collisions of the colliding nuclei. At low Bjorken x the gluon distribution is dominant, and it is therefore expected that gluon dynamics will dominate the initial stage of the collision. An interesting conjecture is that at some scale of x and Q^2, the gluon distribution in the incoming nuclei is saturated, and that this may be reflected in the observed multiplicity [94].

Charm quark production in relativistic heavy ion collisions is particularly sensitive to the early gluon dominated stages of the collision. It can occur during initial parton-parton collisions, during the subsequent secondary parton cascade, and during the thermal expansion and rescattering processes which happen later [95, 96]. Most $c\bar{c}$ production is expected to occur during the early partonic stages, much of it via hard gluon fusion, $gg \rightarrow c\bar{c}$ production during the initial stage. The cross section for this process is known. During the later stage of the hot partonic system $c\bar{c}$ production is also expected to occur, but the amount of such production depends strongly upon the initial temperature, thermalization time scale, and longitudinal space-momentum correlations [95]-[97]. Because the yield of charm is sensitive to the details of the early stages, the measurement of the charm production rate is very important for determining a proper description the initial conditions and the early stages of relativistic nucleus-nucleus collisions.

The information afforded by the measurement of charm production, and specifically by D mesons, is particularly robust since the yield of mesons with open charm is affected only weakly by final state interactions within the medium; charm quarks are produced during the initial stages; subsequently they are not created or annihilated; during final state rescattering they emerge from the collision, primarily as mesons or baryons with open charm. Studies of open charm differ in this respect from studies of the J/ψ, since the observed yield for charmonium is sensitive to screening in a color deconfined medium and final state hadronic scattering (medium) effects. The measurement of open charm is indeed an important "calibration" for the study of J/ψ suppression [98] or enhancement (the latter has been conjectured to be possible due to the coalescence of open charm [99]).

Studying the energy loss of partons in QCD matter is an exciting new possibility afforded for the first time by the high energy of the RHIC machine. Recently, the measurement of the suppression of high p_T particle production [100, 95], the identification of jet fragmentation, and the possible disappearance of "away-side" jets have generated considerable interest[102]. When a parton propagates through QCD matter, it loses energy by gluon bremsstrahlung. For a heavy quark, the amount of energy loss in the medium is expected to be lower than for a light quark due to suppression of gluon radiation at small angles (the "dead cone" phenomenon)[103]. This is expected to result in charm enhancement at moderate p_T. A calculation by Ref.[103] shows a factor of 2 enhancement of D/π ratio at 5 GeV in hot QGP matter compared to the yield expected in p+p collisions. The enhancement is about a factor

of 1.2 in cold nuclear matter.

For the reasons stated above, measurement of the yield and spectra of particles with open charm (in particular, D mesons) is particularly important to fully understand the nature and evolution of the new matter being produced at RHIC. Within STAR, the beam time and analysis effort required to perform a systematic study of open charm yields and spectra are prohibitive without the additional particle identification capability provided by the proposed large acceptance MRPC barrel TOF detector.

With the proposed barrel TOF, a systematic study of open charm is possible. It will focus on:

1. placing important constraints on the gluon structure function of the colliding nuclei through comparison of measured yields and spectra of D mesons with pQCD calculations of open charm quark production via gluon-gluon fusion

2. establishing a baseline for studying possible quarkonium (J/ψ) suppression in a deconfined color medium by determining the amount of open charm being produced

3. probing charm quark dynamics in the partonic state through the measurement of transverse radial flow and possibly elliptic flow of mesons with open charm;

4. measuring possible energy loss of charm quark jets in the dense medium at intermediate p_T.

Without the proposed MRPC barrel TOF detector, the beam time and analysis effort required to achieve these goals are prohibitive. For example, with the present STAR detector (without TOF), to make a significant measurement of the yield of D mesons (integrated over pt) at the 3σ level of significance requires $\sim$12 million events. (Measuring D meson spectra out to 4-6 GeV/c requires $\sim$85 million.) Based on previous experience, the time necessary to analyze 12 million events is $\sim$10 months. With the full barrel TOF detector, the number of events (and the time needed) are reduced by a factor of $\sim$5 (2.6M events). Since measurements with several beam species will need to be studied as a function of centrality, for a full systematic study, the measurement of open charm quickly becomes problematic without the additional PID capability provided by the proposed barrel TOF detector.

In STAR, D mesons will be measured by reconstructing their invariant mass through the K-π decay channel. Two approaches will be used: the event-mixing technique, subtracting combinatorial background from the invariant mass distribution for all possible D meson (K-π) candidates, and direct reconstruction of D mesons by detecting a displaced decay vertex. To fully utilize the second technique a new STAR micro vertex detector will be needed. Currently this detector is in the R&D stage.

The proposed barrel TOF upgrade is absolutely essential to make a systematic study of the yield and spectra of open charm in STAR. Specifically, this upgrade will:

- allow the identification of a significantly greater percentage of the kaons and pions from the $D^0 \rightarrow K^-\pi^+$ and $\bar{D}^0 \rightarrow K^+\pi^-$two-body decay channel, greatly improving the signal to background ratio in the reconstructed D^0 invariant mass distribution. The centroid of the p_T distribution for kaons that survive STAR's acceptance and efficiency cuts is about 1 GeV/c. For kaons, PID based on dE/dx in the STAR TPC cuts off at ∼0.6 GeV/c. The proposed barrel TOF will extend PID for kaons to 1.7 GeV/c. As a consequence, 5× more kaons will be identified, and a better sampling of the kaon p_T distribution will be possible, greatly increasing the efficiency for D meson detection and reconstruction. The improvement will mainly be due to the reduction of combinatoric background. This reduction could be even greater in the future with the addition of a possible microVertex detector.

- significantly reduce the time and resources needed to perform a systematic study of open charm. Without the additional PID capability provided by the barrel TOF detector, the beam and analysis time required to utilize the large acceptance of STAR to systematically investigate the dependence of open charm production on beam energy, centrality, and beam species are prohibitive.

3.4.1 Simulation Results

This section presents results from simulation studies made to estimate STAR's capabilities for detecting neutral D mesons. These studies used TPC tracking and dE/dx-based particle identification (PID). Varying amounts of TOF coverage were then added. The event-mixing technique was used to extract an open charm signal by subtracting a combinatorial background. The resulting simulated invariant mass distribution was used to draw conclusions about STAR's ability to determine D meson yields and spectra. This technique will be used for real data as well, and is expected for a sufficiently large number of events to yield a peak at the D meson mass. It has been used successfully in STAR already to measure the yield of the $K^{\star 0}$. The effects of flow and nearby resonances are manageable.

The expected yield and spectra of D mesons is uncertain at RHIC. Recent PHENIX results [104], using single leptons at high p_T from the Au+Au $\sqrt{s_{NN}} = 130$ GeV data, report $dN_{c\bar{c}}/dy = 2.1$ with large statistical and systematic errors. Assuming most $c\bar{c}$ production goes into D mesons and that 1/2 are neutral ($c\bar{u}$ and $\bar{c}u$), the estimated relative yield of $(D^0 + \bar{D}^0)/h^-$ is 0.007. The slope parameter for the neutral D mesons' m_t spectrum is assumed to be approximately 300 MeV based on a general extrapolation of inverse slope versus mass [106] and extrapolations of the J/ψ slope versus energy density [107]. A Gaussian rapidity distribution with σ_y=2.0 (typical for mesons produced at RHIC) is assumed.

Given these assumptions, the two-body decay channels $D^0 \rightarrow K^-\pi^+$ and $\bar{D}^0 \rightarrow K^+\pi^-$ were simulated; their branching fractions were taken to be 3.8%. The resulting D^0 peak in the reconstructed $K^-+\pi^+$ invariant mass spectrum (pure decays only, no background) using all K^- and π^+ particles which survive acceptance cuts, decay

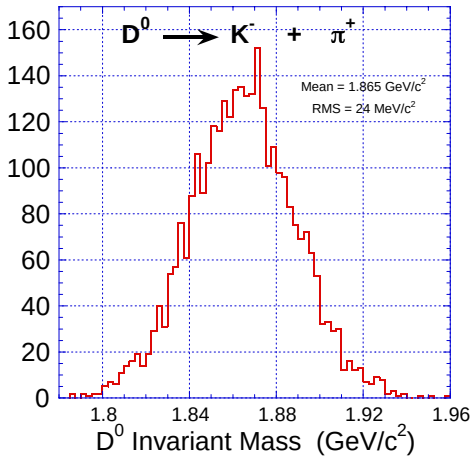

Figure 18: The resulting D^0 peak in the reconstructed $K^-\pi^+$ invariant mass spectrum (pure decays only, no background) using all K^-, π^+ particles which survive the acceptance (including decay losses) and tracking inefficiency.

losses and tracking inefficiencies is shown in Figure 18. The observed width of 24 MeV/c^2 is mainly due to momentum resolution (typically 2-3%).

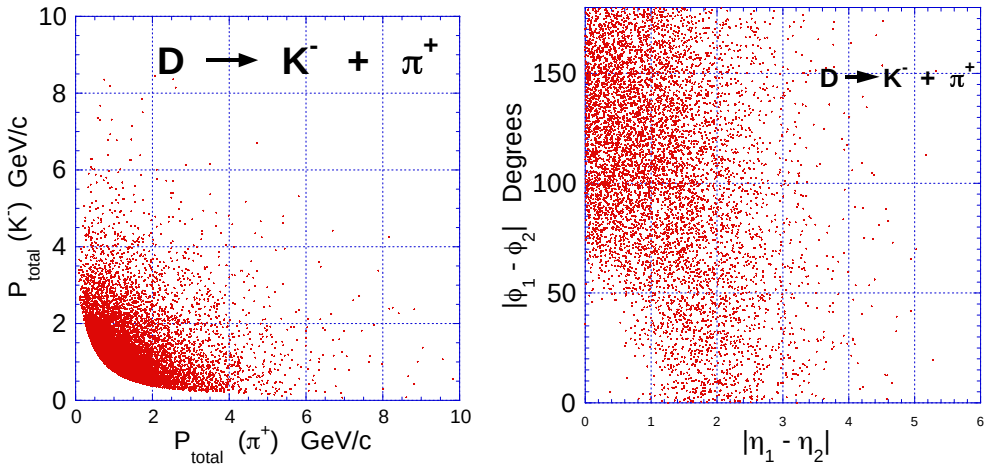

Figure 19: (left) Scatter plot of the total momenta of the daughter kaon versus the pion, and (right) the azimuthal angle – pseudorapidity correlation ($\Delta\phi - \Delta\eta$) between the kaon and pion daughters from D^0 decay.

Particle identification is most important for correctly identifying the charged kaon daughters from the D^0 and $\bar{D}^0$ two-body Kπ decay branches. This mainly serves to reduce the large combinatorial background in the invariant mass distribution. Precise measurement of the momentum of the daughter kaon is also necessary for good D meson invariant mass reconstruction. A scatter plot of the total momenta of the daughter kaon versus the pion from D^0 decay is shown on the left in Figure 19. From

this figure it is seen that if TPC dE/dx PID were required for both decay daughters there would be *no D meson signal*, as TPC PID is only effective for momenta p<600 MeV/c. However, the TPC is capable of some limited identification of the daughter kaons. The azimuthal angle - pseudorapidity correlation ($\Delta\phi-\Delta\eta$) between the kaon and pion daughters shown on the right in Figure 19 demonstrates the necessity of having a large acceptance TOF detector for efficient D meson measurement.

Table II: Statistical significance of D meson signal for a variety of particle ID options as a function of p_T. The last two columns are the number of events N_{events} required for a 3σ signal in the invariant mass distribution for $D^0+\bar{D}^0$ mesons under different assumptions. HIJING was used as the basis for simulating the effect of TOF PID to provide data on backgrounds and charm production.

Description	$S(D^0)$	mass width	TPC PID	100% TOF
All p_T	0.066	23(MeV)	12M	2.6M
$4 > p_T > 2$ GeV	0.011	25(MeV)	59M	23M
$6 > p_T > 4$ GeV	0.0012	37(MeV)	85M	42M
$p_T > 6$ GeV	0.0002	45(MeV)	115M	115M

Background simulation and subtraction were performed for various assumed configurations using the p_T, η distributions of charged pions, kaons, protons, and antiprotons from the year 2000 STAR and PHENIX Au+Au top centrality data. An overall multiplicity rescaling factor (1.14) was used for 200 GeV data as well as the K^-/K^+ and $p/\bar{p}$ ratios for 200 GeV. The monte carlo generator MEVSIM was used to generate events, without D mesons, from which the background K+π invariant mass histogram was formed. Using the expected width of the D^0 peak (assuming $\pm 2\sigma$) the rate of background pairs was obtained for a variety of PID options. Using the same analysis approach, the D signal from simulations of pure D^0s was obtained. The signal-to-background ratio was determined by scaling the simulated signal to the assumed production rate for D^0 (assumed to be 1.1 per unit rapidity) with the branching ratio, normalized to the rate of background pairs. With this information, the statistical significance of the signal was determined as a function of the number of events. The signal is obtained from S=Y-B, where Y is the total yield and B is the background under the peak. For this analysis the statistical error of the mixed event background was assumed to be much smaller than the signal sample so that the statistical error in the signal was dominant, $\sqrt{Y}\approx\sqrt{B}$. The statistical significance of the D^0 signal is then,

$$\frac{S}{\Delta S}\,|_{D^0} = \frac{\bar{S}(D^0)}{\sqrt{\bar{B}}}\sqrt{N_{events}} \tag{4}$$

where $\bar{S}(D^0)$ and $\bar{B}$ are the number of true reconstructed D^0s per event and the number of background pairs under the peak per event, respectively. The statistical

significance of the combined D^0 and $\bar{D}^0$ signal was determined by multiplying this amount by $\sqrt{2}$ assuming equal yields for D^0 and $\bar{D}^0$.

Table II shows the sensitivity of D^0 reconstruction to particle identification as function of p_T. With the addition of the full TOF detector, the measurement of the D^0/π ratio with 20% error at $p_T \simeq 5$ GeV requires $\sim$40 million events. This measurement will directly test theoretical predictions about the energy loss of heavy (charmed) quarks in the early gluon-dominated stage of the collision, providing essential information about the properties of the produced matter. This measurement is challenging but feasible. Without the barrel TOF it is not possible.

In summary, with the present configuration of STAR the observation simply of the D meson yield requires $\sim$12 million events based on the statistical calculations presented here. With the proposed barrel TOF detector the number of events required is reduced by a factor of $\sim$5. Using the barrel TOF detector the statistical significance of the D meson signal is maximized by requiring particle identification of (at least) the daughter kaon. In this scenario a robust measurement of the yield of neutral D mesons should be possible in a single (nominal) RHIC year of running. This measurement will provide an essential baseline on charm production to help "calibrate" J/ψ suppression (enhancement) studies. It will also provide a first measurement of the spectra (p_T dependence) for D meson production, providing important initial results concerning the D/π ratio as a function of p_T to study heavy quark energy loss and suppression of gluon bremsstrahlung due to the "dead cone" effect in hot partonic matter. These studies are not possible with the projected amount of running time and analysis capability available without the additional particle identification provided by the proposed barrel TOF detector.

3.5 Physics of Resonances at RHIC

In a thermal statistical description of nucleus-nucleus collisions the dynamical evolution is thought to be marked by two epochs: chemical freeze-out when particle production stops and kinetic freeze-out when particle interactions cease and stable particles free-stream to the experimental detectors. Between these times, particles continue to interact through elastic collisions without changing particle flavor. In this picture, the chemical freeze-out stage separates the partonic (early) stage from later hadronic evolution.

In order to understand the evolution of the produced matter after hadronization, it is necessary to understand the properties of the system between chemical and kinetic freeze-out. This can be accomplished using resonance production to probe dynamics between these stages. After their initial formation, the number and kinematic distribution of resonances continues to evolve through decay, rescattering, and re-generation. By systematically measuring a number of different resonances with a range of lifetimes (from a few to several tens of fm/c) it is possible to map out the dynamical evolution of nucleus-nucleus collisions between chemical and kinetic freeze-out.

Within STAR the resonances studied thus far include the ρ, Δ, f_0, K^*, $\Sigma(1385)$, $\Lambda(1520)$, and the ϕ. The physics goals of these resonance measurements are:

1. to provide stringent constraints on theoretical models of particle production at RHIC. Resonances contribute significantly to the production of stable particles in the final state and the contribution from various resonances must be accounted for in detail by models of particle production.

2. to study the effect of the dense medium on resonance properties. In particular, properties such as the mass and width of short-lived resonances such as the ρ meson (which contributes to the dilepton mass spectrum) have been predicted to be sensitive to the properties of the medium in which they are formed.

3. to provide an important probe of the time evolution of the system from chemical to kinetic freeze-out. Since the lifetime of short lived resonances is comparable to that between chemical and kinetic freeze-out, their survival probability depends strongly on the time duration of the evolution and the density of the local medium.

4. to provide a measurement of flavor dependence of particle production at intermediate p_T ($\gtrsim$2-3 GeV/c) for studying the transition between the soft physics and hard scattering regimes.

The study of resonances provides essential information unavailable otherwise about the evolution of the later stages of the collision from hadronization to the final state. Without the proposed barrel TOF detector, this study is seriously compromised due to the amount of combinatoric background and the limited range of p_T over which resonances can be studied. The proposed barrel TOF detector will:

- provide PID for the decay products of resonances. Since the K/π ratio is $\sim$15% and the p/π ratio is $\sim$10%, the combinatoric background in the present STAR setup for decays containing a kaon or a proton is very large. The additional PID capability from the barrel TOF will significantly reduce this background.

- reduce significantly the background from correlated pairs (decays of real particles) from the same event that lie underneath the resonance mass distribution of interest so that reliable information on the invariant mass, width, and branching ratio can be extracted for a given resonance. This is particularly important for resonances with very short life-times, such as the ρ, Δ, and $\Lambda(1520)$, which have irregular underlying background shapes. (K^* decays, for example, form a significant background under the ρ mass peak.)

- allow the measurement of rare and wide resonances such as $\Lambda(1520)\rightarrow$p+K, which cannot be measured well in central Au+Au collisions with the current STAR configuration due to background.

- extend the measurement for many resonances to the intermediate p_T region, which is essential to disentangle collective expansion dynamics from hard-scattering contributions. Collective expansion results in a p_T dependent modification of the primordial production of resonances which depends on the resonance lifetime.

- allow STAR to fully detail final state hadron (in particular resonance) production at RHIC as a function of beam energy, collision centrality and colliding species. This can only be achieved with the proposed barrel TOF detector with an acceptance matching that of the existing SVT, TPC and barrel EMC.

Resonance Production in Heavy Ion Collisions:

In order to understand collision dynamics in nucleus-nucleus interactions it is imperative to make precise measurements of resonance production because it is a key process dominating the yield of most stable particles in the final state. In order to fully characterize properties of a possible new form of matter at RHIC, the features of resonance matter must be understood. Because of its large acceptance STAR is uniquely positioned at RHIC to make a comprehensive study of the full spectrum of produced resonances, provided it has the additional particle identification capability provided by the barrel TOF detector. Without the proposed barrel TOF system large combinatoric backgrounds and the limited range of p_T accessible for identified particles with the existing STAR setup are a limiting factor.

The proposed barrel TOF detector upgrade will significantly extend STAR's ability to make a comprehensive study of resonances. Specifically, precision measurements of the ρ, Δ, and $\Lambda(1520)$ resonances over a wide p_T range will be made to extract their yield and p_T spectra in central heavy ion collisions. The measurement of the p_T spectra in particular is problematic with the present SVT+TPC only. In addition,

the barrel TOF upgrade will significantly improve the measurement of the ϕ and the K* compared to what is possible using the STAR TPC alone. With the improved signal to background afforded by the barrel TOF, important measures such as elliptic flow will be determined with precision over a broad range of p_T.

The precise measurement of resonance production possible with the barrel TOF detector will also provide essential information needed to constrain models of particle production. The soft processes of QCD (e.g., hadronization) are not calculable using a perturbative approach. Progress in understanding such processes relies instead on testing the predictions of phenomenological models of particle production. In e^++e^- collisions, string fragmentation has been successfully used in Monte Carlo Models in an empirical approach to describe the data [116]. In nucleus-nucleus collisions, thermal statistical models of particle production have been used with success to fit experimental data and extract thermal parameters such as temperature and chemical potential at the AGS, SPS, and RHIC [118]. Important questions remain as to whether thermal models truly provide a fundamental description of the collision. An important factor in understanding the extent to which these models fully describe heavy ion collisions will be to understand in detail the yield of stable particles coming from the feed-down of resonance decays. This will provide stringent constraints on thermal statistical models, as well as transport models such as UrQMD and AMPT [119]. The comprehensive study needed to acquire information for a large number of resonances over a range of p_T can only be accomplished with the additional particle identification capability provided by the proposed barrel TOF detector.

Medium Effects in Hot and Dense Matter:

In heavy ion collisions, one of the most interesting predictions about the hot, dense medium produced at RHIC is that it may result in a modification of hadron mass, width, and branching ratios (see [110, 114] and references therein). To study this effect in detail, precise measurements are necessary. Recent RHIC results [115] indicate that resonances with large width can have a different mass from the nominal one due to the phase space population of the particles which create the resonance (e.g. π^++π^-→ρ). Rescattering can also modify the resonance mass and width.

Fig. 20 shows the invariant mass distribution of π^++π^- from Au+Au and p+p collisions. These measurements represent the first direct observation of ρ decays into the $\pi\pi$ channel in relativistic heavy ion collisions. Despite this important achievement, the most important information potentially available from this measurement is significantly compromised, since the ρ mass distribution, particularly for p_T>1 GeV/c, contains a sizeable contamination from misidentified particles. The contamination is mainly due to misidentifying the K*→K+π daughters as a $\pi^+\pi^-$ pair. This is a prime example of how contamination poses a fundamental limitation in extracting crucial information about possible in-medium modification of the resonance mass and width (in this case the ρ as a function of p_T). With the proposed barrel TOF, the ρ would be cleanly identified up to a p_T of ∼3 GeV/c. This is an example of why the barrel TOF detector is essential. With the additional PID capability afforded by this detector, STAR will be able to extract essential information on the characteristics of

the medium in which resonances are produced and the effect of the medium on their hadronic decay channels.

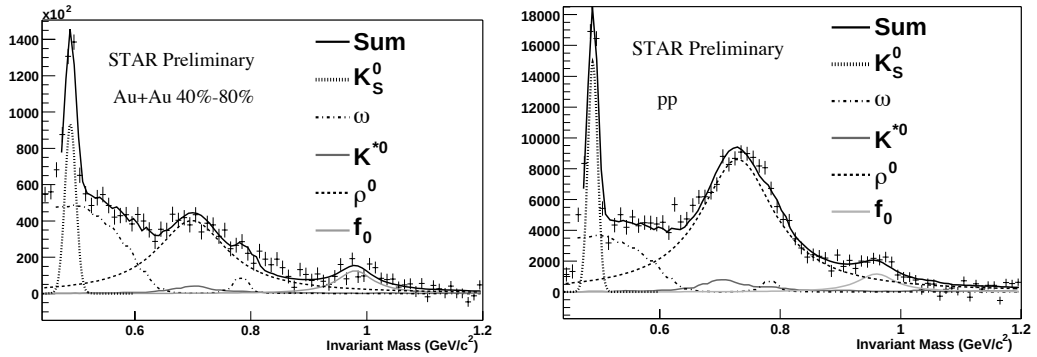

Figure 20: The $\pi^+\pi^-$ invariant mass distribution after background subtraction from 40%-80% Au+Au (left) and p+p (right) collisions.

Simulation Results

STAR's enhanced capabilities for resonance studies with the TOF are illustrated here using the $K^{\star 0}$, ϕ, and $\Lambda(1520)$ resonances. Both the $K^{\star 0}$ and ϕ were observed in STAR's first run [105, 121], with spectra measured out to about $p_T \sim 2$ GeV/c. The yields for these resonances were obtained from invariant mass distributions after subtracting a mixed event background. In principle, particle identification is not required to simply observe these short lived resonances. However, precise measurement requires the PID capability of the proposed barrel TOF detector to reduce the combinatorial background, and increase the ratio of signal-to-$\sqrt{\text{background}}$ per event. A further improvement afforded by the barrel TOF would be to remove other residual backgrounds and peaks which remain after mixed event background subtraction due to nearby resonances, misidentified decay daughters, and particle correlations from other dynamical sources. These residual backgrounds are clearly seen in the $K^{\star 0}$ analysis [105] and other preliminary resonance analyses of STAR data. A significant reduction in the combinatorial background will reduce this background as well, further enhancing the signal to background ratio.

Simulations were performed for the $K^{\star 0}$ and ϕ resonances using a mixed-event background for Au+Au $\sqrt{s_{NN}}$=200 GeV collisions similar to the one described in the preceding section for D mesons. The statistical significance per event, $\bar{S}/\sqrt{\bar{B}}$, was determined with and without the proposed TOF upgrade. The quantity $(\bar{S}/\sqrt{\bar{B}})^2$ indicates the reduction in the number of events required for the same level of significance on the signal. This is taken to be a figure of merit for the improvement possible with the proposed barrel TOF. The results are shown in Table III.

Fig. 21 (left panel) shows the contamination in the $K^{\star} \rightarrow K + \pi$ invariant mass spectrum due to the misidentification of pions as kaons. The uncertainty in the determination of the $K^{\star}$ signal is about 20%. It is strongly dependent on the detailed shape of the background. The barrel TOF detector will remove this contamination

Table III: For the K^{*0}, ϕ, and $\Lambda(1520)$, the ratio as a function of p_T of the figure of merit $(\bar{S}/\sqrt{\bar{B}})^2$ obtained with full TOF + TPC to that for the TPC only. The inverse of these numbers equals the reduction factor in the required number of events while still achieving the same statistical significance of the signal.

Resonance	Parent p_T (GeV/c)	TPC+TOF
K^{*0}	0 - 1	2.0
K^{*0}	1 - 2	1.85
K^{*0}	2 - 3	1.74
K^{*0}	3 - 5	1.39
$\phi(1020)$	0 - 2	5.0
$\phi(1020)$	2 - 5	3.42
$\Lambda(1520)$	0 - 1.6	11.4

and significantly reduce this uncertainty. A full GEANT simulation with the present STAR detector and the inclusion of the barrel TOF detector was performed to study the background, detector response, occupancy and efficiency of the TOF. Fig. 21 (right panel) shows the dramatic improvement possible in reducing the residual background with the addition of the barrel TOF detector. In this case the background is essentially gone.

The proposed barrel TOF detector will significantly reduce the combinatorial background for the entire spectrum of resonances of interest in STAR. A further example of particular interest is the $\Lambda(1520)$. The proposed barrel TOF will cleanly identify both its decay products (proton and kaon), removing the large combinatorial background from pions. This background reduction is particularly important for the higher p_T region where both the proton and kaon are beyond the PID capability of the existing TPC+SVT.

The simulation performed here was for decay daughters with p_T up to 1.6 GeV/c. HIJING was used to simulate the background. The yield of $\Lambda(1520)$ per central Au+Au collision was estimated to be 0.6 using Au+Au data from RHIC. With the proposed barrel TOF detector, the level of significance of the $\Lambda(1520)$, *i.e.* the signal divided by the square root of the background, increases relative to that for the TPC alone (2.1) to 7.1. This corresponds to a factor of $\sim$3.4 resulting in a reduction in the number of events required to achieve the same level of significance by a factor of $\sim$11.4.

Figure 22 shows the expected $\Lambda(1520)$ signal from approximately 1.7M central Au+Au events. With the proposed barrel TOF detector, precision measurement of the $\Lambda(1520)$ p_T spectrum is possible from several million events. Without it, measurement of the p_T spectrum would require approximately an order of magnitude more.

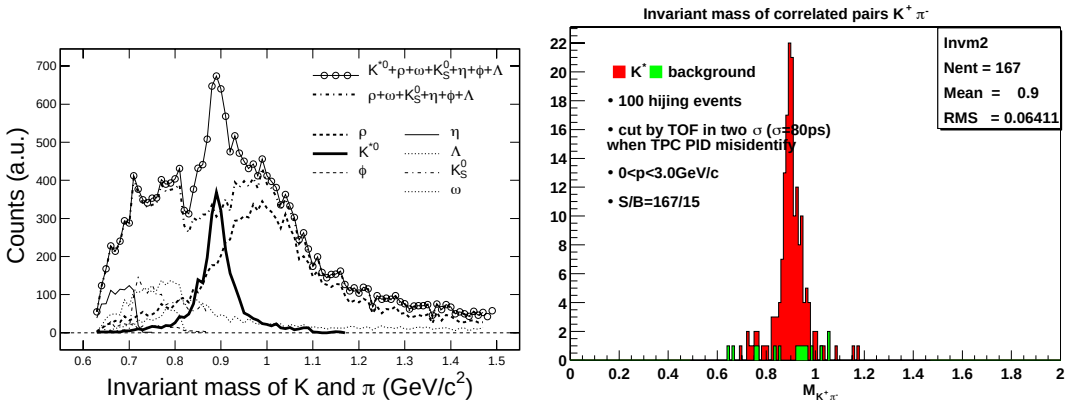

Figure 21: Left: Correlated K+π pairs from K^{*0} decay (open symbols). For K^0_S (thin dot-dashed line), ρ (thick dashed line), ω (thin dotted line), and η (thin solid line), assuming of their decay pions is misidentified as a kaon. For the ϕ (thin dashed line), one of its decay kaons is presumed to be misidentified as a pion. For the Λ (thin short-dashed line), the decay proton is misidentified as a kaon. These are realistic assumptions given the limitations of particle identification in the STAR TPC. The total background for K^{*0} is shown as thick dot-dashed line. The K^{*0} signal is shown as thick solid-line. Simple PID from specific ionization (dE/dx) in the TPC was used for this simulation. The events are HIJING Au+Au collision at 130 GeV. Right: Correlated K+π pairs from $K^{\star 0}$ after applying the PID cuts from the proposed barrel TOF detector.

In summary, a comprehensive systematic study of resonance production is crucial to fully understand particle production at RHIC, and details of the later stages of Au+Au collisions. Due to its large uniform acceptance, STAR is uniquely positioned to carry out this study, provided it has the additional PID capability afforded by the the proposed barrel TOF detector.

Without the proposed upgrade, the measurements discussed here will require many tens of millions of events throughout the lifetime of the experiment. With the proposed barrel TOF detector the required amount of data for precision studies of the K^*, ϕ, and $\Lambda(1520)$ is reduced by factors of 2, 5 and 11.4, respectively.

The savings in the required data volume makes the difference in determining whether a comprehensive study of resonance production and a full understanding of particle production at RHIC are possible or not. Without the additional PID capability from the proposed TOF barrel, correlations from particle misidentification result in considerably larger systematic uncertainty in resonance measurements. This will prevent detailed conclusions to constrain models of particle production and to study in-medium modification of hadron properties. The proposed barrel TOF is essential to increase the statistical significance of the signal available for resonance studies and decrease systematic uncertainties. Precision measurement of resonances is an important step to disentangle conventional hadronic dynamics from properties of the new matter created in nucleus-nucleus collisions at RHIC.

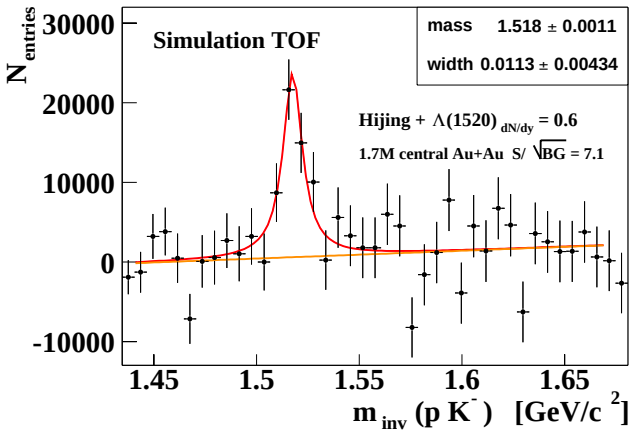

Figure 22: Expected Λ(1520) signal from 1.7M central Au+Au collisions with the proposed TOF detector. Without the barrel TOF detector the significance of the Λ(1520) is only 2.1 for p_T up to 1.6 GeV/c. The proposed barrel TOF upgrade increases the significance of the signal by a factor of ∼3.4, resulting in a reduction of 11.4 in the number of events required to achieve the same level of significance. With the proposed barrel TOF detector, precision measurement of the Λ(1520) p_T spectrum is possible from several million events. Without it, measurement of the p_T spectrum would require approximately an order of magnitude more.

3.6 Searches for Exotic Dibaryons

Nucleus-nucleus collisions provide a unique environment for possible production of multiply strange dibaryons, which could be formed through coalescence of hyperons in the final state or hadronization of the quark-gluon plasma. Initial STAR measurements of anti-deuterons at RHIC indicate that the coalescence probability is not significantly reduced at RHIC compared with that at lower energies [136]. There are several advantages for formation of strange dibaryons by coalescence at RHIC energies. First, the absolute yield of hyperons at RHIC is significantly higher than that in nucleus-nucleus collisions at lower energies, which compensates for a possible reduction in the coalescence probability. Second, at RHIC energy the production of anti-baryons is comparable with that of baryons. This allows a systematic study of particles and anti-particles, which have different backgrounds. Third, searches for certain exotic particles such as a [Ω-Ω], are feasible at RHIC energy since there are enough Ω's produced per collision that coalescence formation for the [Ω-Ω] dibaryon is possible.

Three dibaryon candidates are of particular interest: the H or [Λ-Λ], the [Ξ-p] (J), and the [Ω-Ω]. The H particle was the original dibaryon (uuddss) state proposed by Jaffe over two decades ago [138] (sometimes denoted[Λ-Λ] if very weakly bound). The decay channel suitable for the STAR detector system is H→Λ+p+π^-, where the Λ further decays to p+π^-. The [Ξ^0-p] dibaryon [139] is above the ΛΛ threshold. It cannot decay to two Λ hyperons because of charge conservation. The [Ξ^0-p] can decay

weakly into a Λ+p in the final state, which could be detected in the STAR TPC.

The proposed TOF detector will add two important capabilities which are critical for a sensitive search for exotic dibaryons: 1) the time-of-flight measurement provides crucial particle identification (PID) needed for the decay daughters to reduce the background level. This is particularly significant when the decay daughters are protons or kaons; 2) with the reduction in background afforded by TOF PID, geometrical cuts in decay topology such as the cut on the distance of closest approach of the decay daughters and the decay vertex of the parent can be modified to increase the detection efficiency while keeping similar signal to background ratios. This increase in the detection efficiency is critical for searches of exotic particles, in particular for the [Ω-Ω] dibaryon.

Recent theoretical calculations based on a chiral SU(3) quark model and analyses of the symmetry properties of two-baryon systems indicate that the $[\Omega\text{-}\Omega]_{0^+}$ is the most interesting possibility for a dibaryon state [140, 141, 142]. It is predicted to be deeply bound, with a binding energy close to 100 MeV; it is also a very compact object with the mean-squared distance between the two Ω's being approximately 0.63 fm, much smaller than the size of the deuteron. It is possible that a tightly bound di-Omega state may even be a six strange quark state, rather than a dibaryon configuration. The [Ω-Ω] is a charge two state. The Coulomb interaction was included in the estimate of the mass. Both two-body and three-body decay channels are available: the three body decay modes are,

$$[\Omega - \Omega]_{0^+} \rightarrow \Omega^- + \Xi^- + \pi^0,$$

$$[\Omega - \Omega]_{0^+} \rightarrow \Omega^- + \Xi^0 + \pi^-,$$

$$[\Omega - \Omega]_{0^+} \rightarrow \Omega^- + \Lambda + K^-,$$

The two body decay mode is,

$$[\Omega - \Omega]_{0^+} \rightarrow \Omega^- + \Xi^-.$$

These are all weak decay modes with an expected mean lifetime time on the order of 10^{-10} sec. Although these predictions are from a chiral SU(3) quark model, it is noted that the symmetry property of $[\Omega\text{-}\Omega]_{0^+}$, and in particular the quark exchange effect between the two Ωs, plays an important role in forming the $[\Omega\text{-}\Omega]_{0^+}$ as a deeply bound state. The qualitative physical picture for the [Ω-Ω] does not depend sensitively on details of the theoretical model.

There is no solid theoretical framework which can be used to reliably estimate the production rate of a possible [Ω-Ω] dibaryon in nucleus-nucleus collisions at RHIC. A comprehensive experimental program to search for these dibaryons is the only approach to deepen our understanding of the possibility for its production. Phenomenological estimates based on coalescence and/or statistical production predict an [Ω-Ω] yield ranging from 10^{-4} to 10^{-7} per central Au+Au collision [143, 144]. For example, in a thermal statistical hadronization model, the particle yield is proportional to $m^{3/2}e^{-m/T}$. Assuming a T∼170 MeV at chemical freeze-out, the ratio of

[Ω-Ω] to Ω yield is found to be approximately 1.5×10^{-4}, corresponding to a rapidity density of [Ω-Ω] in central Au+Au collisions at 200 GeV of $\sim5\times10^{-5}$. In order to reach a meaningful sensitivity for the [Ω-Ω] search, it is essential to use a large acceptance detector with high detection efficiency for hyperon decays.

The proposed barrel TOF detector, which matches the TPC acceptance in the mid-rapidity region, will significantly enhance the hyperon detection efficiency. Figure 6 shows the detection efficiency of Ω with and without the PID capability afforded by the proposed barrel TOF. The increase in the Ω detection efficiency due to the TOF PID over that of TPC+SVT is p_T dependent. For Ω $p_T\sim2$ GeV/c, where most of the reconstructed Ω's yield is, the enhancement in the detection efficiency is between a factor of 5 and 10.

It is estimated that a sensitive [Ω-Ω] search program can be carried out using the barrel TOF system with a data sample of ∼100 million central Au+Au collisions. The measurement will challenge the limits of STAR's present capability but it is feasible. Without the proposed barrel TOF system, it is not possible.

In conclusion, it is emphasized that experimental searches for dibaryons at RHIC will potentially provide a major scientific advance in the understanding of multi-hyperon systems based on a QCD inspired physical picture. In spite of the many theoretical and experimental uncertainties which must always be confronted when entering a new regime, the experimental search for dibaryons is a worthwhile scientific endeavor at RHIC. The STAR TOF upgrade will greatly aid in the search for a possible di-Omega state.

3.7 Additional Important Physics Benefits

In addition to the science measurements described in the preceding sections, there are additional studies in STAR where the PID capability provided by the proposed TOF upgrade results in a quantitative improvement. Two such studies are momentum/space-time correlations of identical and non-identical particles, and production of anti-nuclei.

3.7.1 Identical and Non-identical Two-Particle Correlations

The measurement of momentum/space-time correlations for identical and non-identical particles in nucleus-nucleus collisions can provide important information on particle production regarding the source geometry, temporal emission pattern, and geometrical correlations with the reaction plane. Initial measurements in STAR of Hanbury-Brown Twist (HBT) correlations of pions indicate that $R_{out} \sim R_{side}$, where R_{out} and R_{side} are the radii of the pion emission source projected to the outward and sideward directions respectively. This observation is in clear contradiction to predictions from hydrodynamic descriptions of nucleus-nucleus collisions, particularly in the instance of a long-lived mixed phase [125].

This result was a surprise, given the success of hydrodynamic models in predicting the magnitude and p_T dependence of elliptic flow for light mesons and baryons having $p_T \leq$1-2 GeV/c. It continues to be an important unsolved problem in attempting to understand the hadronic evolution of nucleus-nucleus collisions. Further analysis with identical and non-identical particles is needed to understand this result as well as the hadronic evolution of the collision in general. The proposed barrel TOF will contribute significantly to these studies by extending the p_T range in which particles can be cleanly identified.

Specifically, the proposed barrel TOF upgrade will:

- allow for systematic investigation of non-identical particle correlations to disentangle particle flavor dependence of temporal emission and flow patterns;
- extend the p_T coverage of the HBT measurement

The ability to study identical and non-identical particle correlations, and, in particular, to extend the p_T range over which these studies can be made to $\sim$2-3 GeV/c is very important to place significant constraints on models proposed to describe the evolution of the hadronic matter in the collision. A prime example is the Blast-Wave parameterization Ref [127]. It is capable of predictions consistent with the observed ratio of R_{out}/R_{side}, but only if the duration for particle emission is exceedingly fast ($\sim$1.5 fm/c). If this picture is correct, it is interesting and important, and quite different from the behavior expected for a long-lived mixed phase.

The Blast Wave model makes specific predictions for non-identical particle HBT as a function of p_T, but these predictions are only definitive in a range of p_T for pions, kaons, and protons that is above that where these particles can be identified by dE/dx in the present TPC + SVT. Above some transverse momentum in the few GeV

range, the dominant source of particle production must switch from soft (expanding fireball) to hard (prompt production from the collision of incoming partons) processes. The space-time emission pattern of soft and hard processes is completely different. Particles arising from hard processes are emitted after ∼1 fm/c, while particles from soft processes which participate in the transverse expansion are emitted after ∼10 fm/c. Since π-p, and π-K correlation functions are sensitive to the relative emission times of pions, kaons, and protons, they can be used to study the transition from soft to hard processes, provided particle identification is possible in a high enough range of transverse momentum. It is in this intermediate p_T range – the transition region between soft physics and hard scattering–that models are significantly constrained by their predictions. Without the barrel TOF upgrade, HBT studies of identical and non-identical particle correlations will be compromised and will be limited in their ability to place significant constraints on models of particle production. Important information will be lost.

3.7.2 Nucleus & Antinucleus production

The addition of a full TOF system affords STAR the possibility of extending its measurement of nuclei and anti-nuclei significantly.

First, the proposed barrel TOF detector will give STAR the ability to measure deuterons in a range of transverse momentum where beam pipe related backgrounds are no longer dominant (this is presently a limiting factor for this measurement). This will allow first measurements of the $\bar{d}/d$ ratio at RHIC in addition to accurate measurements of the inverse slope parameters for ant-deuterons and deuterons. This is not possible using TPC dE/dx identification alone. The same comment is true for tritons and anti-tritons. In this case, the additional particle identification capability provided by the proposed barrel TOF upgrade will result in the first measurement of the $\bar{t}/^3\overline{He}$ ratio at RHIC. The barrel TOF detector will also significantly enhance STAR's chances to make a discovery observation of $^4\overline{He}$ due to the improved particle identification capability and candidate separation possible at high p_T.

With the additional capability afforded by the barrel TOF, thorough searches for nucleus and anti-nucleus production will be made. This will result in significant constraints on the models of the sources for nucleon and anti-nucleon production and upon the factors influencing nucleon (anti-nucleon) coalescence such as nucleon and anti-nucleon number density and radial flow profiles in heavy ion collisions.

4 Detector Design

To meet the physics objectives outlined in the previous section, the TOF system must measure time intervals with a specific precision using information on the track momenta and positions determined by a separate system (the TPC). In section 4.1, the Time Of Flight approach in this environment is first described which will relate the necessary precision for the time interval measurements to particle identification requirements. The requirements on the design of the TOF system driven by the physics objectives are then outlined in section 4.2. This is followed by detailed descriptions of the resulting design of the MRPC detectors (section 4.3), the mechanical components (section 4.4), the gas system (section 4.5), and the electronics (section 4.6).

4.1 The STAR Approach to Time Of Flight

The TOF system measures time intervals with two detectors – an event "start" detector near the beam pipe (see section 4.9) and a charged particle "stop detector" (the barrel of MRPCs), each of which has a specific resolution on particle arrival times. Following offline corrections, the difference of these times is the sole quantity of interest provided by this system. These time intervals, Δt, are associated with reconstructed tracks in the STAR TPC by track extrapolation to the TOF detectors. The TPC thus provides the momentum, p, and total path length, s, and so allows the calculation of the inverse velocity, $1/\beta$, for each TPC track via,

$$1/\beta = \mathrm{c}\Delta\mathrm{t}/\mathrm{s}, \tag{5}$$

where c is the 29.98 cm/ns speed of light. It is this inverse velocity versus the particle momentum that provides the basis for the particle identification (PID) capabilities of the system. That is, the track momentum and the associated inverse velocity give the particle mass, M, via,

$$\mathrm{M} = \mathrm{p}\sqrt{(1/\beta)^2 - 1}. \tag{6}$$

The TPC is a large cylinder with an outer(inner) diameter of 4(1) m which extends $\pm$2.1 m on either side of the beam intersection region, or approximately two units of pseudorapidity from -1 to 1. Its track momentum resolution, Δp/p, is 1-2% in the momentum range of interest for this TOF system, and its resolution on track total path lengths is less than 0.5cm. This makes the TPC an extremely powerful particle tracker for use in combination with the TOF system.

A TOF system in STAR at the cylindrical radius of the TPC with a total time interval resolution of 100 ps thus has the PID capabilities indicated in Figure 23. Shown in this figure is the particle mass via TOF for each of four charged hadrons of interest - pions, Kaons, protons, and deuterons, as labelled, versus the particle momentum for the STAR geometry and for the momentum and path length resolutions of the STAR TPC. Plotted for each particle are a pair of lines indicating the dependence of M+ΔM (upper line in pair) and M$-\Delta$M (lower line in pair) versus the momentum. The solid pairs of lines correspond to tracks in STAR near pseudorapidity $\eta\sim$0 (the center of the

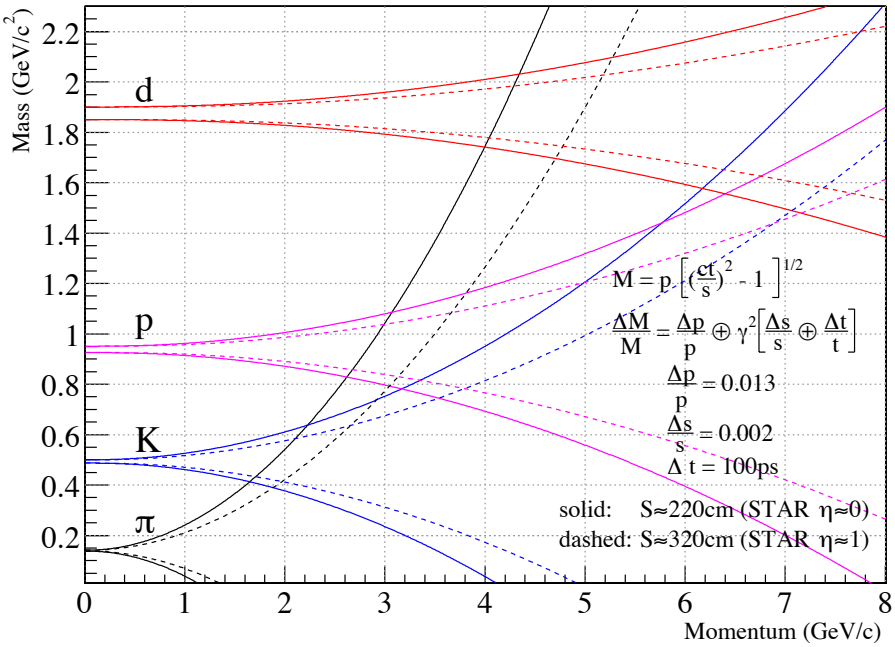

Figure 23: The momentum dependence of the particle mass resolution for a 100ps total resolution TOF system in the STAR environment. In regions where the lines are non-overlapping, the corresponding particle can be identified by the proposed system.

TPC), while the dashed pairs of lines correspond to tracks near pseudorapidity $\eta\sim1$, which have a ∼50% longer path length. The lowest momenta at which an upper line for a particular particle touches the lower line for another particle is the maximum momentum for which "2σ" PID is possible via a STAR TOF system with a 100 ps total time interval resolution after corrections. From the figure, such a system would provide direct π/K/p identification up to momenta of ∼1.7(1.9) GeV/c, and direct p *vs.* (π+K) identification up to ∼2.6(3.1) GeV/c, for tracks near $\eta\sim0(1)$. Deuterons can be directly identified out to ∼4(4.7) GeV/c. It is also interesting to note from this figure that, with increasing momentum, pions, not Kaons, are the first particles to lead to a significant background in the proton identification, and similarly pions, not protons, are also the first background to deuteron identification.

4.2 Requirements

The primary requirement for the system to meet the physics objectives is on the total time interval resolution of the TOF system. Other constraints must also be considered.

- The total resolution after all corrections must be 100 ps. For a start resolution of ∼50 ps (attained by the existing start detector for TOFp called the pVPD), and a 30 ps contribution from the timing corrections, this dictates a pure stop

resolution of less than ∼80 ps. The detectors developed for this project have demonstrated pure stop resolutions in the range from 50-70 ps, satisfying this requirement. For high-multiplicity heavy ion collisions, the start time can be determined to negligible error event by event using the stop timing, so the total time resolution will be less than 80 ps in these events.

- The detector segmentation must be such that the occupancy per channel is below 10-15%, in order to retain this timing performance even for the highest multiplicity events.
- The system must fit into the integration envelope for the present CTB system, which it would replace.
- The system must be able to operate inside the 0.5T STAR magnetic field, and not be negatively impacted by a possible future upgrade of the STAR magnet to reach higher fields.
- The system must be able to operate at particle fluxes up to ∼200 Hz/cm^2. The particle flux in Au+Au collisions at the 1500 Hz maximum interaction rate seen in the FY2001 run was 2.2 Hz/cm^2. The RHIC-II era will see the maximum rate increase by a factor of 16. The interaction rate in p+p collisions at 2×10^{32} cm^{-2}s^{-1} will be 8 MHz, with a resulting flux of 175 Hz/cm^2.
- The system must be inexpensive.
- The system must be safe.
- The system must not impair the performance of other STAR detectors. This concerns the effects of the total interaction and radiation lengths of the detectors on the EMC performance, as well as the effects on the TPC and FTPC performance if the MRPC gas containment is incomplete.

To address these design requirements, it is proposed to use a new technology developed at CERN and approved for use in the ALICE experiment [5]. This design has a high timing resolution, a high granularity, is impervious to magnetic fields, is inexpensive, reliable, and relatively easy to construct. A number of authors of the present proposal participated directly in the development of this technology at CERN. In November 1999, members of the STAR collaboration who participated in the development efforts at CERN submitted a Letter of Intent to STAR management and DOE for an MRPC-based TOF system for STAR [6]. Since that time we have pursued an extensive testing program on TOF modules constructed as prototypes for a STAR TOF system [7], leading finally to the present proposal.

4.3 Design

The multi-gap resistive plate chamber (MRPC) technology was first developed by the CERN ALICE group [145]. It has proved to be inexpensive and capable of the necessary timing resolution.

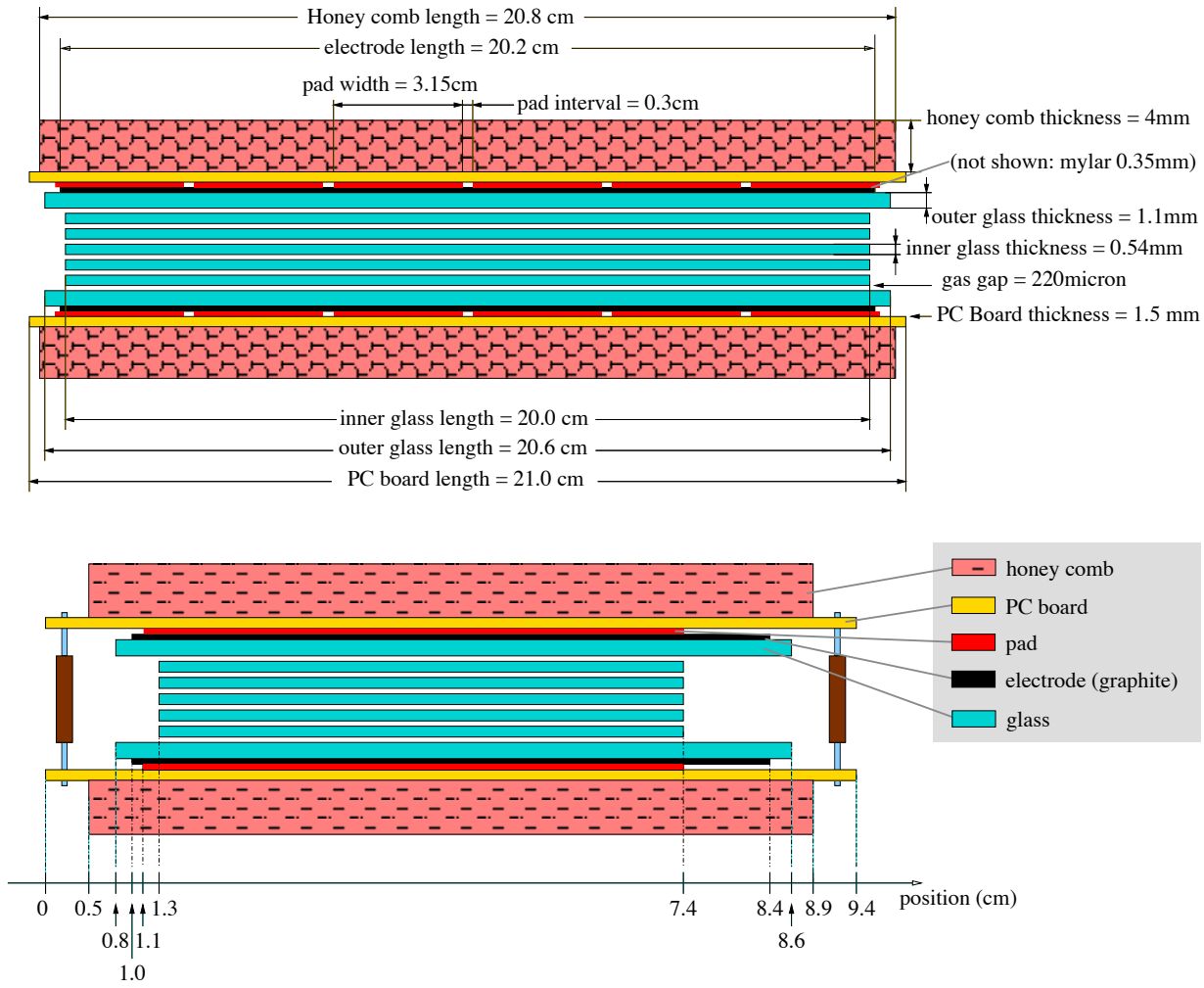

Figure 24: Two side views of the structure of an MRPC module. The upper(lower) view shows the long(short) edge. The two views are not shown at the same scale.

57

Figure 24 shows two side views of an MRPC module appropriate for STAR. The upper(lower) view in this figure shows the long(short) edge of a module. The two views are not shown at the same scale. An MRPC is a basically a stack of resistive plates with a series of uniform gas gaps. Electrodes are applied to the outer surface of the outer plates. A strong electric field is generated in each sub-gap by applying a high voltage across these external electrodes. All the internal plates are electrically floating. A charged particle going through the chamber generates avalanches in the gas gaps. Because the glass plates are resistive, they are transparent to charge induction from avalanches in the gaps. Typical resistivity for the glass plates is on the order of 10^{13} Ω/cm. Thus the induced signal on the pads is the sum of possible avalanches from all gas gaps. The electrodes are made of resistive graphite tape and are also transparent to charge. Copper pickup pads are used to read out the signals. A view of these pads for the present MRPCs is shown in Figure 25.

The graphite electrodes have a surface resistivity of 10^5 Ω and cover the entire active area. The outer and inner glass plates are 1.1 mm and 0.54 mm thick, respectively. They are kept parallel by using 0.22 mm diameter nylon fishing line as a spacer. The signal is read out by an array of copper pickup pads. The pickup pad layers are separated from the outer electrodes by 0.35 mm of Mylar.

Figures 26-28 show beam test results from a module produced by the China TOF group with six 0.25 mm gas gaps, 0.7 mm inner glass, and a 2×6 array of 3cm×3cm pickup pads. For these tests, the signal from the pads is amplified by Maxim 3760 fast current amplifier connected to a discriminator which is based on the AD96685 comparator. The output from the amplifier and discriminator is connected to CAMAC ADC (LeCroy 2248) and TDC (LeCroy 2228) modules, respectively.

The prototype MRPCs were tested at the CERN PS T10 beam line with a 7 GeV/c pion beam. The gas mixture used is 90% C2H2F4, 5% iso-Butane and 5% SF6.

The upper left frame of Figure 26 shows the raw time distribution for the 7 GeV/c test beam. In the lower frame is the Time *vs.* Amplitude correlation, or "slewing." The upper right frame of Figure 26 shows the time resolution after the slewing correction and the subtraction (in quadrature) of the start time resolution, which was measured independently. In both of the upper frames and on the ordinate of the lower frame, the time distributions are shown in units of TDC channels, each of which are ∼50 ps wide.

The sigma of the raw time distribution (before the slewing correction) is approximately 120 ps. After slewing and start corrections, the stop resolution is 1.33 TDC ch, or ∼67 ps. For a number of chambers we observed stop resolutions of 50-60 ps.

Figure 27 shows the efficiency (left frame), the corrected time resolution (middle frame), and the time walk (right frame) as a function of the high voltage. The detection efficiency exceeds 97% for a wide range of high voltage settings from 15.5 to 17 kV. In this region of high voltage, the stop resolution is always less than 65 ps, decreasing to 60 ps at the highest voltage settings. The time walk decreases linearly with increasing high voltage with a slope of ∼30 ps/kV.

Figure 28 shows the corrected TOF distribution for a 3 GeV/c test beam. The

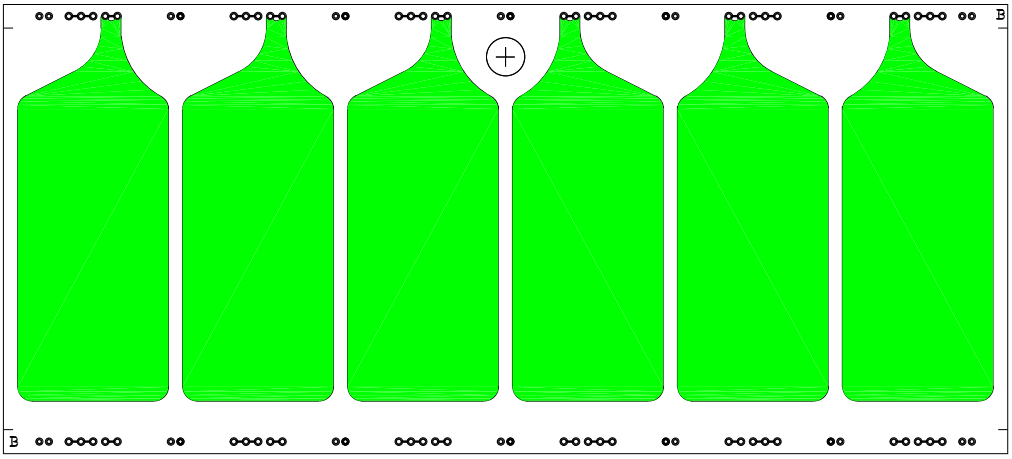

Figure 25: The circuit board with the copper read-out pads for the present MRPC detectors.

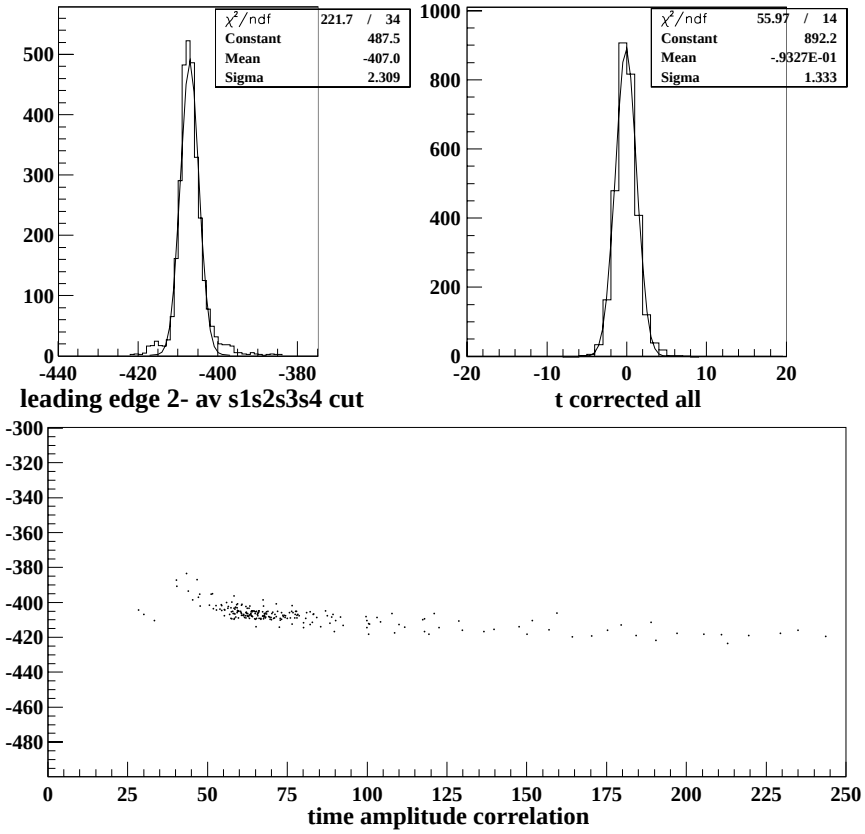

Figure 26: The raw time distribution (upper left), the time-amplitude ("slewing") correlation (lower), and the pure stop time resolution after the slewing and start resolution corrections (upper right).

flight path for these data was 2.8 m, which is comparable to that in STAR. The start time resolution was also comparable to that expected in STAR. The π/p separation is about 4σ under these conditions. It is clear that this system will satisfy the requirements set by the physics goals in STAR. In the following section, we describe the mechanical design of the system.

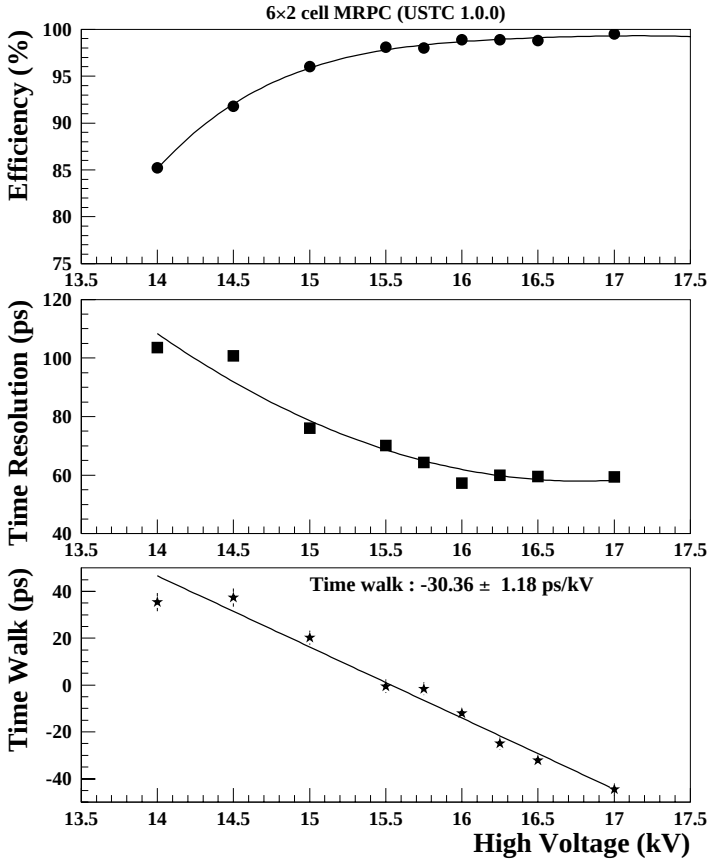

Figure 27: The detection efficiency (upper frame), slewing-corrected time resolution (middle frame), and time walk (lower frame), as a function of high voltage for the 6 gap MRPC.

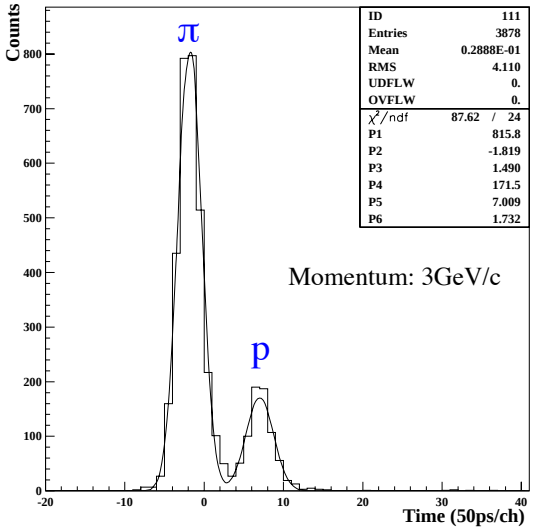

Figure 28: The corrected time-of-flight distribution of pions and protons in a beam of 3 GeV/c momentum. The flight path is 2.8 m.

4.4 Mechanical Design

The primary mechanical structure on the stop side of the system is a "tray." These hold the detectors in three dimensions at specific positions and angles, support the on-detector electronics, and form all but one wall of the gas volume. The trays for the proposed system are similar to those we have used successfully in the CTB (125 trays), TOFp (1 tray), and TOFr (1 tray) systems. (The TOF patch or TOFp is a 41-channel conventional scintillator-based TOF system that was installed for the FY2002 run, see appendix B.) In these systems, a tray is a welded 50 mil-thick aluminum box that slides onto rails attached to the TPC outer field cage. Additional requirements for the proposed system are that the MRPC trays must reside in a gas-tight volume, and that ∼200 signal cables must be passed out of this volume to the on-board electronics. This necessitated modifications to the basic tray design. The design is such that no part of the proposed system exceeds the assigned maximum "integration" radius of 219.5 cm. The welded-aluminum tray appropriate for the present system, as well other mechanical aspects such as the detector and electronics positioning inside this tray, are described in this section.

In this discussion, it will often be convenient to refer to figures shown in the following section (section 5), which describes the full-size STAR prototype MRPC tray, called "TOFr," that we constructed, tested in a BNL radiation area, and then installed in STAR. Most of the construction of the large-area system will use the same techniques and materials we developed during the construction of the TOFr tray.

A tray is an aluminum box with 50 mil (0.13 cm) wall thickness and welded corners. A CTB, TOFp, or TOFr tray is 95" (241.3 cm) long, 8.5" (21.6 cm) wide, and ∼3.5" (8.9 cm) high. It takes 120 trays to cover the cylindrical outer radius of the TPC, which are arranged as two adjoining cylindrical shells of 60 trays each. Each cylindrical shell subtends approximately 1 unit of pseudorapidity. Unlike the CTB and TOFp trays, these trays must be gas-tight. The detectors inside the gas volume are standard MRPC "modules," 6 channels each, with detector channel dimensions of 3.3cm×6.1cm. It takes 32-34 modules to fill a tray depending on the arrangement. The "top" of the tray, which bolts to the tray body via aluminum rails, is a custom 1/8" (0.32 cm) thick FR4 electronics board called the TOF Front End Electronics (TFEE) plate. These TFEE plates are simultaneously the "top" of the gas box, the signal feedthrough mechanism, the actual FEE boards, and the mounting location of the TOF Digitization (TDIG) boards just above the TFEE boards. Thus, the electronics exist as two layers, the TFEE boards themselves are both the first layer of electronics and the tray top. Mounted above these is another layer of boards, TDIG, that perform the digitization. At the high-z end of the tray are two more boards, TCPU and TMIT, which perform the communication of the digital data. The total height of the tray body, plus the thickness of the tray top (the TFEE plates), plus the thickness of the digitization electronics (including components), must not exceed a maximum height determined by the STAR integration envelope for this detector. The length of the tray plus the lengths of the two communications boards at the end of the tray likewise must not exceed a specified maximum length.

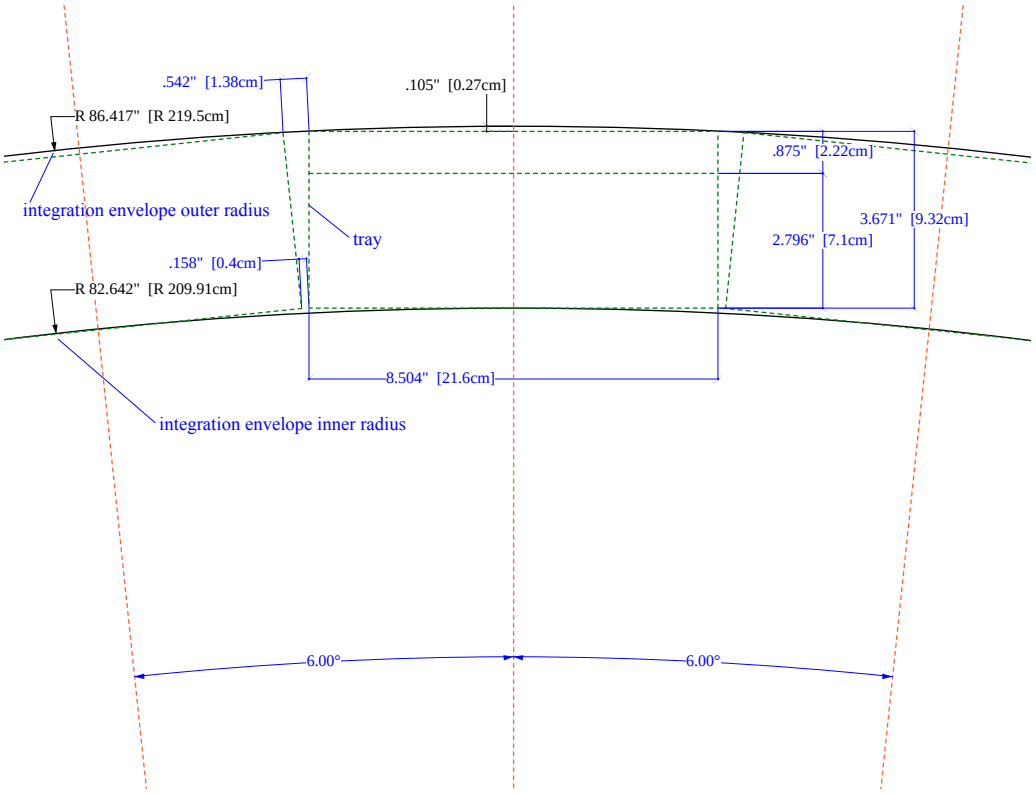

Figure 29: An end view of STAR showing the dimensions of the integration envelope allocated for this system.

Shown in Figure 29 is an end view of the STAR geometry near 12 o'clock and near the radius of interest. The radius of the bottom of the tray, at the centerline of the tray, when installed is 209.91 cm and is shown by the lower black arc. The maximum radius allowed is 219.5 cm, which is shown as the upper black arc. The new trays will be the same width as in the STAR CTB and TOFp systems. This thus defines the maximum total height of each tray (including electronics) to be 9.32 cm.

This distance specifies the rest of the design. It is estimated that 7/8" (2.22cm) of space at the top of this volume is needed for the two layers of electronics (TFEE and TDIG, see section 4.6 below). The height of the upper edge of the side walls of the tray is thus set at 9.32 cm−2.22 cm = 7.1 cm. The rails take up 0.5"+0.05" contingency (1.27 cm+.13 cm) of space just under this height. This space is also a convenient place to put the interior gas piping and HV cabling. With the thickness of the tray bottom of 50 mil (0.13 cm), the height of the space left for holding detectors is thus 5.7 cm.

Shown in Figure 30 is the side view of the tray for this system. Several different arrangements of detectors were studied in Autocad. While they all allowed the 32 detectors to fit into this 5.7 cm height, the arrangement shown in Figure 30 has the detectors placed most projectively to the average primary vertex location at z=0.

The left side of the figure is near STAR z∼η∼0, and the right side is near η∼1.

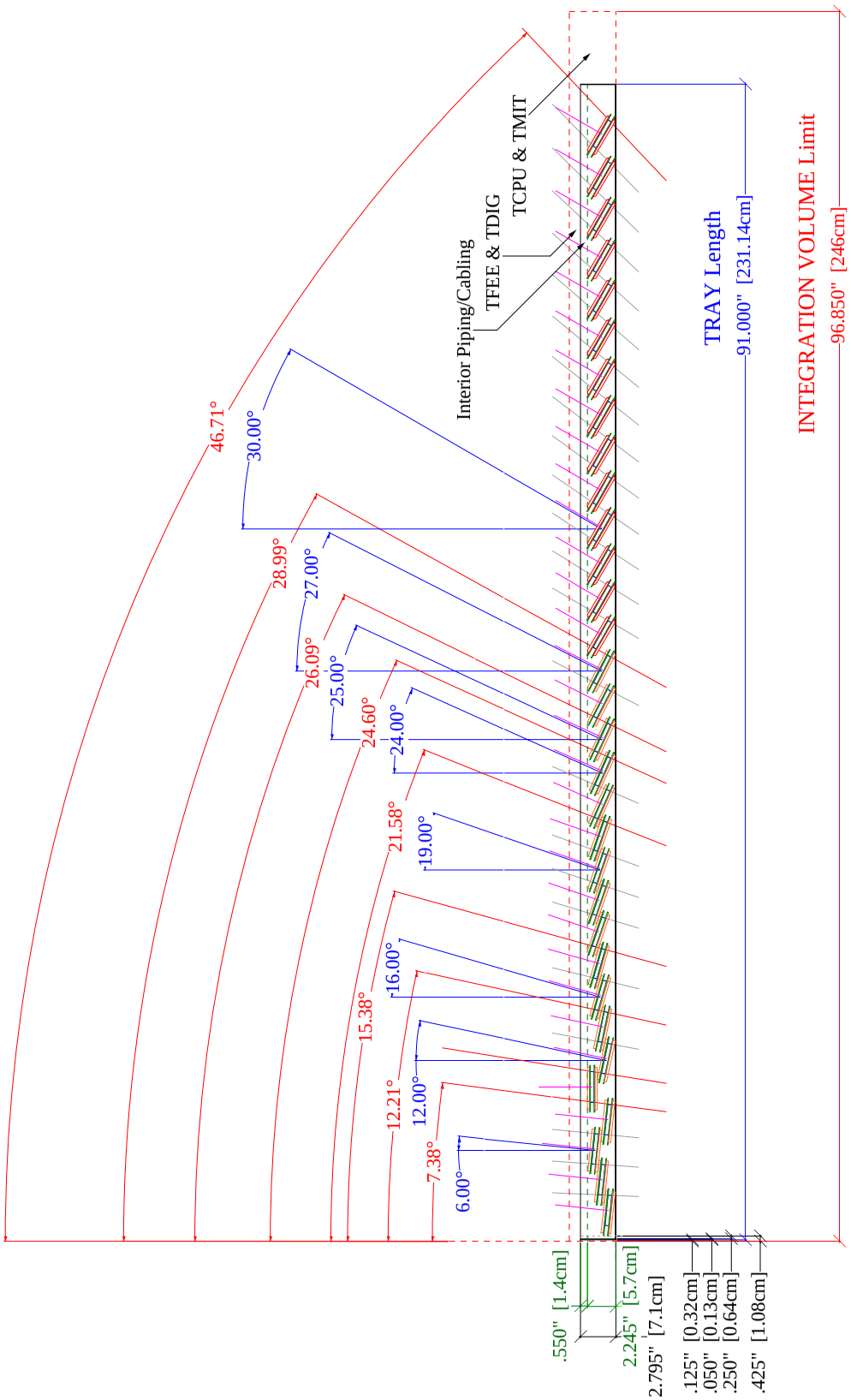

Figure 30: A dimensioned side view of the tray indicating the detector positioning.

The dashed red lines denote the boundary of the integration volume. The STAR z-axis is located 209.91 cm below the lower left corner of this red dashed box. The integration volume extends to z=246 cm. The tray length for the proposed system is 91", slightly shorter than the 95" length of the trays used in the CTB, TOFp, and TOFr systems.

In the present design there are 32 modules in each tray (192 detector channels). Although in a standard 95" (241.3 cm) long tray, there would be room for another module or two, depending on the module arrangement, a 91" (231.4 cm) length has several positive impacts. First, a channel count of 192 is divisible both by 24 and 32, allowing useful simplifications in the design of the DAQ interface and efficient deployment of the CERN HPTDC chips. The shorter-length tray also allows plenty of space for the two electronics boards, TCPU and TMIT, which are mounted at the end of each tray as part of the DAQ interface.

The support for the MRPC modules will be based on the same technique as used in the TOFr tray (see Figures 40 and 41). Phenolic-impregnated Kraft paper honeycomb ("hexcell", which is 1/4" (0.64 cm) thick, light, workable and extremely rigid) panels are machined into specific shapes ("sawtooths"). These shapes are glued to the inner walls of the tray going from the bottom of the tray up to the top, and the detectors are placed in the precisely oriented voids in the hexcell along the way. Thus all detectors are held up/down and in/out by the four sides of hexcell at their edges, and left/right by the walls of the tray itself. A small gap is left between the modules and the tray wall. The sides of the modules which are adjacent with the tray side walls are covered with two layers of Kapton tape before the modules are inserted. The interior bottom of the tray is also covered with a Kapton layer before the sawtooths and detectors are installed.

After the detectors are mounted, the interior HV cabling and then the interior gas piping is installed. The mechanical support for the TFEE cards is the "Rail Assembly". This is a single piece of aluminum, formed by welding flat plates to 4 pieces of 0.5" (1.27 cm) aluminum angle, which fits exactly into the opening of the box and is bolted horizontally to the tray walls with 8-32 brass machine screws. The TFEE plates bolt vertically onto the top of the rail assembly, which closes the gas volume around the detectors. These vertical bolts pass through a layer of 1 mm-thick neoprene rubber, which was found to be the most appropriate gasket material in tests performed during the TOFr construction (see section 5). A view of the TOFr tray with such a rail assembly installed is shown in section 5 on the left side of Figure 42.

With the rail assembly installed, 192 short twisted pair cables that carry the detector signals are connected to the pins on the underside of the TFEE plates. These plates are then bolted down to the rail assembly. After leak checking, gas is flowed through the tray. Then, the low voltage power and threshold distribution to the TFEE boards are attached. After gas has been flowing for $\sim$1/2 day, all tray systems can then be powered up and tested.

GEANT simulations were performed to evaluate the integrated thickness of the tray and detectors in interaction and radiation lengths. The results are shown in Figures 31. The gaps in azimuth between trays are at an angle of ± 0.052 radians in

this figure. In each frame, the three lines correspond to the CTB trays and detectors, the scintillator-based TOFp tray and detectors, and the presently proposed TOF trays with MRPC detectors, as labeled in each frame. In the two views versus the pseudorapidity, one notices 32 peaks for the present TOF system - these tracks are those passing through two MRPC modules. The two views versus the azimuthal angle give a clearer indication of the relative thicknesses of these three detector systems. The CTB is generally always the thinnest in terms of both interaction and radiation lengths. In terms of interaction lengths, TOFp is thicker than TOF, but in terms of radiation lengths, TOF is thicker than TOFp. This is because the thickest component of TOFp is the 2 cm-thick plastic slats, while glass and FR4 printed circuit boards in the MRPCs are the thickest components of TOF. The total interaction(radiation) length of the TOF trays is 21%(26%) more than that for the CTB.

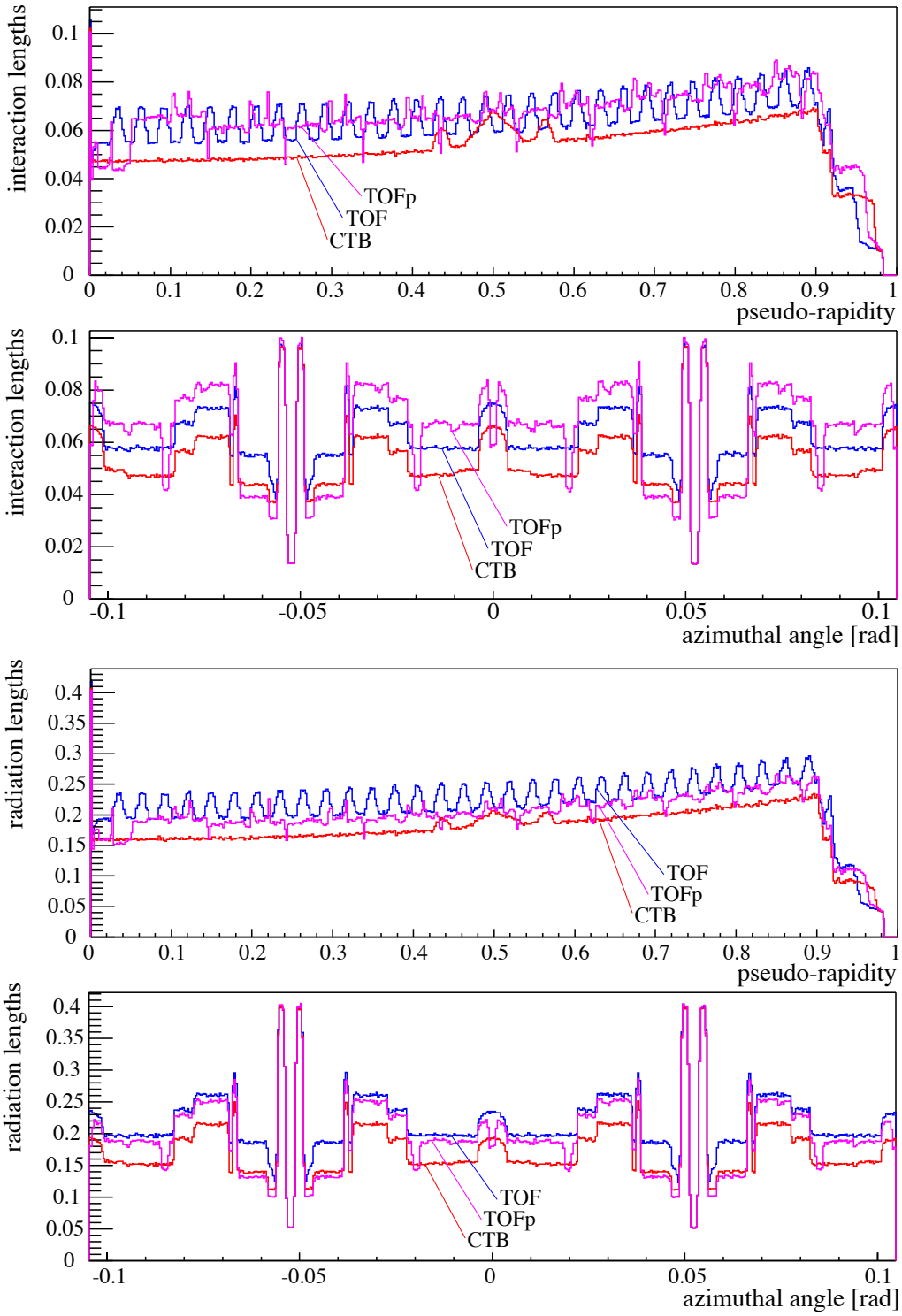

Figure 31: The integrated thickness of the tray and detectors in interaction lengths (upper two frames) and radiation lengths (lower two frames), versus the pseudorapidity and azimuthal angle, as labeled.

4.5 Gas System Design

The primary purpose of the TOF Gas System is to provide a mixture of 90% R134a, 5% iso-butane, and 5% SF6 to the TOF chambers at the correct pressure. This system can regulate the flow rate of the mixture while monitoring mixture temperature, flammable gas content, oxygen and moisture. A computer control/data acquisition system collects and logs the gas system operating parameters while providing a means of remotely controlling system valves. Shown in Figure 32 is the schematic, and Table IV lists the parameters, of the proposed gas system.

The TOFr system was successfully operated for several weeks during the AGS test without SF6, see 5.2. This test will be continued with the TOFr tray installed in STAR. If we continue successful operation, without SF6, we will plan to operate the full TOF system with a 2-component gas system.

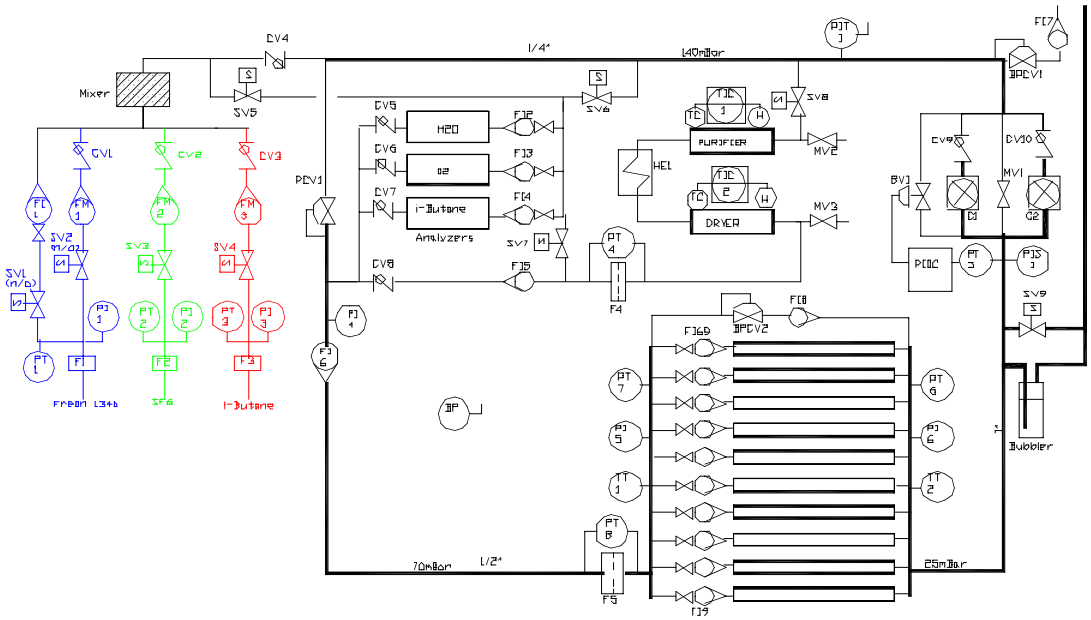

Figure 32: The schematic of the proposed gas system.

The system operates nominally as a closed circuit gas system with the majority of the mixture re-circulating through the TOF chambers and delivery system. During normal operation a small amount of fresh mixture is added and equivalent quantity of the existing mixture is vented. The gas system can be operated in an open system configuration for purging.

The mixture circulation rate through the small membrane compressor is 15 LPM at 140 mbar. The gas system contains two compressors (C1,C2), one active and one spare. The mixture from the compressors goes to the supply line through the check valves CV9 or CV10. The 140 mbar output pressure from the compressor is reduced to 70 mbar by the pressure regulator (PCV1) and this pressure level is maintained with the back pressure regulator (BPCV2).

The return gas manifold is maintained at 2.5 mbar above atmospheric pressure by a

Table IV: The design parameters of the gas system.

Mixture	90% R134a, 5% i-C_4H_{10}, 5% SF_6
Compressor pressure	100-150 mbar
Supply pressure	70±0.1 mbar
Return pressure	2.5±0.1 mbar
Re-circulation flow	700 liter/hr
Mixture flow through TOF chambers	300-600 liter/hr
Purge flow	600 liter/hr
Make-up mixture flow	0.2-2 liter/min
Oxygen content	<30 ppm
Water content	<20 ppm

differential pressure transmitter (PT5) and electro-pneumatic PID Controller (PIDC) that operates bypass valve (BV1). The bypass shunts flow from the compressor discharge line directly back to the compressor's inlet. A second manual bypass valve (MV1) is adjusted to enable the automatic control loop to be used within its optimum range.

The bypass line including the back pressure control valve (BPCV2) allows smoothing the gas system start and rapid response to increased or reduced iso-butane content measured with the iso-butane analyzer upstream of the compressor. Also, it permits *e.g.* the preparation of the mixture with a homogeneous iso-butane content.

Two flow indicators (FI6 and FI8) will measure the re-circulating flows: main and bypass. A difference between them is the flow through the TOF chambers. The measurements of the fresh mixture (FM1, FM2 and FM3) and flow through the flow indicator (FI7) provides an estimation of the tray leakage.

The purity and composition of the mixture is monitored using oxygen, iso-butane and humidity analyzers. A fraction of the re-circulating mixture can be passed through a purifier and dryer to remove moisture and contaminants as needed.

A computer driven data acquisition/control system monitors all of the process variables. The computer system flags quantities which fall outside of predefined limits and initiates corrective action.

It is imperative that the TOF chambers inside pressure accurately track barometric pressure. A rapid change in atmospheric pressure is typical preceding storms and hurricanes. To assure that the TOF chambers follow a fast rise in atmospheric pressure, a relatively large flow of inert gas will be admitted into the TOF chambers in the event that normal pressure controls fail to keep up with falling relative internal pressure. The vent lines and associated valves are sized to allow for rapid venting of the TOF chamber mixture to prevent a high internal pressure in the case of a rapid decline in barometric pressure.

4.5.1 Pressure Control

There are two sources of pressure in the system: the first is the compressors located at the exit of the TOF chambers. The second is the flow of fresh mixture through the mixing manifold. Nominally the pressure within the TOF chambers is controlled by maintaining a constant pressure upstream of the DC and PC via the pressure reducing regulator (PCV1) plus back pressure regulator (BPCV2) and varying the pressure downstream of the TOF chambers by regulating the amount of mixture shunted from the compressor output to inlet. On a longer time scale, the flow of fresh mixture is constant.

The output from the compressor is 700 liter/hr at 140 mbar. A back pressure regulator (BPCV1) in the outlet line is set to 140 mbar thus maintaining a maximum delivery pressure independent of the compressor output. This pressure is reduced to 70 mbar by the pressure regulator (PCV1) and supported with the back pressure regulator (BPCV2) upstream of the TOF chambers. The TOF chambers exhaust pressure, measured at the return gas manifold is maintained at 2.5 mbar by a TESCOM ER3000 electro-pneumatic PID controller. A 0-5 mbar differential pressure transmitter (PT5) on the return manifold produces a 4-20 mA output that the PID controller compares to a set-point value. If the transmitter signal is different from the set point, the controller sends a pneumatic output signal to the bypass control valve (BV1). The bypass shunts flow from the compressor discharge line directly back to the compressor's inlet. Opening the bypass valve causes the TOF chambers exhaust pressure to rise and closing the valve makes the pressure fall. A second bypass valve (MV1), manually adjusted during the initial system set-up, enables this automatic control loop to be used within its optimum range.

The fresh mixture is admitted between the pressure regulator (PVC1) and back pressure regulator (BPCV1). The quantity of fresh mixture is changeable in the range of 0.2.-3 liter/min with the mass flow controllers FM1, FM2 and FM3. To purge the detectors with up to 10 liter/min of inert gas, the flow indicator (FI1) is used. Simultaneously, gas is removed from the system through the back pressure regulator (BPCV1). To have the stable content of fresh mixture, the Freon R134a mass flow controller (FM1) operates the SF6 and iso-butane controllers (FM2 and FM3). This means that FM1 is a master, and FM2 and FM3 are the slaves. These units are normally locally controlled. The quantity of fresh mixture is monitored by the PC data acquisition/control system.

When the internal TOF chamber's pressure as measured by PT6 is more then 3 mbar above the atmospheric one, the gas control system will close the solenoid valves (SV2, SV3, and SV4) in the fresh mixture supply line and open the vent line valve (SV9) allowing mixture to vent directly to the atmosphere. Also, a pressure indicating switch (PIS1) has a set-point of 3 mbar and it can operate SV2, SV3, SV4 and SV9 as the computer control. Should the TOF chambers pressure reach 3.5 mbar, the out-going TOF chamber gas mixture will vent to the atmosphere through the bubbler. With this arrangement, the TOF chambers are protected from either flow controller malfunction, a rapid drop in atmospheric pressure, and/or a failure of

the back pressure regulator.

In the event of a rapid rise in atmospheric pressure, or effectively a fast drop in the TOF chambers internal pressure (up to 6 mbar/min), a dual set point Dwyer differential pressure transmitter (PT6) in the return manifold will trip as the pressure falls below 0.5 mbar causing an audible and visual alarm. When the pressure at PT6 falls below atmospheric (0.1 mbar gauge) a second set-point trips and the computer control system will stop the compressor, shut-off the flow of iso-butane, shut-off the HV, and pass inert gas by opening the solenoid valve (SV1) to supply an additional 5 liter/min of inert gas.

A pressure indicating switch (PIS1) with dual set points is also installed in the return manifold. This switch is not connected to the computer control system but is hardwired to perform the same functions as the computer in the event of a falling TOF chambers pressure. Thus the system is equipped with two separate means of preventing the TOF chambers from experiencing an external over pressure.

In the event of a power failure, the solenoid valves SV1, SV2, and SV9 will open, or remain open and SV3, SV4 will close, causing 5 liter/min of inert gas to flow through the TOF chambers. This flow rate is adequate to assure that fluctuations in the atmospheric pressure will not result in the creation of over- or negative-pressure inside the TOF chambers.

The computer data acquisition /control system will measure the atmospheric pressure with a barometer (BP) to have available the absolute pressure data.

4.5.2 Mixture Control & Temperature Measurement

Along with automated valve control, the gas system's dedicated computer controlled data acquisition provides constant monitoring of the mixture composition via measuring the mass controllers output signals. The iso-butane analyzer will be used periodically to check iso-butane content in the mixture. The mixture ratio is fixed by the Teledyne mass flow controllers (FM1, FM2 and FM3) with the SF6 and iso-butane flow controllers slaved to the freon controller. The stability of the flow controllers is sufficient to make variation in the mixture negligible.

Two temperature transmitters (TT1 and TT2) are used to measure the mixture temperature within the TOF chambers. The data of measured mixture temperature are logged for later use in data analysis.

4.5.3 Gas Sampling & Purification

The gas system is equipped with oxygen, moisture and iso-butane analyzers plumbed such that each section of the gas system can be selected separately for evaluation. The data from the analyzers is read out and archived by the computer data acquisition system and used to control the gas system.

A mixture dryer and purifier withdraws a portion (about 2 liter/min) of the recirculating flow upstream of the pressure regulator (PCV1) and delivers the conditioned gas to the recirculating flow downstream of PCV1. This loop is used only as needed.

Table V: The list of fault conditions in the gas system.

No.	Name	Limit	Action
1	PT-6	<0.1 mbar	Stop Compressor and HV, inert gas purge (open SV1), Alarm (audible, flashing light)
2	PT-6	<0.5 mbar	Alarm (audible, flashing light)
3	PT-6	>3 mbar	Close SV2, SV3 and SV4, Open SV9, Alarm (audible, flashing light)
4	PT-1	<6 PSI	Alarm (audible, flashing light)
5	PT-2	<6 PSI	Alarm (audible, flashing light)
6	PT-3	>5 PSI	Alarm (audible, flashing light)
7	O2&H20	>100 ppm	Stop HV, Alarm (audible, flashing light)
8	O2&H2O	>90 ppm	Alarm (flashing light)
9	iso-butane	> 7%	Alarm (audible, flashing light)
10	iso-butane	< 4%	Alarm (audible, flashing light)
11	FM1-3	>7% iC4H10	Stop iC4H10 supply and HV. Alarm (audible, flashing light)
12	FM1-3	<4% iC4H10	Alarm (audible, flashing light)
13	PIT-1	<50 mbar	Alarm (audible, flashing light)
14	PT-4	>45 mbar	Alarm (audible, flashing light)
15	PT-8	>10 mbar	Alarm (audible, flashing light)

The dryer is made from a stainless steel tube containing 1 pound of molecular sieve (zeolite 13X) as adsorbent. This amount permits the removal of about 0.4 lbs of water vapor to a level 2-3 ppm at room temperature. Filters are installed upstream and downstream of the adsorbent to prevent particles from entering to the mixture stream. A heating element is placed inside the dryer. For thermal insulation, a fiber glass insulation is used. The dryer is regenerated by heating to 350-400 °C with purging of the mixture (Nitrogen + 3% H2). The purge gas enters at the top of the dryer and exits at the bottom carrying with it the water vapor. A temperature transmitter installed inside the dryer is connected to the temperature controller (TIC2) that supports the dryer temperature on the set-pointed level. A moisture analyzer is used to measure the quantity of the water in the circuit before and after the dryer to determine when the adsorbent is saturated.

The purifier is similar to the dryer except that it is filled with pure copper. The oxidization process takes place at 220 °C that is regulated by the temperature controller (TIC1). A heat exchanger (HE1) is used to reduce the mixture temperature exiting into the dryer. This purifier is regenerated with the same mixture as the dryer. Solenoid valve (SV8) installed at the inlet of the purification loop isolates the unit

from the main circuit when it is not in use. If the inside pressure of the purifier/dryer is more than 1/3 PSI, the check valve (CV8) works as the safety valve and prevents the purifier/dryer from damage.

A 10 μm filter is installed after the purifier/dryer to prevent dust from passing into the main mixture supply line. A differential pressure transmitter (PT4) is used to check the plugging of the filters.

4.5.4 Computer Control & Data Acquisition

The gas system includes a computer driven data acquisition and control system. The controlling computer is a dedicated PC with Intel Pentium processor. It reads the data and operates the gas system via National Instruments SCXI system. This computerized system is programmed to acquire the signals from the various temperature, pressure, flow, and content measuring devices and issue warnings and/or take corrective action in the event that predetermined levels are exceeded. All acquired values can be selected and viewed on the terminal. Gas system parameters may be viewed using the World Wide Web. The interface of the gas system with STAR slow controls will be accomplished by an EPICS interface.

4.6 Electronics Design

A Time-of-Flight system measures time intervals, which are defined by independent electronic measurements of one "start time" and some number of "stop times" in each experimental event. While different detectors are used on the start and stop sides, important advantages are gained by performing both the start and stop digitization in the same electronics. This is a common trait of all successful TOF detector systems. In the STAR TOFp and TOFr systems, digitization is performed on the platform using the pVPD signals as direct electronic starts for both the stop detector and the pVPD digitization (see section 4.9 and appendix B). However, for the proposed system, one cannot possibly distribute electronic signals from the start detector to each stop detector (*i.e.* each tray) in time. Also, one could not possibly integrate a system into STAR that digitizes 23k detector channels using long cables and a huge bank of CAMAC or Fastbus electronics. For the proposed system, one must instead digitize versus a clock, and transmit from the detector digital data, instead of logic signals to be digitized elsewhere. The information ultimately needed for timing analyses are still available, as (stop-clock)-(start-clock)=stop-start, so long as the clocks used on both the start and stop sides are the same to 10-20 ps in every event. Additional comments on the start detector are presented in section 4.9 below.

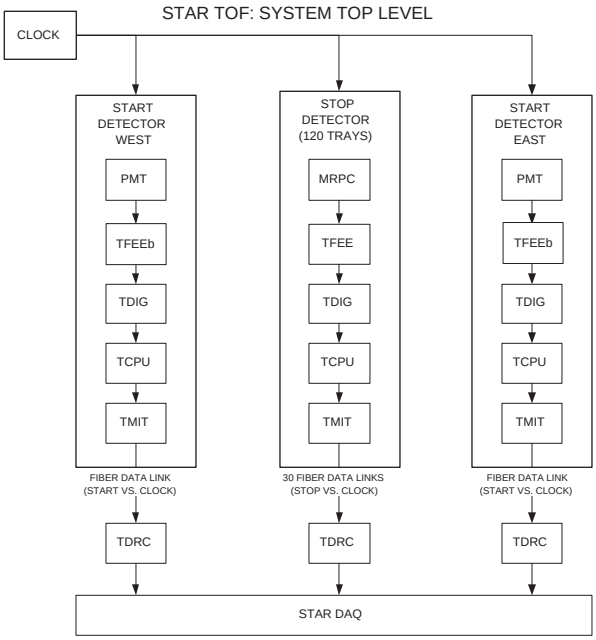

Figure 33: The highest-level diagram of the electronics for the proposed system.

Shown in Figure 33 is the top-level diagram of the electronics for the start and stop sides of the present system. The electronics chain on the start side is very similar to that on the stop side by design. The individual electronics boards seen in this figure are discussed in detail in this and the following subsections.

Each tray consists of 192 detector channels and three different types of circuit cards. These types are called TFEE, TDIG, and TCPU, listed in order of the flow

of information from the detector. Every fourth tray also contains a TMIT card that transmits the data to STAR DAQ. The TFEE contains the analog front end electronics and also serves as the top of the gas box and the signal feedthrough. The ∼10" long twisted-pair cables from the detector pickup pads are connected to the feed-through. The TFEE pass their output to the TDIG, which digitizes and buffers the detector information. This information is passed to TCPU which formats and buffers the digital detector information. This formatted data is passed to TMIT, which transmits it over an optical fiber to the data receiver TDRC in the STAR DAQ room.

Shown in Figure 34 is the top level electronics diagram at the tray level. The system interfaces include:

- a fiber optic data communication link via the TDRC to the STAR DAQ (TDC data and command echo),
- a high speed differential data link (PECL or LVDS) for multiplicity data to the STAR Level-0 trigger,
- a command link for acquisition commands from the STAR trigger,
- a high speed differential line (1 signal) for the beam crossing timing signal from the STAR trigger, and
- a serial bus for connecting the system's embedded CPUs to the network for configuration and status.

Each MRPC module contains 6 detector channels. Four modules feed into one TFEE. Each TFEE feeds one TDIG. The 8 TDIG cards in a tray feed into a single TCPU. Data from 4 TCPUs will feed into a single TMIT located as a daughter board on one of the TCPUs. Figure 35 shows the physical partitioning of these different electronics boards and the data flow between them.

Each TFEE card contains the high-bandwidth amplifiers and leading-edge discriminators for 24 detector inputs (4 modules). These two functions are performed by the Maxim 3760 preamplifier and the Analog Devices AD96687 dual comparator. To reduce noise into the low level MRPC output signal, the TFEE is designed as an integral part of the tray mechanical structure. The TFEE will have test inputs and outputs to allow the simulated MRPC signal input and front-end performance measurements using external test equipment (ADCs, TDCs and high performance oscilloscopes) that is independent of the embedded TDC circuitry. This will allow isolated performance measurements of the pre-amplifier, discriminator, and TDC, as well as the comparison of the TDC measurements by TDIG to those when digitizing in CAMAC or in a fast oscilloscope.

Each TDIG card comprises the time-to-digital conversion function for the discriminator outputs from a TFEE, using the HPTDC ASIC under development at CERN for ALICE and CMS. There are eight TDIG cards per tray, and each sees 24 detector channels via one TFEE card. The 4 HPTDC chips on each TDIG card sample rising

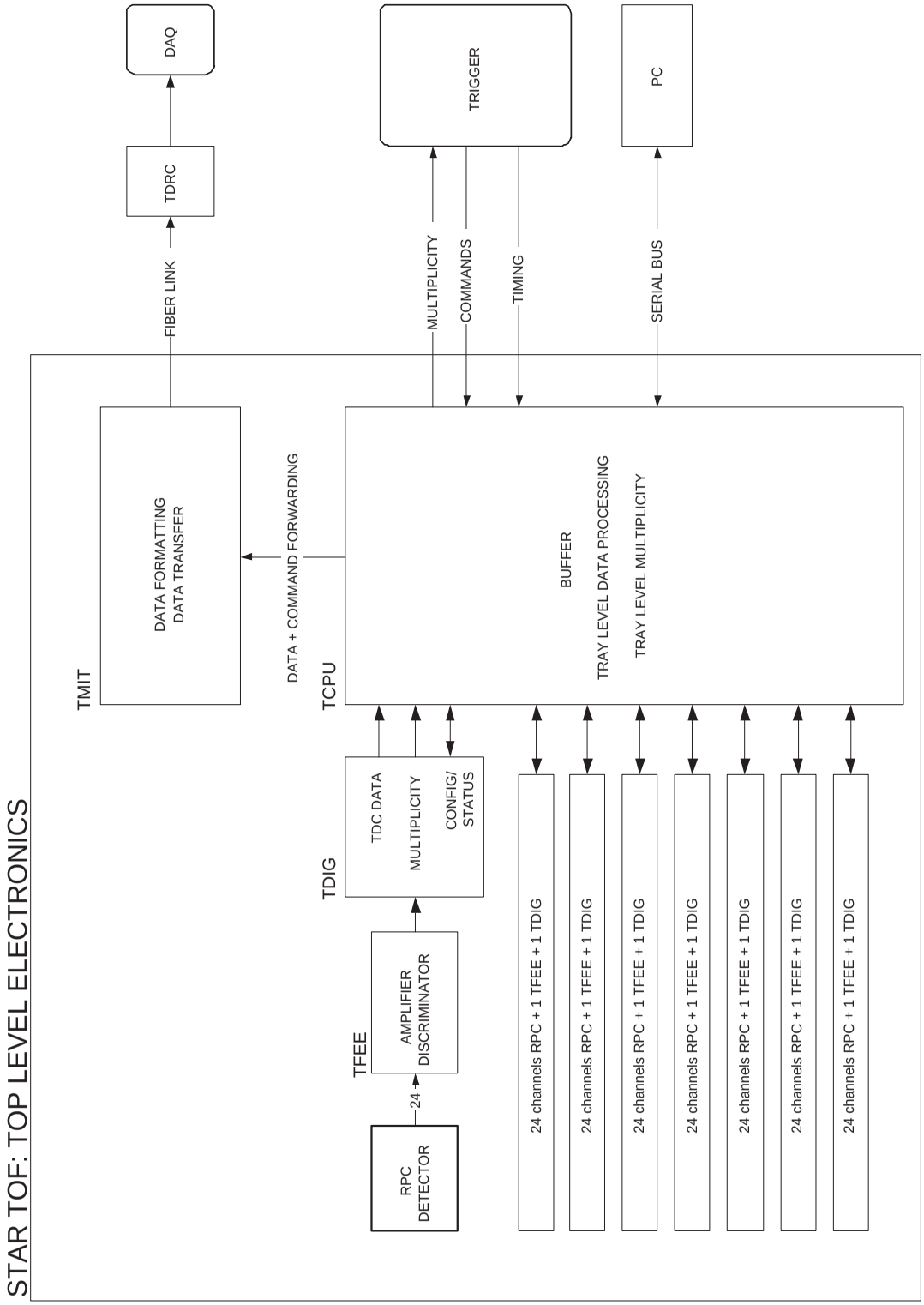

Figure 34: The top level electronics diagram at the tray level.

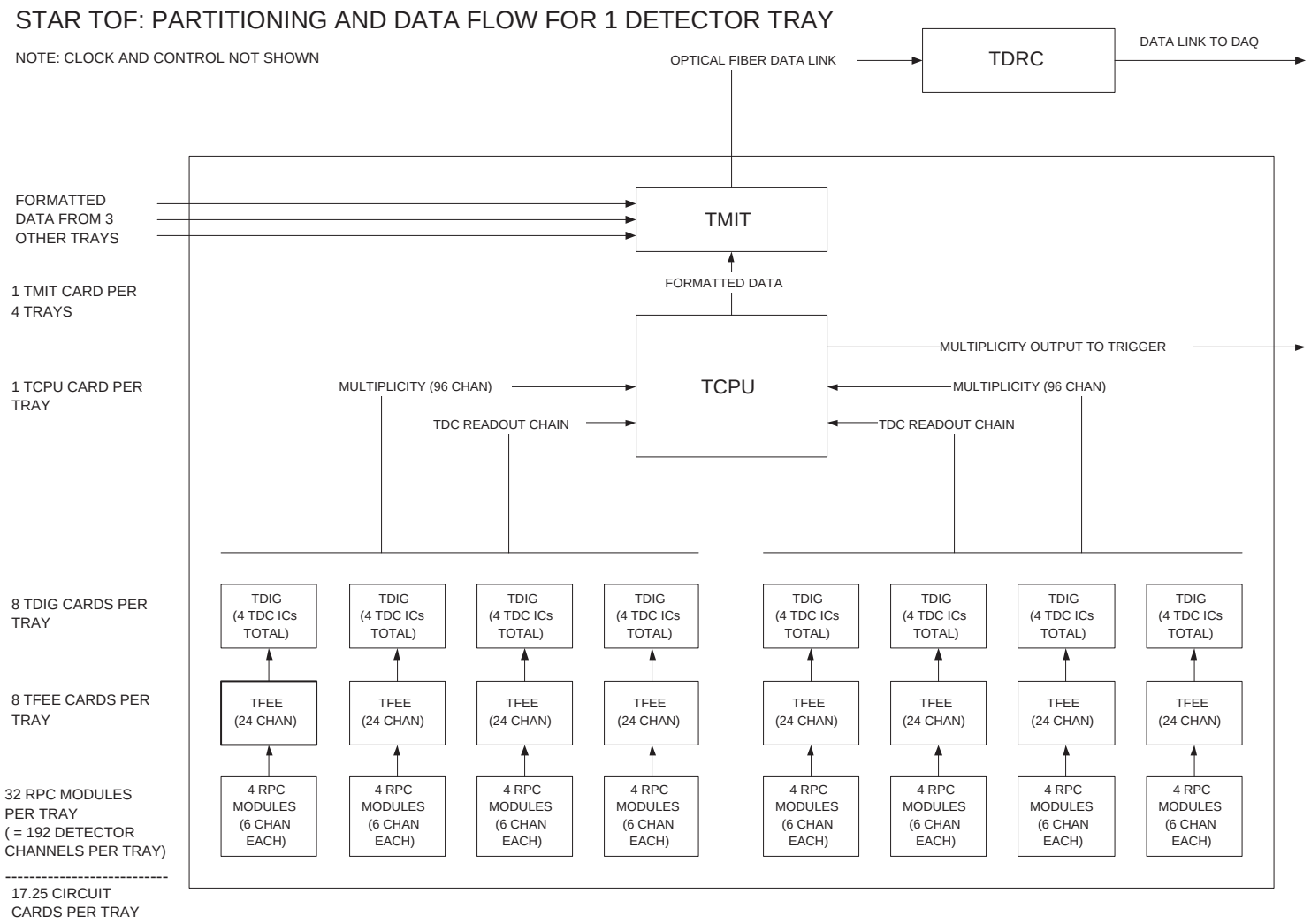

Figure 35: The partitioning of electronics functions between circuit cards.

and falling edges of the discriminated input pulse, giving both leading edge timing and time-over-threshold information (for the slewing correction). The HPTDC chip also contains a buffer for 256 recorded times where stop times are held until read out by the TCPU card. The amplifier/discriminator and TDC functions are physically and electrically separated onto two boards, TFEE and TDIG, to reduce the chance that digital noise from the TDC circuitry will interfere with (i.e. add jitter to) the analog signals in the amplifier/discriminator section.

Each TDIG card also performs the first layer of logic for the multiplicity output, producing the (5-bit) total of active discriminator outputs at each beam crossing interval. This information, aggregated at the tray level by the TCPU card, will be used as an input to the STAR Level-0 trigger. Since the installation of the proposed system implies the removal of the STAR CTB, the system will provide the same kind of multiplicity information for $|\eta|<1$ to the Level-0 trigger that the CTB did.

There is one TCPU card per detector tray. The TCPU card configures the eight TDIG and TFEE pairs in the tray and controls data acquisition cycles based on commands from the trigger. The TCPU also receives TDC data from the TDIG cards, formats and buffers the data, and transfers the buffered data to the TMIT daughter board for transmission to the DAQ via the TDRC card.

The TMIT circuit implements a high-speed serial communications protocol at the physical layer. Separating this function into a separate daughter board allows a protocol change to occur transparently to the TCPU hardware - only embedded CPU or PLD firmware changes would be necessary.

The TCPU receives a beam crossing timing signal from the trigger, cleans it up (if necessary) and distributes it to the TDCs on the TDIG boards. In normal operation, the TCPU will configure itself and operate based on embedded firmware, but the TCPU includes a serial bus connection to a host PC to directly control configuration and obtain status during testing and system integration. This data link will be available for remote diagnostics during final assembly and operation of the system.

The TCPU performs the second layer of logic for the multiplicity output, summing 5-bit inputs from four TDIG cards into a 7-bit multiplicity output for a half-tray (96 channels). The TCPU performs this function for each of the two half-tray signal groups and sends the 7-bit result for each group as a 7-bit differential signal during each beam crossing interval. There are 2 multiplicity outputs for each tray; each is 7 bits in parallel, and each bit is differential (2 signal wires).

In the subsections below, we describe each of the five STAR TOF electronics boards in more detail.

4.6.1 TFEE

This card contains preamplifier and discriminator circuits to accommodate 24 pad signals from 4 MRPC modules. A TOF detector tray will have 8 TFEE cards. Each TFEE card will be 8.4"×10.5". The power dissipation will be about 14 Watts per card, or 110 Watts per tray. The principal functions of the TFEE and TDIG are shown in Figure 36.

The preamp device, a Maxim 3760, is a low noise input trans-impedance integrated circuit whose gain and rise time characteristics are well-defined by internal feedback. This part is commercially available for use as a photodiode receiver preamp in data communication applications. Several designs employing this chip have shown excellent timing performance when connected to actual MRPC pads - the Maxim 3760 has been used extensively for the past two years by both the STAR and ALICE TOF groups.

An ultra-high speed integrated circuit comparator, the AD96685, serves as a simple leading-edge discriminator with externally controlled threshold. This circuit has also been demonstrated successfully in both the TOFp and TOFr systems. The output pulse width, *i.e.* the "Time Over Threshold," will be used to infer the input signal pulse height for the slewing correction.

The TFEE is an integral part of the tray mechanical assembly. This results in the shortest signal path and the maximum shielding. The TDIG cards are stacked above their respective TFEE card to reduce RF cabling. Multiplicity sums have dedicated parallel data paths from each TDIG card to the TCPU. The TDCs on the TDIG cards are read over a dedicated bus in groups of 16 TDCs (four TDIG cards), giving 2 data paths from the TDIG cards to the TCPU. All the TDCs are configured via a JTAG serial bus. The threshold DACs and temperature monitors are configured/read from a separate low speed serial bus.

Provisions will be made during the design of the TFEE cards to optionally bypass the preamp section. This will allow these boards (TFEEb) to operate when the inputs are photomultiplier signals, not MRPC signals. This will allow the identical signal processing chain to be used on the start side with no additional board designs. Access to the preamp outputs will also be included for evaluation of MPRC ADC spectra during the final testing and QA of fully assembled final trays.

A 6-channel version of TFEE was produced for the prototype TOF tray, TOFr (see section 5). This circuit for TOFr had additional functions that will not be required on TFEE such as an amplified analog output and NIM logic signal output. The pre-amplifier, discriminator, and related circuitry will remain the same, so we have a proven design for this card and experience building and testing production boards.

Table VI shows the bench test results for 41 TOFr FEE cards. The jitter in the pre-amplifier was of order 20 ps or less in all but one channel. This is an outstanding result.

These TOFr FEE cards have proved to be reliable. They have been used for testing MRPC modules at CERN, Rice, and in China and 28 six-channel cards were used for the TOFr tests at the AGS. There was one field failure in a single channel, but this channel proved good when re-tested on the bench, so the failure was likely a poor connection to the interface card.

4.6.2 TDIG

The TDIG card measures leading and trailing edge timing for 4 MRPC modules (24 detector channels). These cards are mounted directly on the TFEE cards - one TDIG card per TFEE card. The discriminator signals, clock, multiplicity gate, and

Board	Status	Chan 1	Chan 2	Chan 3	Chan 4	Chan 5	Chan 6
4	OK	16.0	16.0	18.0	16.0	18.0	17.0
5	OK	15.0	16.0	16.0	16.0	16.0	16.0
6	OK	16.2	16.7	15.8	18.8	17.8	16.1
7	OK	16.0	14.0	18.0	18.0	17.0	20.0
8	OK	16.0	19.0	16.0	19.0	16.0	16.0
9	OK	16.7	17.2	15.8	14.8	16.3	16.0
10	OK	16.9	18.6	17.3	18.9	19.7	17.8
11	OK	16.9	18.0	15.0	19.4	16.8	17.3
12	OK	17.4	17.4	20.1	20.5	15.2	16.5
13	OK	17.7	21.0	18.9	17.8	17.8	17.3
14	failed						
15	failed&fixed	14.8	13.9	22.0	15.5	23.2	21.1
16	OK	18.4	18.4	15.8	20.0	19.2	19.7
17	OK	16.5	14.8	20.3	18.5	16.5	20.7
18	OK	15.7	15.0	16.3	19.0	19.2	16.9
19	OK	16.3	16.4	18.0	18.2	17.4	18.8
20	OK	16.2	19.6	17.3	19.7	15.6	18.8
21	OK	16.8	17.0	17.6	17.9	15.3	17.0
22	OK	15.8	15.1	17.1	20.2	20.4	16.9
23	OK	18.3	19.3	15.0	17.6	19.8	16.7
24	don't use	18.2	18.9	33.8	15.5	16.4	17.3
25	OK	15.8	14.5	16.5	15.4	16.7	18.6
26	OK	17.7	18.5	16.2	16.8	17.7	19.2
27	OK	14.7	20.3	20.5	19.3	20.1	18.1
28	OK	18.1	16.8	17.8	16.5	17.5	16.8
29	OK	17.0	16.4	19.2	20.2	18.4	18.2
30	OK	15.8	16.6	18.0	17.3	14.2	17.3
31	OK	19.3	16.8	17.4	17.1	17.9	15.4
32	OK	16.3	17.7	16.2	18.4	19.6	15.4
33	OK	18.1	14.1	18.1	17.7	16.1	16.9
34	OK	13.8	18.0	15.0	15.6	19.3	16.3
35	failed&fixed	16.7	16.1	18.6	23.1	16.9	15.1
36	OK	15.2	14.7	14.1	17.4	17.5	15.1
37	OK	19.8	16.3	16.3	15.6	15.6	15.6
38	OK	14.8	18.1	14.4	16.0	15.4	13.9
39	OK	16.1	17.8	17.3	18.7	15.0	15.7
40	OK	19.3	16.5	19.3	20.3	18.4	14.7
41	OK	17.8	16.7	15.6	15.9	14.6	16.1
43	OK	18.3	17.2	20.2	22.0	21.0	19.2
44	no. not used						
45	bad PCB						
46	OK	15.3	19.1	15.0	24.1	20.1	21.6

Table VI: The bench test results for the TOFr FEE cards. The columns are standard deviations (*i.e.* the resolution) in units of picoseconds. These TOFr FEE cards are very similar to cards proposed for the full system called TFEE.

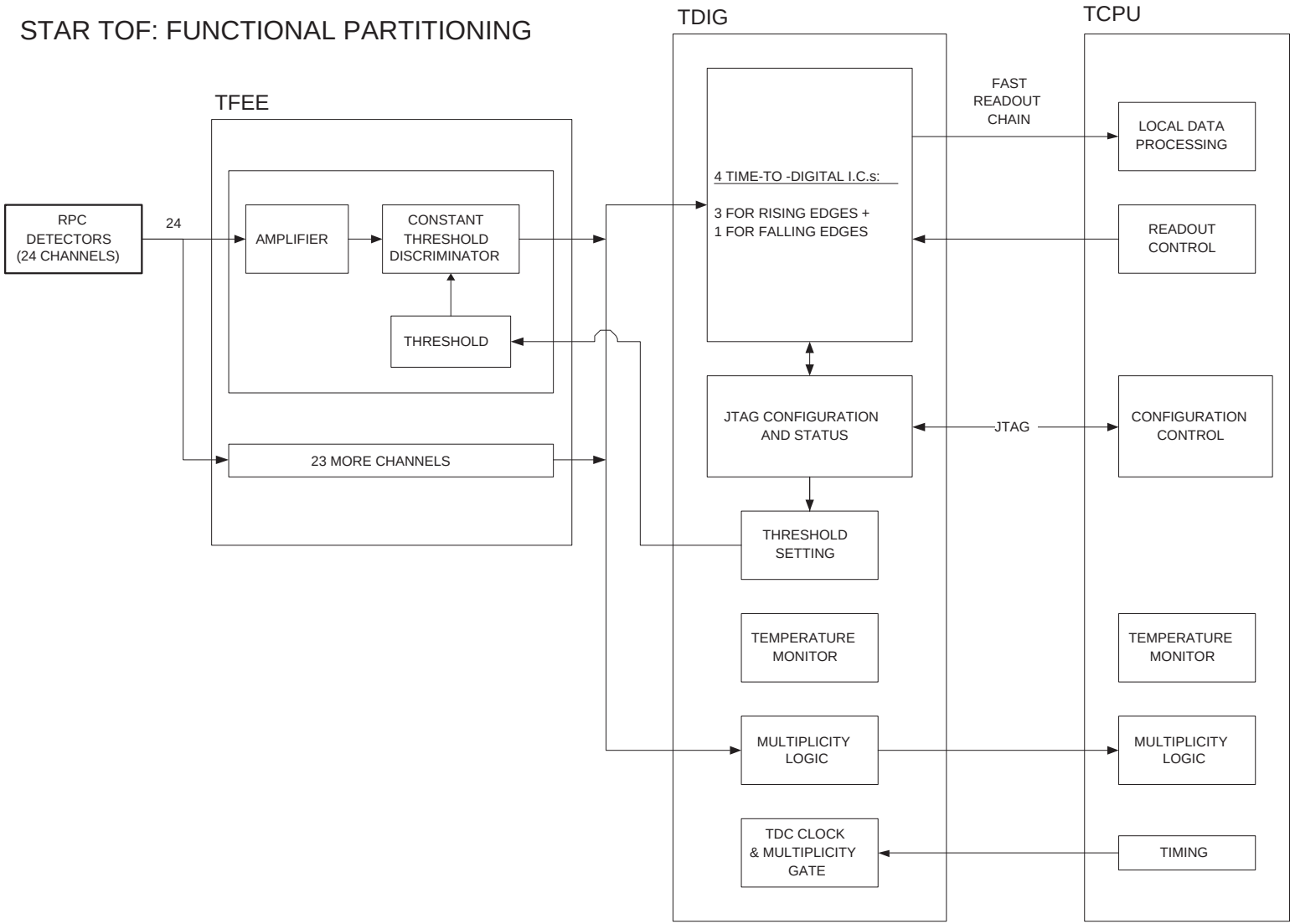

Figure 36: The front end electronics (TFEE) and digital sampling (TDIG) circuit cards.

81

L0 trigger readout commands are primary inputs while the hit edge timing data and 5-bit partial multiplicity sums are outputs. The calculation of the pulse width for the time-over-threshold slewing correction, and any resultant data formatting, will occur downstream of this card.

The multichannel HPTDC ASIC developed at CERN for the ALICE and CMS experiments is our first choice for the TDC measurement. In addition to meeting our time resolution requirements, it has efficient and flexible triggering and readout features. The trigger matching function allows acquired data to be read out from the built-in buffer in an order that accounts for trigger latency. As a backup, we will evaluate a device under development at the University of Oulu in Finland. The Oulu device as specified has adequate timing resolution but does not include readout features of the CERN HPTDC. However, the Oulu TDC is a full custom CMOS ASIC achieving 20 picosecond timing precision with very low power consumption of <5 mW/channel. NASA is currently evaluating chips they have received from Oulu.

Leading edge timing for 24 channels with 25 ps binning will be provided by 3 HPTDC devices operating in 8 channel, Very Hi Res mode. The trailing edge times of all 24 channels will be determined by 1 device operating in 32 channel Hi Res mode with 100 ps time bins. A built in hardware handshake protocol allows 16 HPTDC devices to share a 80 Mbit/sec serial output port so that only 2 data cables are required per CTB tray (4 TDIG boards, 96 MRPC pads each).

Additionally, this card will have slow serial interfaces for TDC and logic configuration, control of discriminator threshold and temperature monitoring. Estimated power consumption is about 10 watts per board or 80 watts per tray.

We have on hand a number of HPTDC chips from the last CERN prototype run and are building a prototype TDIG circuit using the HPTDC. The latest HPTDCs have been bench tested at CERN and have successfully demonstrated 15 ps timing resolution. The low-resolution mode of the HPTDC is available now in a CAEN VME-based TDC module offering 100 ps resolution. However, the current version of the HPTDC is difficult to use in high precision mode and a new prototype run is underway. The next iteration of the HPTDC is expected at CERN in mid-November, 2002. We will receive some of the latest chips for testing once they have been evaluated by CERN.

CERN is currently planning a single production run of the HPTDC chip in mid-to-late 2003 and we would need to order the full complement of HPTDC chips for the TOF system at that time. We could in principle have our own production run at a later time but this would entail some increased cost.

4.6.3 TTST

The purpose of this card is to serve as an interface to allow convenient testing of the completed trays (MRPC modules plus TFEE) without having to communicate with the full STAR DAQ to get the data out. This board has the same footprint as TDIG and plugs into TFEE in the same way as TDIG. The TTST board contains NIM signal level conditioning circuits to make the TFEE preamp and discriminator

outputs compatible with CAMAC TDC & ADC modules. The combination of TFEE and TTST has exactly the same electronic functionality as the TOFr FEE boards (see sections 4.6.1 and 5). Only a few of the TTST boards are needed at each location in the project where fully-assembled trays are being tested.

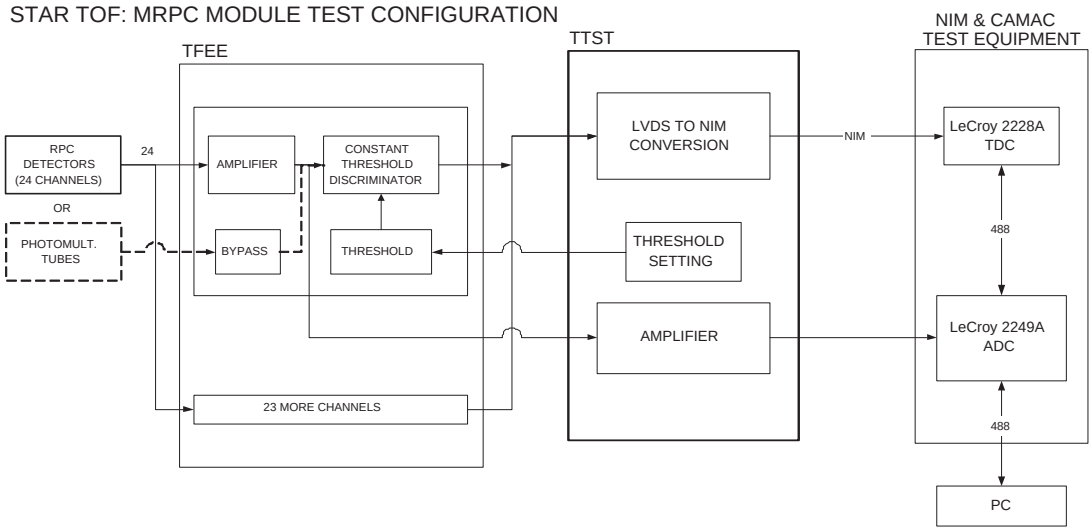

Figure 37: The functional diagram of the construction test electronics chain TFEE to TTST to CAMAC.

4.6.4 TCPU

The TCPU circuit card functions as a data concentrator and interface between the external experimental environment and the STAR TOF data acquisition electronics (TFEE and TDIG). The TCPU is implemented as a combination of embedded CPU and programmable logic. The TCPU functions at the detector tray level, and our design has one TCPU per tray. The TCPU concentrates data from 192 detector channels.

The TCPU performs the following functions (see Figure 38):

- **Multiplicity** – Once per beam crossing, the 8 TDIG cards in a tray each provide multiplicity data as a 5-bit value representing from 0 to 24 hits. From these data, the TCPU computes 2 multiplicity sums, each the sum of 4 TDIG inputs, or 96 channels. Each half-tray multiplicity sum is sent to the STAR Level 0 trigger as 7 differential signal pairs, using either PECL or LVDS drivers.

- **TDC readout** – The TCPU will provide readout signals to the 32 TDCs in the tray. It will receive data from the TDCs, buffer the data, format the data, and send it out via the TMIT daughter board. In the process of building data packets from buffered data for transmission via the TMIT board, the TCPU will perform data token management, using tokens received via trigger commands.

- **System configuration** – Prior to data acquisition, the TCPU configures the TDCs, sets the discriminator thresholds, and initializes the trigger command processing and high speed data transmission blocks. Configuration parameters are loaded from on-board EEPROM storage or read from a host PC over the host serial bus. The TCPU sends configuration data to the TDCs over a JTAG daisy chain. The threshold DAC configuration data travels over a separate 2-wire communication path.

- **System status** – System status information includes TDC configuration echo via JTAG, threshold DAC echo via the 2-wire communication path, and temperature monitor information via the 2-wire communication path. We will likely implement limited built-in self-test capabilities in the TDIG and TCPU cards. This information will be included in the system status.

- **System timebase conditioning** – The TCPU will receive a system level beam crossing clock from the RHIC V124 modules. It conditions this signal by PLL frequency multiplication and filtering techniques to produce a TDC sampling clock with acceptably low jitter characteristics.

- **Trigger command processing** – The TCPU will receive and process commands from the trigger. It will also simply pass some commands such as Abort and L2 Accept on to DAQ via the TMIT card.

4.6.5 TMIT

The TMIT takes formatted data from the data/command buffer, serializes it and transmits it over a fiber optic link to the TDRC. The TMIT will be implemented as a PLD (or a communications chip specific to the communications protocol) and an optical transmitter.

4.6.6 TDRC

The TOF data acquisition receiver card (TDRC) contains the optic link fiber receiver to receive data and trigger events from the on-detector fiber transmitter card TMIT. Each TDRC receives data from 4 TOF trays, resulting in a total of 30 TDRC cards for 120 TOF trays.

The principal components of the TDRC are shown in Figure 39. A fiber deserializer receives the data from the optic link fiber and presents it as 20 bit words to a Header Decoder. The Header Decoder determines the type of event received. Fiber data consists of two possible event types: data events and trigger events. On receipt of an event from the fiber, the TDRC decodes what kind of event it is and takes appropriate actions.

On receipt of a data event, the TDRC stores the associated data in one of a possible 4096 buffer locations locally, which correspond to the 4096 tokens possible from the trigger system. The addressing of these buffer locations is determined by

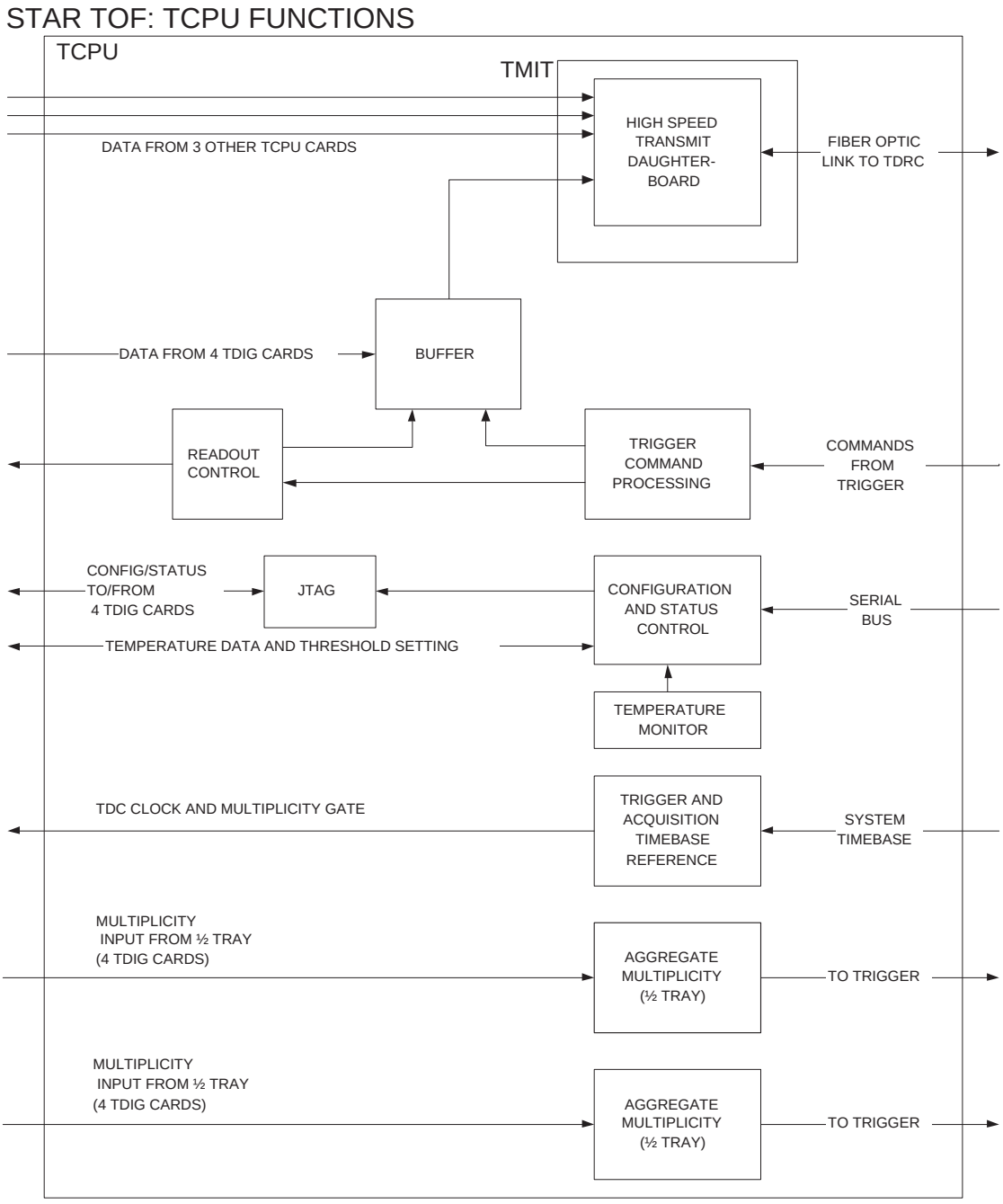

Figure 38: The tray level CPU (TCPU) and high speed data transmit (TMIT) circuit cards.

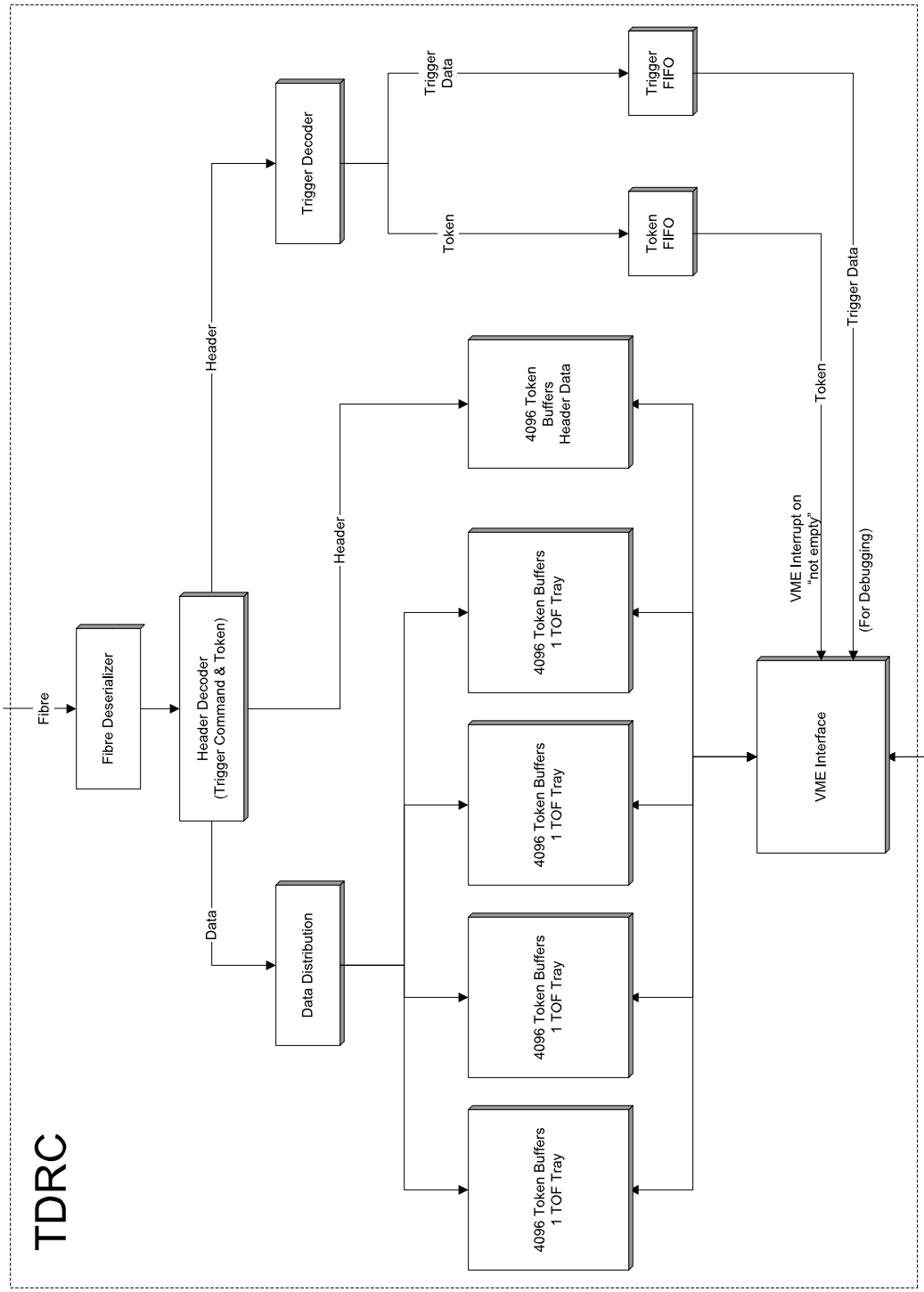

Figure 39: The principal components of the TDRC.

the token number associated with the event. To simplify the buffer structure, the data is subdivided into data from each of the 4 TOF trays, which are stored in one of four buffer regions (possibly implemented as different mezzanine cards to the TDRC). Since the data width from each channel is 20 bits, and the VME interface is 32 bits, it is necessary to store each 20 bit word in a 32 bit memory location (4 bytes). Each event contains 4 sections of up to 384 twenty-bit data words, so for a total of 4096 possible tokens the memory requirement is 384 * 4 * 4096 bytes or 6,291,456 bytes. Since the TCPU of each tray will readout data from two TDC readout chains, the data can further be subdivided into two sections for each tray if memory size is a concern. Each token memory location has associated with it an "invalidate" flag. Before data is written to a token memory location, the invalidate flag is checked to confirm that the previous content of this location is no longer needed. In case of a missing invalidate flag for a token, an error condition is indicated to VME.

On receipt of a trigger event, the data is passed on to trigger decoder logic. Trigger events contain the trigger command word, the DAQ command word, the trigger token, and possibly additional trigger information. Depending on the kind of trigger command word received, the buffer location associated with the token in the trigger event will either be validated (in case of an L2-accept) or invalidated (in case of an abort). In case of a validated event, the associated token is pushed into a FIFO accessible from VME. A VME interrupt can be used to notify the processor in the VME crate of the arrival of a new event. The VME processor will then read the token from the FIFO, read the associated event fragments from the memory locations identified by the token, and invalidate the token memory locations (by setting the associated invalidate flag) so they can be reused. In case of an abort trigger event, the invalidate flag of the token memory location associated with the trigger token will be set, so that this location can be reused for future events. For debugging purposes, a second FIFO will be filled with a subset of the trigger information for each trigger received. This FIFO can also be accessed from VME to verify correct functioning of the trigger logic. For regular running conditions, this second FIFO can be disabled.

A VME interface allows read and write access to the different token memory regions, access to the token and trigger FIFOs, and handles interrupt generation and acknowledgment from VME.

The L2-accept rate from the trigger system is currently limited to 100Hz (the TPC readout rate) but will be upgraded to 1 kHz, so that the data rate from each TDRC presented to the VME interface is 384 words $\times$ 4 bytes/word $\times$ 1000 events/sec $\times$ 4 buffer regions = 6M bytes/sec. Abort triggers need to be handled at rates up to 10 kHz, the same rate as the L0 trigger rate, but those events are never presented to the VME bus.

For economy, two or more of these TDRCs might be combined on one 9U VME card, with one VME interface for those TDRCs. With one TDRC on each VME board, 30 cards are needed to handle all 120 trays. One VME crate can contain up to 10 TDRCs. A total of 3 VME crates is needed for the TOF, each crate with a single board computer and all necessary network connections (Myrinet and Ethernet).

A possible simplification of the TDRC logic can be achieved by not using the

invalidate flag at all. The STAR trigger system is supposed to assure that no two events in the system will have the same token associated with it. A token can only be reused by trigger after it has been returned to the trigger subsystem by DAQ, or an abort has been issued. This architecture should guarantee that an event will never arrive at the TDRC with a token that is currently in use on the TDRC. So the TDRC should always be able to assume that the token buffer for an event received can be reused, either because the previous event has been processed by DAQ and therefore the token has been returned to the trigger subsystem, or because trigger has issued an abort for this token, and the associated event is no longer needed further downstream from the TDRC. The decision as to which logic to use can be made later in the design of the TDRC, since this will probably only require a reprogramming of the programmable logic on the TDRC.

4.7 Power Systems

Low voltage supplies on the STAR platforms are needed to power the on-detector electronics. High voltage of +8 kV and −8 kV is needed to power each MRPC detector. We will evaluate high-channel-density commercial supplies to fill these two roles.

4.8 Test & Monitoring Software

A small-scale DAQ system has been developed for MRPC testing. The digitization is done using CAMAC TDC and ADC modules. To allow flexibility and possibly further test automation a GPIB-based CAMAC controller was used in these test experiments. Object oriented DAQ software, already successfully used in earlier TOFp tests, allows for optimum flexibility in introducing new or adding additional CAMAC modules, controllers, or online analysis software modules. The CERN HBOOK functionality is wrapped in the C++ code such that the output files are written in the standard ntuple format and therefore directly analyzable on any platform at any institution.

For the AGS tests of the TOFr prototype (discussed in section 5 below), additional scripting software allowed the operation of this DAQ in a daemon-like fashion. The software ran extremely reliably and has collected many millions of test beam events so far.

The main purpose of the online software for this system will be monitoring and control. The STAR Slow Controls system is now mature and well-understood and most if not all operational parameters will be set and monitored through this system. Typically the operations include monitoring of temperatures, controlling and monitoring the high voltage and low voltage, monitoring the comparator thresholds, reading/setting the TDC configuration, and monitoring the parameters of the gas system. Including these parameters in STAR Slow Controls system also means that they are automatically added to the online database. This will be helpful in advanced stages of the data analysis to correct for long term drift such as that related to electronics temperatures or from the gas system parameters.

4.9 Start Detector Design

In this section, we present comments on the current start detector, the pVPD, and discuss the advantages of an upgrade to this detector.

The existing pVPD detector was constructed and commissioned within the contingency of the STAR TOFp construction funding. Its purpose is to provide copies of the raw PMT signals and high-resolution discriminator logic signals to be used in NIM electronics on the platform as the the electronic start for the TOFp and pVPD digitization. The pVPD was installed in STAR in Spring 2001 and ran throughout the FY2002 RHIC run. This detector subsystem of STAR-TOFp consists of two identical assemblies of three magnetically-shielded Pb+Scintillator+PMT+Linear Base detectors in the "flashlight" design. These detector assemblies are mounted very close to the beam pipe at a STAR $|Z|$ position of $\sim$5 m; one on the East and one on the West. The front-end electronics are single boards of the same TOFp FEE as are used inside the TOFp tray.

In the most recent RHIC run ending in January 2002, we observed that the pVPD is practically 100% efficient for all but perhaps the most peripheral 5% of the (ZDC/CTB triggered) STAR-standard minimum bias events. (The zero degree calorimeter, ZDC, is detects remnant neutrons at zero degrees.) Another observation was that the pVPD fired in $\sim$60% of the BBC triggered STAR events taken in the January 2002 p+p running. (The beam-beam counter, BBC, coincidence is the minimum bias trigger in p+p running.) After the ZDC, the pVPD is the most forward detector in STAR. There are areas of common acceptance between the pVPD detectors and a few of the most-inner BBC detectors.

In the Au+Au data from this run, we observed sub-50 ps timing resolution of the pVPD. This was achieved by running the pVPD "hot," meaning we ran the pVPD PMT high voltage to the largest possible values for which the pulse area distributions were still >90% on-scale for the LeCroy 2249A ADCs and 8 dB attenuators at each pVPD ADC input. In the Au+Au data, there are numerous hits in each detector channel from very energetic photons which convert in the Pb layer resulting in a large number of prompt photoelectrons. The result is an excellent start time resolution. For the p+p running, the 8 dB attenuators were removed from the TOFp ADC inputs and the pVPD PMT gains were increased by approximately a factor of nine (9) above that used (with ADC attenuators) during the Au+Au running. The data from the p+p run indicate that, when a pVPD channel fires, it is firing on a single particle. The probability that one detector on the east fired and one detector on the west fired in the most recent p+p run was approximately 12%.

There are immutable penalties to the start time resolution when comparing the operation of such a "small-area" start detector in p+p to that in Au+Au. The fact that p+p data means single particle start timing in detectors of this size implies a relatively low number of photoelectrons and hence the intrinsic resolution of the detectors are worse compared to Au+Au (many 10's of prompt hits per detector channel per event). Also, the sparse number of final state particles in p+p data implies that only rarely can one use the average times of many start detectors in the

same event in order to further improve the total start time resolution beyond the intrinsic single channel timing resolution.

The requirements on the performance of the start detector for the proposed large-area TOF system in full energy Au+Au collisions are minimal. In Au+Au with many tens of square meters of TOF coverage, there are many TPC tracks matched to TOF channels. In this case, the start time can be inferred event by event from the stop times with nearly arbitrary precision. According to simulations performed for the TOFp proposal [3], one only needs ∼10 TPC→TOF track matches to be able to infer the event start time solely from the stop times with a resolution of ∼40 ps. This is sufficient to meet the physics requirements for the whole system (start plus stop plus corrections).

However, for p+p collisions and peripheral light-ion collisions, an increase of the acceptance of the start detector would have a significant positive impact in the system as a whole. Obviously the efficiency per event improves. The resolution of the start detector adds in quadrature to the stop resolution of the large area TOF system. An increased acceptance on the start side also enables multiple independent measurements of the prompt particles in the same event, improving the start resolution. This makes some aspects of the offline analysis, which involves a number of corrections independent of those related to the start detector, easier. Initiating an analysis with an intrinsically high-resolution start time in a "large" acceptance reduces the magnitude and uncertainty in all other corrections. Examples of stop corrections made considerably easier by better start timing are the hit position correction and the slewing correction.

The pVPD upgrade would involve:

- replacing the 3+3 pVPD shielded PMT assemblies with approximately 20+20 unshielded mesh-dynode PMT assemblies. This number of unshielded mesh-dynode PMTs fits easily into the same volume occupied by the present pVPD. As almost all of weight of the pVPD is in the six steel plus μ-metal shield assemblies, the upgraded detector as a whole may be lighter than the present pVPD despite the increased channel count.

- replacing the FEE and CAMAC digitization with the same electronics being developed for the stop side in this proposal (see 4.6). Only one minor modification of one board type (TFEE) is needed to make the same electronics chain applicable for both the MRPC input (stop side) and PMT input (start side).

- building two new small light-weight aluminum and Delrin mounting assemblies. Since magnetic shielding is unnecessary for the mesh-dynode PMTs, there are no longer magnetic forces on the mounting structure.

The upgraded pVPD would occupy the same integration volume as the present pVPD, which is close to the beam pipe near $|Z|$∼5 m. This volume does not conflict with the PMD, FPD, and BBC detectors in the vicinity. With the magnetic shields gone, the largest source of backgrounds in other detectors from particle interactions in

the pVPD is removed. The same FEE plus digitization plus communication electronics chain that is presently proposed for the stop side will be used for this upgraded system. The start side like the stop side will be digitized versus a common clock with digital data transmitted off the detector. The economy of using the same basic electronics design for both the start and stop sides of this system requires that the TFEE boards (see section 4.6.1) be designed so that a simple retrofit of 3-4 boards will allow PMT inputs. This involves bypassing the Maxim preamp which is straightforward. The rest of the TFEE circuit remains the same.

The PMTs could be obtained in principle from the STAR CTB, which will have to be decommissioned to make way for the proposed system. However, these PMTs have been damaged by large LED pulses and they afterpulse, a typical problem for Hamamatsu mesh-dynode PMTs as they age. If the TOFp system were decommissioned in the Summer of 2005, there would exist $\sim$40 more mesh dynode PMTs which will have higher gains and better resolution than the CTB PMTs (but which may also afterpulse by then). A possible approach would be to decommission both TOFp and the CTB before the FY2006 run, and take the best $\sim$50 PMTs available. However, the cost estimate for the pVPD upgrade includes the purchase of 50 new Hamamatsu R5946 PMTs.

Twenty detector channels per upgraded PVPD detector is well-matched to the 24 channel TFEE boards. There would be a single TFEE board mounted close to upgraded pVPD detectors, one on each side of STAR. Power to the PMTs would be provided by the HVSys system presently powering the TOFp PMTs. One HVSys bus would power the 20 PMTs on the east, and second bus would power those on the west (there are 4 HVSys busses total).

This upgraded pVPD system, with a high channel count and crossing-by-crossing clocking of the start timing information, would provide multiplicity information to the STAR Level 0 trigger in the same way as the TOF barrel. Providing Level 0 with the primary vertex location via east/west timing differences event by event requires further design but appears to be feasible using the electronics model described in section 4.6.

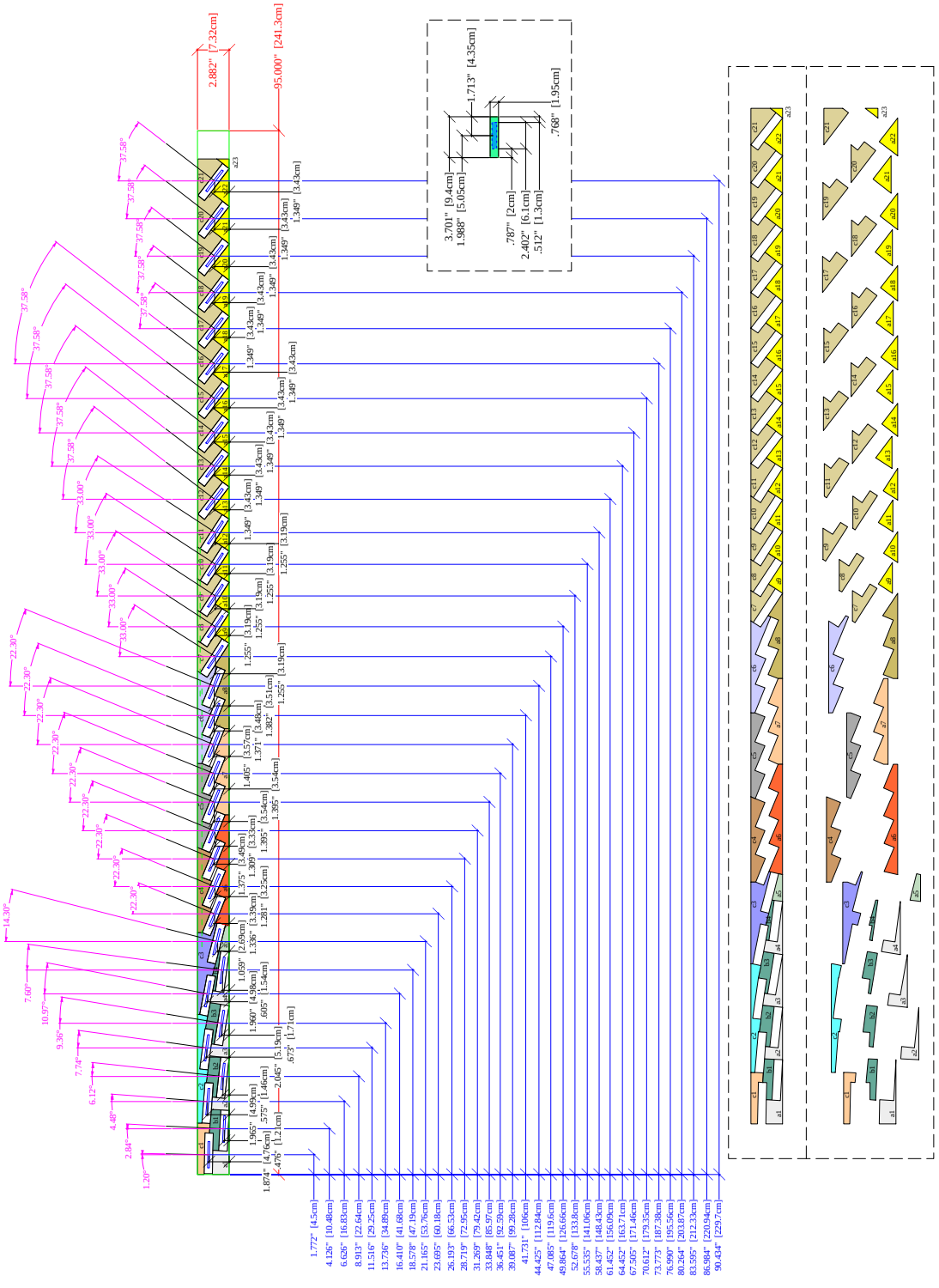

Figure 40: A dimensioned side view of the TOFr tray indicating the detector positioning.

5 The Prototype: TOFr

The MRPC design incorporating six electrode pads was perfected over several years of testing modules at CERN. The test beam setup and other assistance was provided by the ALICE TOF group. We next proposed a 30-module prototype tray [9] with the requisite on-tray electronics, gas system, and high and low voltage distribution. The shape of this tray is identical to those in the STAR CTB (125 trays) and TOFp (1 tray) subsystems built by the Rice group.

The construction was completed in February 2002 and the system was transported to BNL where it was tested in a radiation area near the E949 experiment at the AGS for 70 days in the spring, 2002. It is now installed in STAR and will be operational for the FY2003 RHIC run. Section 5.1 describes the construction of this prototype tray, TOFr, and section 5.2 discusses the results obtained from the AGS tests.

5.1 Construction

The dimensioned side view of the module geometry of the TOFr tray is shown in Figure 40. The $\eta\sim0(1)$ end is on the left(right) side. The design supports the insertion of 33 MRPC modules. For TOFr, 28 modules were installed, 24 of these produced by the Chinese groups and 4 produced at CERN. The CERN modules were slightly thicker than the CN modules, which was handled by simple retrofits.

The mechanical support of the MRPC modules in three dimensions was accomplished using so-called "sawtooths". These are shown at the bottom inset of Figure 40. The sawtooths are 48 differently-shaped pieces of "hexcell" (phenolic-impregnated Kraft paper honeycomb, 1/4" thick) which are glued to the inside walls of the tray. The modules rest inside precisely located voids in the hexcell sawtooths. To fabricate these sawtooths, each pattern was printed to scale on paper. Two layers of hexcell were attached to each other and the pattern by double-sided tape. A band saw was used to cut out the pattern. This resulted in two sawtooth pieces for each shape, one attached to the left side of the tray and the other to the right.

The 96 sawtooths required in total are categorized as "A", "B", and "C". The A sawtooths were glued to the bottom inside walls for the full length of the tray. The TOFr tray after this step is shown in the left side of Figure 41. Next the lower row of modules was installed, resting on the upper edges of the A sawtooths. Then the B sawtooths were glued on the tray inside walls, just above this layer of modules. Then the rest of the modules were installed. Finally, the C sawtooths were glued into position. At this point all modules were mechanically secure inside the tray. The TOFr tray after this step is shown on the right side of Figure 41.

Once the detectors and sawtooths were installed, the interior high voltage and gas piping was installed. The 28 modules in the TOFr tray are connected to one of two interior HV busses, A and B. The "A" bus powers the 19 best chambers (lowest noise rate and dark current), while the "B" bus powers the other 9 modules. The gas piping is $\sim$3/8" OD plastic tubing running from the end plate at the high-z end all the way to the low-z end inside the box.

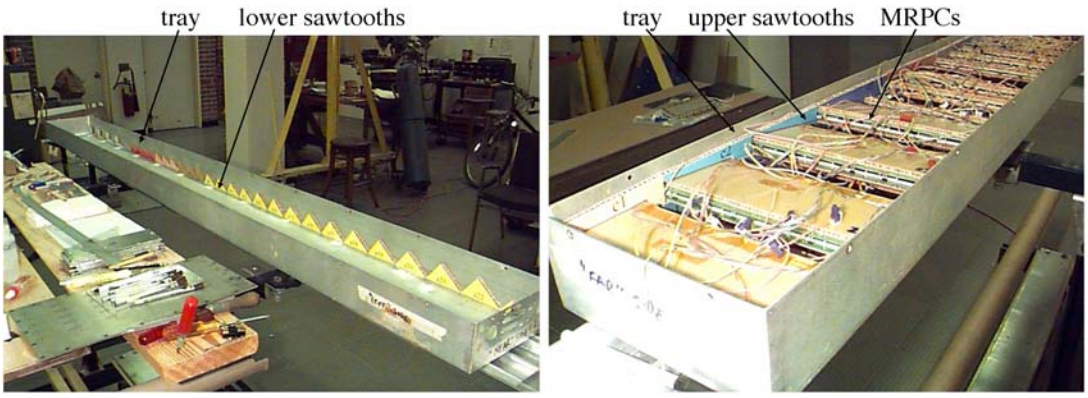

Figure 41: On the left, the lower sawtooths in position in the TOFr tray, and on the right, the TOFr tray filled with 28 MRPC modules snugly positioned by all three layers of sawtooths.

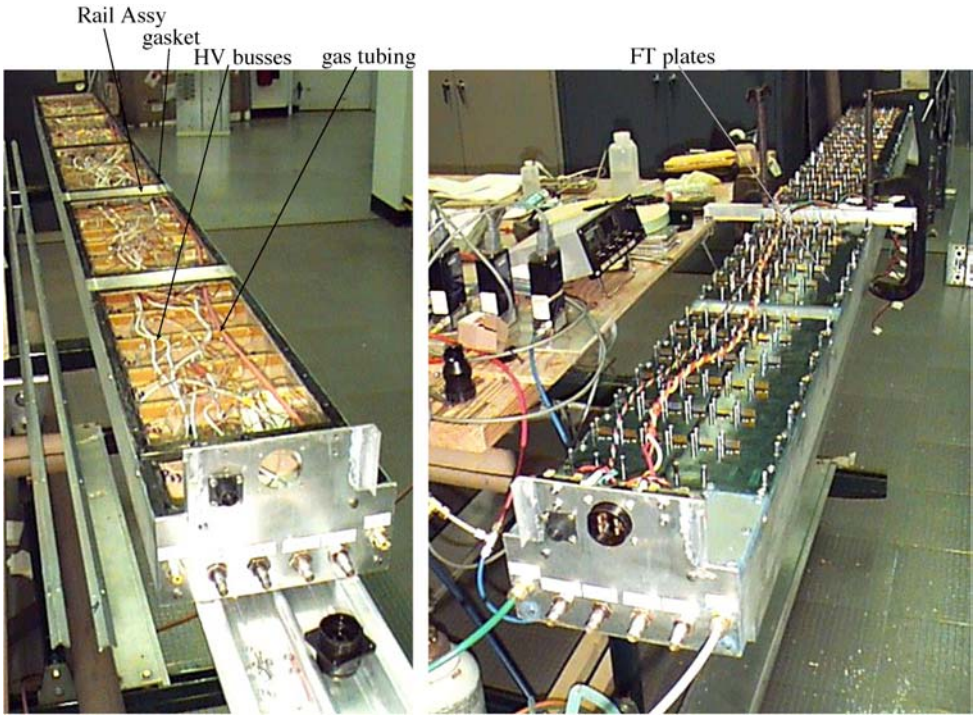

Figure 42: On the left, the TOFr tray after the completion of all interior piping and cabling and the installation of the gasketed rail assembly, and on the right, the TOFr tray with the feedthrough plates installed.

Next, the "Rail Assembly" was installed, which supports the feedthrough (FT) plates from below. The rail assembly is a single piece of aluminum, formed by butt-welding flat plates to 4 pieces of tapped 0.5" aluminum angle. The assembly as a whole fits exactly into the top opening of the box. The assembly is bolted horizontally to the tray walls with 8-32 stainless steel or brass machine screws. The FT plates bolt

vertically onto the top of the rail assembly, which closes the gas volume around the detectors. These vertical bolts pass through a gasket of 1 mm-thick neoprene rubber. A view of the TOFr tray with this rail assembly installed is shown on the left side of Figure 42.

With the rail assembly installed, the 28×6 short twisted-pair cables that carry the detector signals from the modules were connected to pins on the underside of the FT plates. These plates were then bolted down to the rail assembly.

For leak checking, Freon gas was flowed through the tray. We found some leaks at the rail assembly/FT plate interface. The leaks were stopped with small amounts of RTV silicone. The leak checking was performed using a Freon sniffer with a maximum sensitivity of 0.4 l/year.

Once gas was flowing through the TOFr tray without leaks, the 28 TOFr FEE boards (see section 4.6.1) were mounted on the top of the FT plates using screw posts. Connectors on the underside of the TOFr FEE boards mount onto the same pins to which the detector signal pigtails are connected underneath the FT plate inside the gas box. The low voltage needed by these boards is ±6.5 V, which is distributed to the 28 FEE boards on two busses of 14 FEE cards (14 modules) each. These low voltage busses are individually fused at the high-z end of the tray. Each of the TOFr FEE boards also independently includes overvoltage protection, overcurrent protection, and input protection.

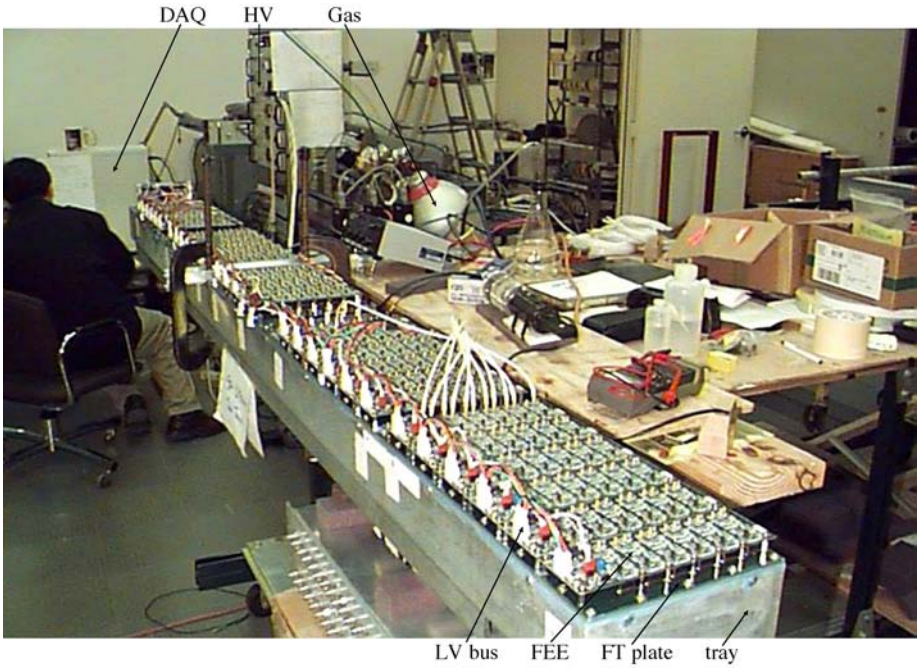

Figure 43: The completed TOFr tray, now with all FEE boards installed and gas flowing for cosmics and noise testing at Rice.

Shown in Figure 43 is the fully constructed TOFr tray under test at Rice in February 2002. The low-z end of the tray (left side of Figure 40) is closest to the

observer. The feedthrough side is at the other end. One can see the individual TOFr FEE boards mounted onto the FT plates on the top of the tray. The low voltage and discriminator threshold distribution is seen above the electronics along the long side of the tray closest to the observer.

Once gas was flowing for ∼24 hours, the high and low voltage systems were powered up. Noise rate data was then collected for all 168 channels as well as the total dark current as a function of time for the A bus and the B bus and cosmic ray data in a few select channels.

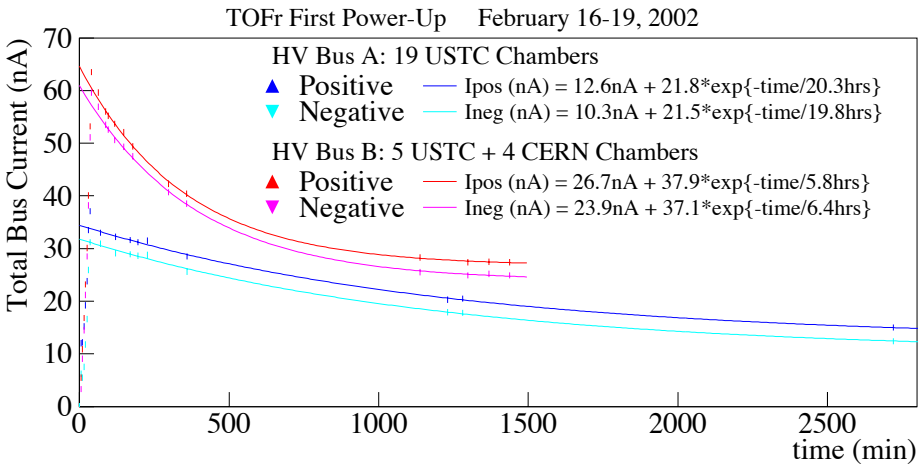

Figure 44: Results on the total HV current draw from the very first power-up of the TOFr tray.

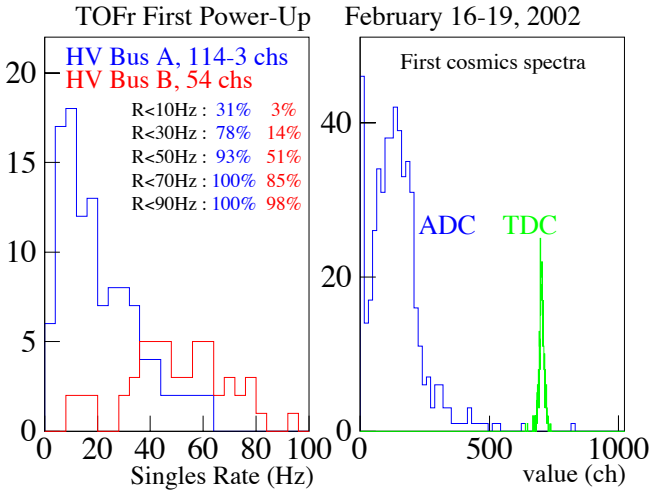

Figure 45: Results on the noise rates from the very first power-up of the TOFr tray.

Figures 44 and 45 summarize the results from these tests from the first power-up of the TOFr tray in February, 2002. In Figure 44, the total bus current for the A bus (blue & cyan) and the B bus (red & magenta) are shown. Anything below ∼50 nA on a single bus is acceptable. One observes however that, given ∼24 hours for the

system to settle down once the HV was applied, the total bus current on the A(B) bus was <20(30) nA, or <1(∼3) nA/module for the 19(9) modules on this bus. The total dark current was thus as expected based on the dark current measured in single chambers.

Shown in the left panel of Figure 45 are histograms (one entry per MRPC channel) of the noise rates from TOFr - the A bus channels are the blue histogram while the B bus channels are the red histogram. The percentages labelled in the left frame are the fractions of the total number of MRPC channels with noise rates less than the labelled rates. As expected from previous measurements, the A bus chambers are less noisy than the B bus chambers. That is, ∼93% of the bus A channels have noise rates below 50 Hz, while only ∼51% of the bus B channels have noise rates below this value. We conclude that the tray environment does not significantly affect the noise rates of the chambers. On average, the B bus modules have noise rates of ∼50 Hz, larger than the 10-20 Hz noise rates for the A bus chambers. This is still acceptable for operation in STAR. The right frame of Figure 45 shows an ADC distribution (blue) and uncorrected TDC distribution (green) using small paddles above and below the tray to trigger on cosmic rays. The ADC distribution obtained is comparable to those obtained in CERN test runs, another indicator of the excellent performance the TOFr tray.

These results were from the first power-up of the TOFr tray. The system has since been transported to BNL and is now installed in STAR. The results from the testing of this tray in an AGS radiation area in the spring of 2002 are discussed in section 5.2 below.

The bench tests at Rice and the extensive testing at the AGS constitute a proof of principle for the proposed large-area TOF system. The MRPC technology is mature and the feasibility of the proposed system is not in question. The TOFr construction exercise has successfully removed most of the uncertainty from the construction of a large-scale system.

While most of the construction techniques used to build the TOFr tray are appropriate for the proposed system, there are a few aspects of the TOFr construction that can be improved for construction of 125 such trays. These areas include:

- **Sawtooths** – Constructing 96∼120 sawtooths for the full system using the technique used for TOFr would be overly labor-intensive. As the detectors are positioned by the shapes of these pieces, it is important for the overall performance of the system that these pieces be made with tight tolerances. We aim to minimize the number of different sawtooth shapes required and to find a way to cut the pieces automatically.

- **Tapping** – In each rail assembly, there are approximately 200 tapped holes in the angle aluminum. We will study alternate designs that involve fewer tapped holes in the rails, and/or welds in place of machine screws in certain locations.

- **Rail Assembly** – The rail assembly for TOFr was produced in-house, and was labor-intensive even after all the holes had been tapped. The rails and cross

plates must be temporarily-installed in a tray, removed as a single unit, and then welded together at many points. This procedure insured a solid custom rail assembly for TOFr, but the fabrication of many of these assemblies might best be shopped out (presumably to the same company making the trays).

- **Gasketing** – In TOFr, the gaskets were glued to the rail assembly. This was very difficult, and it was by far the most labor-intensive aspect of the TOFr construction. In the full system, the gaskets will not be glued to the rail assembly, only greased. As the gaskets are held in place all the way around their periphery by the vertical bolts through the TFEE plates, there is no concern a gasket could "squeeze-out" in such a geometry.

- **Unnecessary holes** – The trays used for the CTB and TOFp detectors include some holes in the bottom of the tray which are unnecessary for this system. Also the tray feet are riveted to the tray body, which adds ∼20 more holes in the tray, all of which must be individually sealed against gas leaks. For the proposed system, unnecessary holes will be eliminated and the tray feet will be welded to the tray body by the manufacturer. This not only removes many holes but also strengthens the feet's connection to the tray body.

We are now in the process of exploring the various alternatives in order to simplify as much as possible the construction of the full system. Also, as discussed in section 7, we plan to install eight trays in time for the FY2005 RHIC run. The commissioning of these eight production trays during the FY2005 run will allow us to integrate and test a substantial system before the remainder of the full system is installed for the FY2006 run.

5.2 TOFr Testing at the AGS

The TOFr tray containing 28 6-channel MRPC TOF modules was transported to BNL for testing and was set up on the floor of the AGS near Experiment 949 on March 18, 2002. The modules in this tray are identical to those we plan to use in the full TOF system. The FEE cards are nearly the same as the TFEE cards in the final design (see sections 4.6.1 and 5.1). The TOFr system contains no on-board TDCs, so the test setup at the AGS used CAMAC TDC and ADC modules to record the start and stop times and to make the various corrections.

The TOFr tray was tested in this beam for a total of ten weeks. Shown in Figure 46 is a photograph of the TOFr tray during this running.

The beam is not actually a test beam but rather a radiation area on the floor of the AGS near Experiment 949. We were able to determine that the beam contained a significant non-relativistic momentum spread by looking at the width of the time distribution in a scintillator separated 20 cm from the start scintillator and then 190 cm from the start scintillator. There also seems to be significant radiation of the entire tray during the two-second spill. The dark current was 60 nA during the 2 s

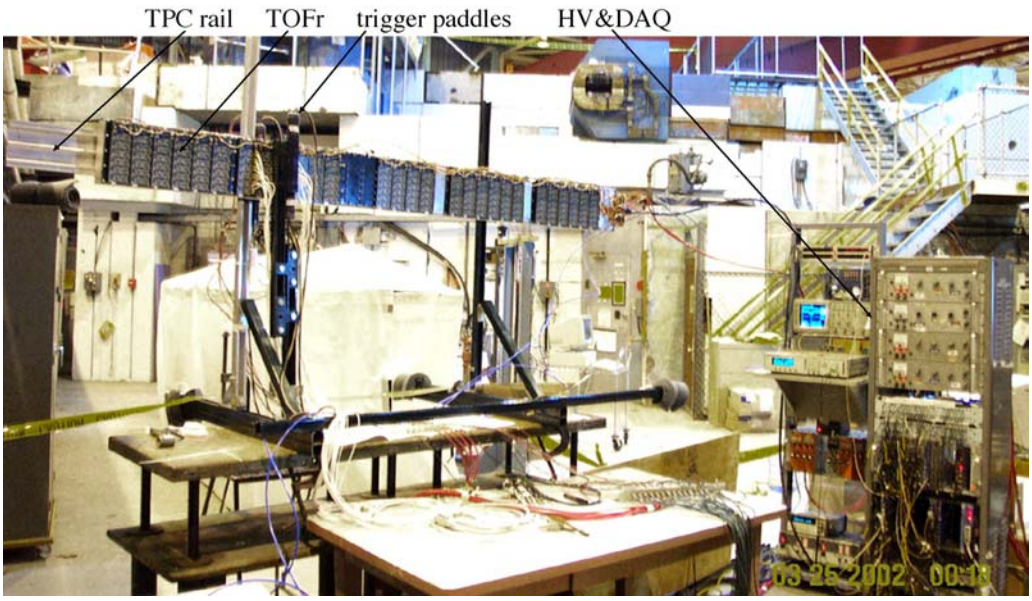

Figure 46: The TOFr tray operating in an AGS radiation area near E949.

spill and dropped to 30 nA during the quiet 3 s of the cycle. The dark current was otherwise 10 nA when the AGS was not operating.

The active region of a 6-channel MRPC module is defined by the transverse dimensions of the five inner glass sheets, 6.1×20.0 cm. The trigger defined a rectangular beam spot of 4×19 cm so most of the active area was covered and hits could occur in any of the six channels in a module. When testing with a large-area trigger like this, one calculates a single efficiency for the module rather that an efficiency for each pad, as was possible in the CERN tests. That efficiency is just the number of triggered events with a TDC stop in any of the six channels divided by the total number of triggered events.

One of the important tests made at the AGS was to determine the optimum threshold and high voltage for operating the chambers. The previous test at CERN with earlier versions of the module and FEE design used a threshold control voltage equivalent to 2.1V in the current FEE. In these previous tests, it was observed that one can operate the modules with 95-97% efficiency at 15.0-15.5 kV. The typical noise rates for the modules tested at CERN were 60-90 Hz. The noise rate is the number of signals above the discriminator threshold (which includes actual hits from cosmics as well as the intrinsic detector noise).

The noise rates for the latest modules built in China in the prototype tray were almost a factor of 10 lower than the rates seen on previous modules. Data was collected at thresholds of 2.2V, 1.7V, and 1.2 V at operating voltages from 13-16 kV to determine the efficiency and time resolution at each threshold and high voltage setting. The results are shown in Figure 47.

A start-subtracted time resolution of about 80 ps was achieved. The signals propagate along the length of the 3.0cm×6.1cm copper pick-up pads at a rate of

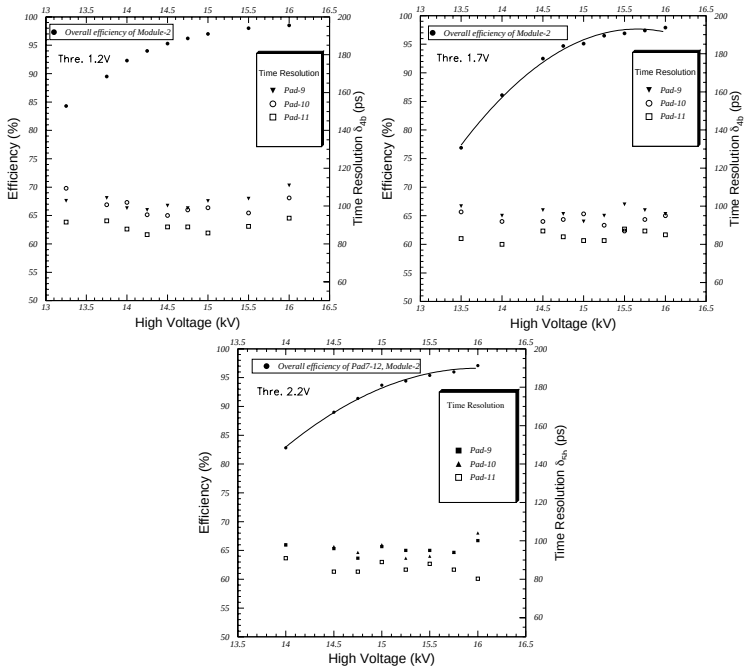

Figure 47: The efficiency (left axes) and time resolution (right axes) versus the high voltage at specific thresholds, 1.2V (upper left frame), 1.7V (upper right frame), and 2.2V (lower frame), obtained from the AGS tests of the TOFr tray.

40 ps/cm. Since the particle firing the trigger can be distributed along any 4 cm of this pad, there is a 45 ps smearing of the stop time by the signal propagation time inside the pad. Subtracting this in quadrature from the 80 ps stop resolution indicates that a 70 ps stop resolution would be achieved if the particle position were known to a few mm as it will be in STAR. Given the beam condition at the AGS, the results are very good and fully consistent with the 60 ps result achieved in the CERN test beam runs.

Table VII: Results from the AGS tests of TOFr giving the noise rates at HV and threshold settings leading to module efficiencies of $\geq$95%.

Efficiency (%)	Threshold (V)	HV (kV)	Noise (Hz)
95.2	2.2	15.5	7.5
95.0	1.7	15.0	7.9
95.2	1.2	14.5	7.1

High voltage and threshold settings were chosen at which the module is 95% efficient. The results are shown in Table VII. It was concluded that it is optimum to operate the modules at 14.5 kV with a 1.2V threshold. This lower operating

voltage will increase the width of the plateau at which the modules operate efficiently without streamers. This should also allow the modules to be somewhat more robust to mechanical imperfections that might occur during construction.

The TOFr system was operated without SF6 for the final two weeks of testing at the AGS. The results showed that the system could be operated at a reduced voltage of 14 kV and 95% efficiency. The high voltage plateau above 95% efficiency with streamer-free operation was slightly smaller but still of order 500 V. The dark current was unchanged and the noise rates were either unchanged or only slightly larger. Although the AGS tests did not constitute a precision test of timing resolution, the preliminary indication is that the timing resolution was the same with the 2-component gas without SF6. We plan to operate the TOFr system in STAR without SF6 to confirm that this mode of operation is possible.

5.3 TOFr in STAR in RHIC Run-III

While the MRPC detectors performed well at the CERN test beams (section 4) and in an AGS radiation area (section 5.2), an additional important proof of principle test was to show that MRPC technology, and more importantly an integrated system with a large number of channels could work well in the STAR environment. To test this, the TOFr protoype tray was installed in STAR and run continuously throughout RHIC Run-III. A summary of the results of this test including preliminary results on timing performance during the d+Au portion of RHIC Run-III are presented in this section.

The specific technical goals of this test included:

- Installation and integration of an MRPC-based TOF system in a collider experiment for the first time.
- Operation of a multi-detector prototype in a quasi-steady state over the entire run to gain experience on the reliability of the system and assess possible aging effects.
- Collection of sufficient data in specific configurations (based on the choice of the gas mixture, detector high voltage, and discriminator threshold) to make statistically significant evaluations of the timing and PID performance to optimize the final design. (The choice of gas is one example. It is not clear that SF-6, a gas used during the detector development phase, is necessary. This gas is potentially detrimental to the STAR TPCs.)
- Comparison of the performance of TOFr to TOFp (see appendix B) in the same RHIC data. Both systems use exactly the same start signals from the pVPD, so the stop timing performance from the two systems can be compared directly, given consistent cuts on the sample of tracks matched to the two systems. This provides an important apple-to-apples comparison of the well-understood conventional technology of scintillators and PMTs to the new MRPC technology.

RHIC Run-III provided significant TOF data sets for full energy d+Au and p+p collisions. Twelve MRPC modules (72 channels total) were read out. These included the nine lowest rapidity modules, and two others at higher rapidity. The FEE were the same as those used in the TOFr AGS tests (see also section 4.6.1). The high voltage was provided by a new CAEN SY-127 unit that is also a candidate for use in the full TOF barrel system. The signal cabling was the same as that for the TOFp detector; it is based on high performance Belden 9310 signal cable, and fast, cross-talk free, line driving before digitization by Phillips Scientific 706 Discriminators. The analog(timing) signals were digizited in LeCroy 2249A ADCs(2228A TDCs). The digitization control and the interfaces to the STAR Trigger and DAQ Systems were provided by the existing components of the TOFp System.

Since the acceptance of TOFr subtends only $\sim 1/300^{th}$ of the outer cylindrical surface of the TPC, a special STAR Level-0 trigger was set up to trigger on events with TOFr hits and a valid pVPD coincidence. The unused second outputs of the line driver PS706 discriminators were "or'ed," leading to a single yes/no logic signal if any active channel in TOFr was struck. This signal was "and'ed" with two signals active if any channel in the pVPD East and West detectors, respectively, were struck. Also included in the logic was a simple primary vertex cut based on maximum allowable values of the timing difference of the pVPD East and West signals. This trigger enhanced the valid TOFr hits by a factor of 40 and 400 in d+Au and p+p collisions, respectively. The special trigger data sets in d+Au and p+p collisions were taken in March and May of 2003, respectively.

In the d+Au running, significant data sets were collected in two specific TOFr configurations - one in which the gas was only Freon R-134A, and the other with 95% Freon R-134A and 5% isobutane. During the period of RHIC Run-III days 24 to 70, STAR collected approximately 25M d+Au events with minimum-bias triggers. The pVPD fired in 6.6M of these events. Approximately 700k(1.6M) total TOFr(TOFp) hits were collected without the special trigger, and 2.4M(0.6k) total TOFr(TOFp) hits were collected with the special trigger. Per detector channel, the totals were $\sim$12k(45k) without the special trigger, and $\sim$35k(20k) with the trigger, for TOFp(TOFr). These samples are sufficiently large to allow detailed analysis and comparison of the timing and PID performance between the different technologies and for different MRPC configurations.

In addition to providing essential data for assessing detector performance, the data acquired during these tests provided important scientific results not possible with the particle identification capability of the TPC alone. Examples include:

- Identified particle "Cronin" effect up to 3 GeV/c in transverse momentum.
- Proton/anti-proton spectra up to 3 GeV/c; dE/dx for these particles from the TPC alone extends only to transverse momenta of $\sim$1 GeV/c
- Distinguishing flow effects from other dynamical effects by comparison of the identified particle transverse momentum spectra for p+p, d+Au, and Au+Au

collisions; distinguishing flow effects arising from the partonic versus the hadronic stage of the collision.

The analyses of the Run-III data are ongoing. Fig. 48 shows the preliminary results of particle identification from $1/\beta$ from time of flight measured by TOFr as a function of the particle momentum measured by the TPC tracking. Although the calibrations are still being optimized, a stop time resolution of ∼100ps from the 72 TOFr channels in the d+Au data set is observed. The data set from p+p collisions is being analyzed.

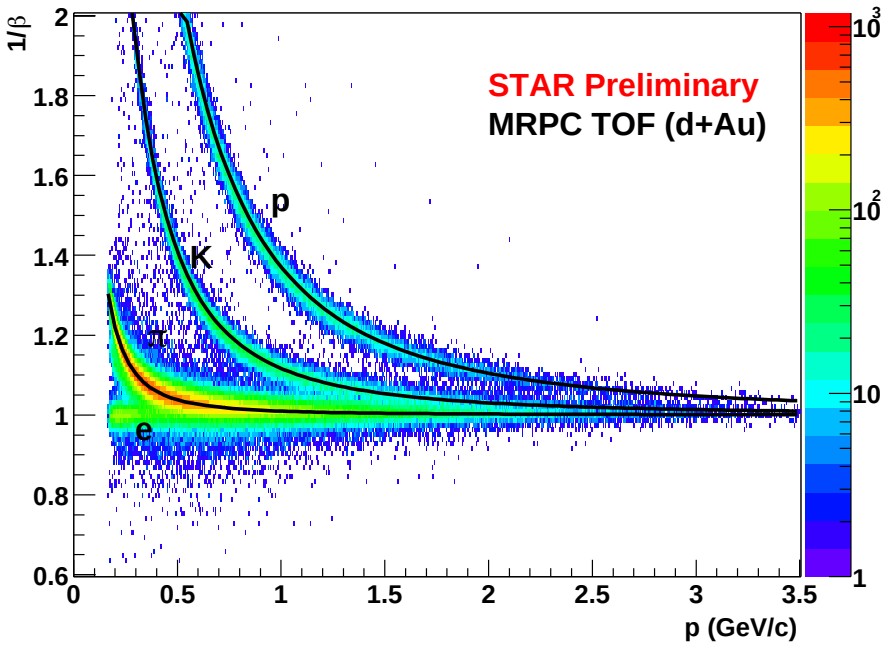

Figure 48: Inverse velocity vs momentum from 2.6 million TOFr+pVPD-triggered events in d+Au collisions.

In addition to the hadron PID capability, with the combination of TOF information and TPC dE/dx information, it is possible to cleanly identify electrons from low p_T (≃0.2 GeV/c), where the EMC has poor energy resolution and low electron identification capability, to very high p_T (≃3 GeV/c) where the EMC can do a good job. The new electron identification capability combined with large coverage of TOF and TPC will enable STAR to effectively reconstruct the J/Ψ and other vector mesons. The left top panel of Fig. 49 shows the charged particle dE/dx from the TPC as function of the momentum. At p<1.5 GeV/c, there are substantial overlaps between the electron dE/dx and the hadron (pion, kaon, and proton) dE/dx. The left bottom panel of Fig. 49 shows that an electron band can be cleanly separated in the entire momentum range by requiring $|1-\beta| < 0.03$ from TOFr. The dE/dx distribution after the TOFr PID selection for $1.0 < p < 1.5$ GeV/c is shown in right panel of Fig. 49. Only pions and electrons are visible and they are well separated.

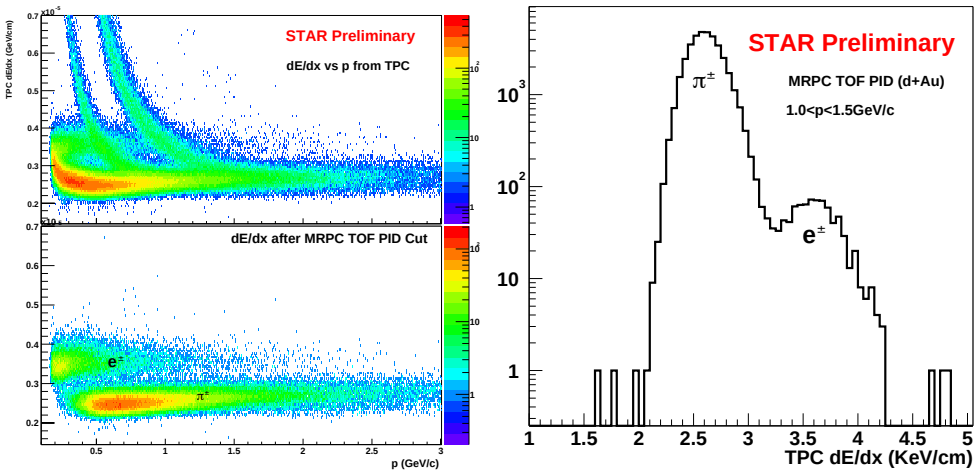

Figure 49: Left top: TPC dE/dx vs the momentum in d+Au collisions. Left bottom: TPC dE/dx vs the momentum after TOFr PID selection of $|1-\beta| < 0.03$. Clean electron identification is achieved. Right: dE/dx from TPC after TOFr PID selection (left bottom panel) for 1.0<p<1.5 GeV/c.

6 Construction

The basic design of the proposed system, embodied by the TOFr prototype (section 5), is described in section 4. In this section we present details on the specific quality assurance tests to be performed during the module construction (section 6.1), the tray assembly (section 6.2), and the electronics construction (section 6.3). Also discussed below in section 6.4 are specific issues regarding the integration of the proposed system into the existing STAR apparatus.

6.1 Module Construction & QA

There are six Chinese groups in STAR participating in the TOF project: USTC, Tsinghua, SINR, IMP Lanzhou, IPP Wuhan, and IHEP Beijing. It is anticipated that the Chinese groups will be responsible for MRPC module production for the STAR TOF detector with financial support from the Chinese funding agencies.

The USTC group produced 26 modules in 2001, of which 24 were installed in the TOFr tray. Of the 26 modules, 20 were characterized by low dark currents and normal ADC spectra in all six channels. The other six modules had slightly higher dark currents and had abnormal ADC spectra in one or more channels. The abnormal ADC spectra have a pronounced high tail in the spectra which is due to a phenomenon known as streamers. Streamers are a class of events with abnormally large signals that can result from the glass plates approaching each other too closely, or in extreme cases, from the presence of foreign material or rough places on the glass. Devices that streamer are usable but do not provide as good timing resolution and are therefore

undesirable in the system.

Research is underway at USTC and Tsinghua on how to improve the yield when assembling modules. Research is also underway to investigate methods and procedures to maintain quality while constructing thousands of modules.

There will be 32 MRPC modules in each of 120 trays, or 3840 total modules. The production yield for high quality modules, based our experience from the module production for the TOFr prototype tray, is estimated to be 70%. In order to meet the envisioned construction schedule (complete installation of a full MRPC TOF detector in two years after the approval of the project), two production facilities will be established. The Tsinghua group will lead the mass production effort. Both the Tsinghua and the USTC groups are preparing MRPC mass production facilities. Tsinghua will be responsible for 70%, and USTC for 30% of the total production. All Chinese groups will participate in the MRPC production effort by providing resources and manpower.

The Chinese STAR TOF group is responsible for testing each MRPC module during production. This will include quality tests for every module and detailed characterization for selected ($\sim$20%) modules. The USTC group will coordinate the testing effort in China.

R&D efforts on the production technique and quality assurance procedures are underway at both USTC and Tsinghua. Significant progress has already been made including 1) partial construction of clean space for MRPC assembly; 2) training of qualified personnel for production supervision; 3) preparation of a procedure manual for module construction; 4) establishment of quality assurance procedures; and 5) test equipment setup.

There will be sufficient manpower and technical expertise available to meet the proposed STAR TOF construction schedule once the STAR TOF project is approved by the respective funding agencies in the US and China.

The total space needed for the production at each institution is 800 m^2.

We assume a 70% yield in material preparation. Approximately 30% of materials may not meet our requirements for module assembly during the preparation.

There will be a test setup for module production quality assurance at both production sites, USTC and Tsinghua. There will be two levels of testing for each MRPC module: module quality test and module characteristics test. The quality assurance effort will be led by a team of physicists including graduate students. The USTC group will be responsible for the overall coordination of MRPC production testing.

The module quality tests will be performed for each MRPC production module. This test includes:

- The leakage current for a module should be <10 nA at 15 kV using the regular operating gas mixture.
- The noise rate should be <50 Hz/pad with pad size 31 mm×61 mm.
- The probability for ADC values larger than 3 σ above of the mean ADC value should be less than 10% at 14.5 kV.

The module characteristics tests will measure the amplitude response of each MRPC module from cosmic rays. We propose that only 20% of the produced modules will undergo the test of time resolution and efficiency. With a prototype testing setup at USTC, a timing resolution better than 100 ps has been achieved with cosmic rays. Relative efficiency in a standard setup can also be measured accurately. It is expected that these requirements will be determined when a final testing setup is established for mass production.

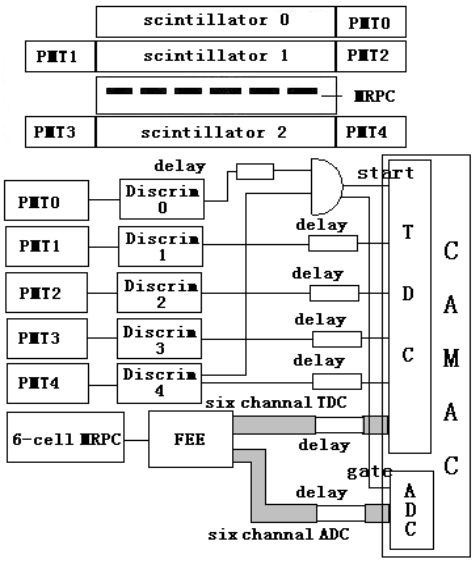

Figure 50: The block diagram of the USTC cosmic ray test apparatus.

The cosmic ray test setup is built using three 22cm×5cm×3cm plastic scintillator counters with photo-multiplier tubes. Figure 50 shows the block diagram of the electronic readout system. A LeCroy 621 discriminator is used for signals from PMT0, PMT1 and PMT2. A constant fraction discriminator ORTEC 851 is used for the signals from PMT3 and PMT4. The coincidence signal between PMT0 and PMT4 provides the cosmic ray trigger for the ADC gate and the start time used for the MRPC digitization. The electronic start is set by the leading edge of the PMT0 pulse. All timing signals (NIM signal from the discriminators) from PMT0 through PMT4 are fed into a CAMAC TDC for digitization. The MRPC module is connected to an FEE card identical to those in use on the TOFr system. The FEE card includes a preamplifier and discriminator for the signal from each MRPC cell. The analog and digital outputs from the FEE card are connected to the ADC and TDC modules. The ADC gate signal has a width of 100 ns. The counting rate for the USTC cosmic ray test setup is approximately 7000 triggers per day covering the 6 channel MRPC module.

The USTC group has established a manual of procedure for MRPC production. This procedure will be refined and used for mass production of MRPC modules in China.

6.2 Tray Construction & QA

The tray which will contain the MRPC modules produced in China will be manufactured in Houston and then shipped to other participating institutions where the final assembly will be performed. A sample of the modules from each shipment from China will be retested before installation in the trays to insure there is no damage to the modules during shipping.

The following quality tests will be performed on the fully-assembled trays.

- All trays will be measured to assure uniformity. The criteria used will be similar to those used for the STAR-CTB trays.
- After tray assembly with FEE cards, gas-tightness tests will be preformed with a freon sniffer and by pressurizing the tray and measuring the decay rate of the pressure versus time. The gas flow rate will be checked with bubbler at a flow rate <2 l/h.
- The leakage current at 15kV will be measured with the operating gas mixture. The current should be <20nA.
- The noise rates should be less than 50 Hz per pad.

These tests will be performed with an electronic setup very similar to that shown in Figure 50. The TTST boards (see section 4.6.3) will be used as the interface between TFEE and the standard CAMAC electronics that will perform the digitization during full tray testing.

6.3 Electronics Construction & QA

Electronics design will take place in Houston. The design will include the additional markup of the bare boards necessary for the fabrication of the electronics ("stuffing") by local industry. Experience has shown that several companies in the Houston area are capable of fabricating stuffed electronics boards appropriate for fast timing systems. The 16 boards for the TOFp system, as well as the ∼40 boards for the TOFr system, were designed at Rice and then shopped out in Houston with great success and with significant cost savings. This model will be used for the construction of the electronics for the proposed system. The specific quality assurance tests to be performed on the electronics are described below.

Once the boards are produced, the following tests will be performed to assure that the boards function adequately. These tests can be generally performed using pulsers for the input signals. For the digitization, a very high resolution oscilloscopes such as the HP Infinium (8 GS/s) used at Rice as well as CAMAC equipment can be used. The following QA tests are envisioned.

- Basic functionality will be checked.

- TFEE – Single channel pure time interval resolution at fixed input pulse height must be below 20 ps. The same test for the TOFr electronics was described above in section 4.6.1 and table VI.

- TFEE – Analog cross-talk must be below 2%, checked on 1-2 pairs of neighboring channels in a random subset of ∼10% of the TFEE boards.

- TFEE – Timing cross-talk must be below 20 ps, checked on 1-2 pairs of neighboring channels in a random subset of ∼10% of the TFEE boards.

- TDIG – The TDC values obtained locally using TFEE+TDIG must be consistent with those obtained independently using TFEE+TTST and digitization in CAMAC equipment, or obtained independently using TFEE+TTST and digitization by a high-sampling-rate oscilloscope.

Additional specific tests are envisioned and will be developed during the design phase of these electronics.

6.4 Integration Issues

Precise details (utility distribution, cabling, etc.) related to the integration of the barrel MRPC TOF detector will be worked out as part of the STAR review process prior to installation. An initial study of integration issues has indicated there are no obvious "show-stoppers", and that the cost of integrating the detector should be modest ∼100 k$. Several potential major issues have been examined including the weight of the detector, and the amount of cooling needed.

Weight

The total weight of a Central Trigger Barrel (CTB) tray, of which there are 120 presently installed, is about 50 lbs, resulting in a total weight for the CTB of ∼6000 lbs. An MRPC TOF tray weighs approximately 70 lbs, so that 120 TOF trays would weigh ∼8400 lbs, or about 20% more. The means of support for both CTB trays and the TOF barrel trays which will replace them is the TPC. The three mechanical elements of the TPC that must carry the additional load are the rails, the support arms, and the gas vessel.

The rails are long aluminum extrusions glued onto the outer field cage of the TPC. Brackets on the bottom of each CTB or TOF tray register the tray's position on these rails and hold them in place. The shear strength of the adhesive used for the rails is ∼3000 psi, and the tensile strength is ∼4000 psi. The peel strength is conservatively estimated to be 20 pounds per linear inch. Assuming a TPC rail behaves rigidly and the weight of the TOF tray is distributed over its entire length (160 inches or ∼4 m), given that the glue bond is is ∼3.5" wide (∼90 mm), the rails should be able to withstand 3200 lb of peel force (load twisting edge away from skin), 1.68 Mega-lb shear (load tangential to skin), and 2.24 Mega-lb tension (load normal to skin). The safety factor for adhesive joints is conservatively estimated to be ∼3, so it is estimated

that a TOF tray could weigh up to ∼1000 lbs (14 times more than design) without endangering the glue bond between the rails and the TPC.

The TPC support arms are two very large aluminum brackets on each end of the STAR detector that support the entire TPC from the steel of the STAR magnet. The weight that each TPC arm was engineered to hold is 25,000 lb, with a safety factor of 3-5 (Star Note 105A)(see LBL EN M7681 and 7682). The TOF detector would increase the present load on each arm by approximately 12% to 28,000 lbs. The original saftey factor was 4.08 for the worst case bolt. The safety factor on the support arms including the additional weight from the TOF system is reduced slightly to 3.6, which is still felt to be conservative.

Additional work will focus on a Finite Element Analysis (based on ANSYS) of the TPC gas vessel to assess the impact of the distributed load over the "as-built" cylinder. This is not expected to present a fundamental problem.

Cooling

Each tray dissipates approximately 200W of power when running. Hence 120 trays dissipate ∼24 kW of power. This generates heat inside the STAR detector and the Wide Angle Hall (WAH) which must be removed.

The baseline plan to address the additional heat load resulting from the TOF barrel is to use air flow for convective cooling of the detector electronics. There is approximately 1.5" of radial space between the present TOF integration envelope and the front face of the STAR barrel EMC. The option being examined is to extend the integration volume of TOF by ∼1" radially, and to install a closed aluminum cover (∼30-40 mils thick) over each TOF tray, about 1" above the electronics, to create a confined space for channeled air flow which would enter and exit through the small ends of the tray. During tray installation, a rail fixture would be used to hold two trays at the same time in a position from which the pair could be slid into STAR as one object. This would allow one to "join" the two trays mechanically and seal together the skins of the trays where they meet end to end. With appropriate ducting near the STAR pole tips, air would be directed through these channels from one end of STAR to the other, insuring a strong and consistent flow of air over the entire length of the electronics. This plan requires the TOF system to be installed from the East side of STAR in the Assembly Building.

The warmed exit air would need to be handled by the A/C system in the Wide Angle Hall (WAH) once the STAR detector was positioned for data acquisition. It is likely that the additional heat dissipated by the barrel TOF detector, along with that of other recently installed STAR subsystems would require an upgrade to the air handling system for the WAH.

Cabling

The plan for the total number of cables, gas lines, fibers, and air cooling ducts that have to be routed from outside to inside the magnet is under development. This will need to address the limited space available for these utility penetrations.

Installation

In addition to the rail fixture used to install the trays onto the TPC rails in pairs, a second fixture will also be necessary. The TPC support arms at 3 and 9 o'clock make it impossible to slide trays onto the rails behind them. A fixture is therefore needed to support the STAR TPC while installing pairs of trays on the rails behind the support arms. The cost of this fixture is estimated to be less than 75 k$.

7 Cost, Schedule, & Management

7.1 Cost

The cost estimate for the TOF construction project is presented in Table VIII. The costs have been estimated based on a combination of engineering estimates and experience constructing similar STAR detectors including the 168 channel TOFr prototype system. Costs shown are in FY2004 dollars.

This cost estimate and the corresponding schedule assume that in FY2004 approximately 234 k$ will be provided for the completion of project R&D and the construction of selected electronics components through a combination of RHIC detector R&D (134 k$) and STAR capital equipment funds (100 k$).

The total cost for the U.S. supported construction project, including an average contingency of 27%, is $4.1M.

Subject to approval by the Chinese funding agencies, the Chinese institutions involved in this project are committed to the construction and testing of ∼4000 MRPC chambers, the full amount required for this detector. This represents a projected in-kind contribution of approximately $2.3M by the participating Chinese institutions.

The fully burdened labor rates used for this estimate were $260/day for technicians at Rice and Texas, $420/day to $480/day for engineers at Rice, $640/day for senior engineers at Rice, and $720/day for mechanical engineers at BNL.

7.2 Schedule

The construction project schedule begins in October 2004 (FY2005) and is predicated on R&D continuing throughout FY2004. A 4-tray prototype system is scheduled to be installed by October 2004. This will allow commissioning of a 4-tray system in the FY2005 run. This experience will help to insure that all components perform as expected, prior to construction of the full system. The project schedule is shown in Figure 51.

The installation of the full system is scheduled to be completed by October 2006, in time to commission and run the full system during the FY2007 RHIC run. Thirty production trays with their on-board electronics and connections to STAR DAQ and trigger are scheduled to be installed by October 2005. The remaining 90 trays are scheduled to be installed by October 2006.

7.3 Management/Project Responsibilities

The management structure for the construction project is shown in Figure 52.

The MRPC modules will be produced in China. This includes QA of the parts used, and a suite of specific tests on each completed detector module. The detectors will then be shipped to the United States in batches. The trays and the tray mechanical pieces will be designed at Rice University, and fabricated out-of-house in Houston. Once delivered to Rice and checked for tolerances, the trays will be shipped to the

University of Texas for tray assembly and testing. The electronics design and integration will be the responsibility of Rice University, while the electronics fabrication will be shopped out. Electronics testing will occur at Rice and UCLA. All collaborating institutions will be involved in the detector installation and commissioning once the system arrives at BNL.

Table VIII: The construction costs, FY2005-2007.

Item	Parts (k$)	Labor Engin. (k$)	Labor Tech. (k$)	Labor (man-days)	Contin-gency (k$)	Contin-gency (%)	Total (k$)	Basis of Estimate
Mechanical&Infrastructure								
Tray Mechanical	100		130	500	58	25	288	TOFr experience
LV System	184				46	25	230	Off-the-shelf
HV System	47				5	11	52	Off-the-shelf
Gas System	32				7	22	39	TPC experience
Racks and Infrastructure	172				43	25	215	TOFp experience
Mechanical Design		30		42	10	33	40	STAR experience
pVPD upgrade	95				15	16	110	pVPD experience
Totals:	630	30	130		184		974	
Electronics								
Design and Integration		291		610	116	40	407	TOFr experience and
			95	375	24	25	119	Engineering est.
TFEE	675				173	26	848	Off-the-shelf parts and
TDIG	730				191	26	921	std. fabrication prices
TCPU	291				78	27	369	-same-
TMIT	30				12	40	42	-same-
TDRC	138				40	29	178	-same-
Testing	12		130	500	36	25	178	Engineering est.
Connections to TRIG/DAQ	49				12	25	61	Engineering est.
Totals:	1925	291	225		682		3123	
U.S. project totals	**2555**	**321**	**355**		**866**		**4097**	
MRPC modules								
contributed by China (U.S. $ equivalent cost)	**1800**				**450**	**25**	**2250**	TOFr experience

113

ID	Task Name	Duration	Start	Finish
1	Four (4) Tray System Installed	0d	10/1/04	10/1/04
2	Funding	0d	10/1/04	10/1/04
3	Four (4) Tray System Commissioning	88d	10/15/04	2/15/05
4	Final Mechanical Review	0d	10/1/04	10/1/04
5	**TOF Construction**	**620d**	**10/1/04**	**2/15/07**
6	**Module Assembly**	**390d**	**10/1/04**	**3/30/06**
7	order MRPC materials	14d	10/1/04	10/20/04
8	MRPC module construction	390d	10/1/04	3/30/06
9	first shipment of modules	0d	12/15/04	12/15/04
10	final shipment of modules	0d	3/30/06	3/30/06
11	**Tray Assembly**	**451d**	**10/1/04**	**6/26/06**
12	Fab all tray bodies,feet,rail assemblies	44d	10/1/04	12/1/04
13	begin tray assembly	0d	12/15/04	12/15/04
14	tray assembly and test	394d	12/15/04	6/19/06
15	Thirty (30) trays arrive at BNL	0d	6/20/05	6/20/05
16	complete tray assembly	0d	6/19/06	6/19/06
17	Final trays arrive at BNL	0d	6/26/06	6/26/06
18	**Electronics**	**620d**	**10/1/04**	**2/15/07**
19	Design Finalized	0d	10/1/04	10/1/04
20	Purchase HPTDC Chips from CERN	0d	10/1/04	10/1/04
21	Testing & Integration	610d	10/15/04	2/15/07
22	Develop Test Procedures	108d	10/15/04	3/15/05
23	Fab and test 50% of TFEE cards	88d	10/15/04	2/15/05
24	Fab electronics for Thirty (30) trays	44d	2/15/05	4/15/05
25	Testing electronics for Thirty (30) trays	110d	3/15/05	8/15/05
26	Fab and test 50% of TFEE cards	89d	8/15/05	12/15/05
27	Fab electronics for Ninety (90) trays	43d	2/15/06	4/15/06
28	Testing electronics for Ninety (90) trays	110d	3/15/06	8/15/06
29	**Installation & Commissioning**	**469d**	**5/2/05**	**2/15/07**
30	Construct gas system at BNL	45d	5/17/05	7/18/05
31	Install fiber links, VME crates, utilities	89d	5/2/05	9/1/05
32	Thirty (30) Tray System Installation	71d	6/24/05	10/1/05
33	Thirty (30) Tray System Commissioning	90d	10/13/05	2/15/06
34	Ninety (90) Tray System Installation	71d	6/26/06	10/2/06
35	Ninety (90) Tray System Commissioning	90d	10/13/06	2/15/07
36	**Project Complete**	**0d**	**2/15/07**	**2/15/07**

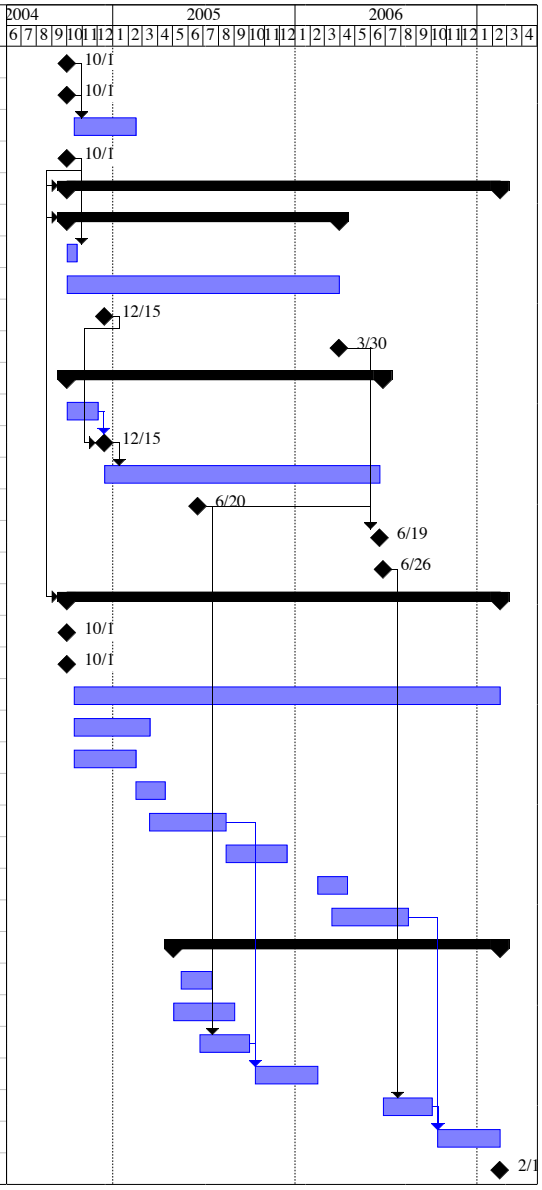

Figure 51: The project schedule for module and tray construction, installation, and commissioning.

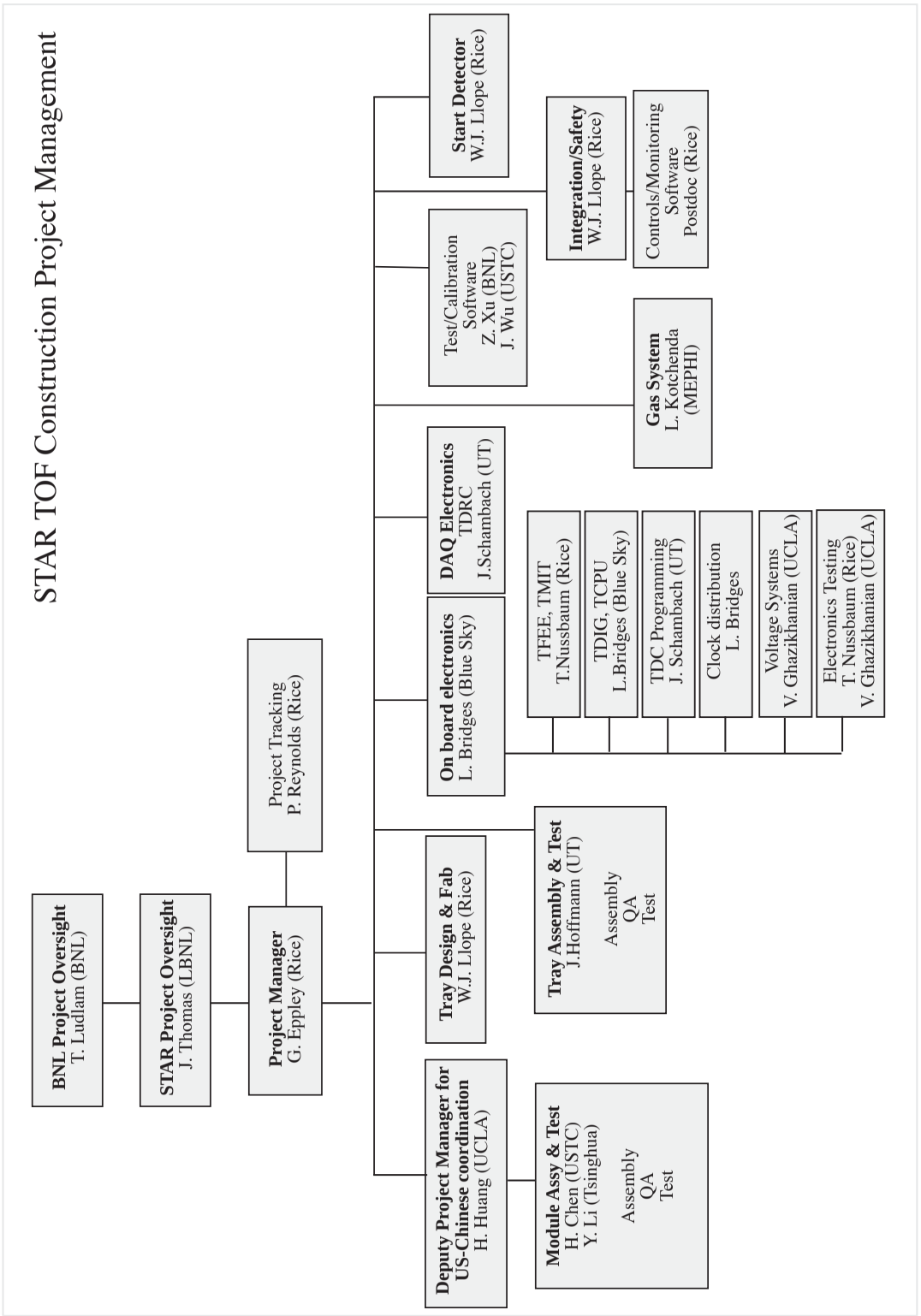

Figure 52: The TOF construction project management structure.

List of Figures

List of Tables

References

[1] http://mac8.rice.edu/~WJLlope/-STAR/-TOF/TOFprop.html; and /TOFpatch.htm;

[2] STAR Notes 36 (1992), 49 (1992), 50 (1992), 52 (1992), 207 (1995), 208 (1995), 209 (1995), 211 (1995), 267 (1996), 326 (1998), and 416 (2000).

[3] W.J. Llope *et al.*, http://mac8.rice.edu/~TOF/TOFp/Documents/TOFp.pdf

[4] STAR Long-Range Plan, http://www.star.bnl.gov/STAR/smd/lrp.html

[5] ALICE Time-Of-Flight Proposal, http://alice.web.cern.ch/Alice/TDR/alice_tof.ps

[6] Letter of Intent, A Time-of-flight System for STAR, November 1, 1999, submitted by B. E. Bonner, G. Eppley, F. Geurts, W. J. Llope, G. S. Mutchler, T. Nussbaum, E. D. Platner, J. B. Roberts and P. Yepes.

[7] M.C.S. Williams, E. Platner, J. Roberts *et al.*, NIM A434 (1999) 362; E. Cerron Zeballos, D. Hatzifotiadou, J. Lamas Valverde, E. Platner, J. Roberts, M.C.S. Williams, A Zichichi; Micro-streamers and the Microgap RPC, document in preparation; A. Akindinov *et al.*, (E. Platner, J. Roberts) Nucl. Instr. Meth. A 456, 16 (2000), B. Bonner, G. Eppley, J. Lamas-Valverde, W. J. Llope, T. Nussbaum, E. Platner, J. Roberts, E. Cerron Zeballos, D. Hatzifotiadou, N-Y. Kim, A. Semak, M.C.S. Williams, "A Multigap Resistive Plate Chamber Prototype for TOF for the STAR Experiment at RHIC," to be published in Procs. Of 9th Vienna Conf. On Instrumentation, Vienna, Feb. 19-23, 2001.

[8] http://www.er.doe.gov/production/henp/nsac/nsac.html

[9] TOFr Proposal, http://mac8.rice.edu/~TOF/TOFr/Documents/TOFr_prop_11132001.pdf.

[10] TOFr Proposal Update, http://mac8.rice.edu/~TOF/TOFr/Documents/TOFr_prop_update.pdf.

[11] S. Bass, private communication.

[12] STAR Conceptual Design Report, LBNL Pub-5347.

[13] M. Gyulassy and M. Plümer, Phys. Lett. B 243, 432 (1990).

[14] X. N. Wang and M. Gyulassy, Phys. Rev. Lett. 68, 1480 (1992).

[15] C. Adler *et al.*, nucl-ex/0210033.

[16] C. Adler *et al.*, (STAR Collaboration) Phys. Rev. Lett. **89**, 232021(2002).

[17] K. H. Ackermann *et al.*, (STAR Collaboration), Phys. Rev. Lett. **86**, 402(2001); C. Adler *et al.*, *ibid*, **87**, 182301(2001); *ibid*, **89**, 132301(2002); *ibid* Phys. Rev. **C66**, 034904(2002).

[18] S. Voloshin, QM02 proceedings, Nantes, France, 18-24 July 2002, nucl-ex/0210014.

[19] P. Huovinen, P.F. Kolb, U. Heinz, P.V. Ruuskanen, and S. Voloshin, Phys. Lett. **B503**, 58(2001).

[20] S. Esumi *et al.*, (PHENIX Collaboration), QM02 proceedings, Nantes, France, 18-24 July 2002, nucl-exp/0210012.

[21] N. Xu and Z. Xu, QM02 proceedings, Nantes, France, 18-24 July 2002.

[22] P. Braun-Munzinger *et. al*, Phys. Lett. **B518**, 41(2001).

[23] N. Xu and M. Kaneta, Nucl. Phys. **A698**, 306c(2002).

[24] G. Baym and H. Heiselberg, Phys. Lett. **B469**, 7(1999).

[25] M. Stephanov, K. Rajagopal, E. Shuryak, Phys. Rev. Lett. **81**, 4816 (1998).

[26] C. Adler *et al.*, STAR Collaboration, "Event-by-event $\langle p_T \rangle$ fluctuations in Au-Au collisions at $\sqrt{s_{NN}} = 130$ GeV," in progress.

[27] J.G. Reid *et al.*, (STAR Collaboration), QM02 proceedings, Nantes, France, 18-24 July 2002.

[28] S. Voloshin and Y. Zhang, Z. Phys. **C70**, 665(1996).

[29] A.M. Poskanzer and S. Voloshin, Phys. Rev. **C58**, 1671(1998).

[30] M. Gyulassy, I. Vitev and X.N. Wang, Phys. Rev. Lett. **86**, 2537(2001).

[31] D. Teaney, J. Lauret, and E.V. Shuryak, Phys. Rev. Lett. **86**, 4783(2001).

[32] C. Adler et al. (STAR Collaboration), Phys. Rev. Lett. **89**, 132301(2002).

[33] D. Teaney, J. Lauret, and E.V. Shuryak, LANL Preprint, nucl-th/0110037.

[34] J.-Y. Ollitrault, Phys. Rev. **D46**, 229(1992).

[35] S. Esumi, *et al.* (PHENIX Collaboration), QM02 proceedings.

[36] Z. Lin and C.M. Ko, e-Print Archive: nucl-th/0207014; *ibid*, Phys. Rev. **C65**, 034904(2002).

[37] M. Gyulassy, I. Vitev, X.N. Wang, and P. Huovinen Phys. Lett. **B526**, 301(2002).

[38] Yu.L. Dokshitzer, V.A. Khoze, and S.I. Troian, Phys. Rev. **D53**, 89(1996); D. Kharzeev, proceedings of "Statistical QCD", aXrive: hep-ph/0111386.

[39] C. Adler et al. (STAR Collaboration), submitted to Phys. Lett. **B**, (2002); e-Print Archive: nucl-ex/0206008.

[40] C. Adler et al. (STAR Collaboration), Phys. Rev. **C65**, 04901(2002).

[41] C. Adler et al. (STAR Collaboration), Phys. Rev. Lett. **89**, 092301(2002).

[42] K. Adcox *et al.*, (PHENIX Collaboration), Phys. Rev. Lett. **88**, 242301(2002).

[43] U. Heinz and P. Kolb, Nucl. Phys. **A702**, 280(2002).

[44] E. Andersen *et al.*, (WA97 collaboration), Phys. Lett. **B433**, 209(1998).

[45] I. Bearden *et al.*, (NA44 Collaboration), Phys. Rev. Lett. **78**, 2080(1997).

[46] H. van Hecke, H. Sorge, and N. Xu, Phys. Rev. Lett. **81**, 5764(1998).

[47] G. Arnison *et al.*, Phys. Lett. B 118, 173 (1982); A. Breakstone *et al.*, Z. Phys. C 23, 1 (1984).

[48] C. Adler *et al.*, nucl-ex/0206006.

[49] D.E. Jaffe *et al.*, Phys. Rev. D 38, 1016 (1988).

[50] H. Heiselberg, Phys. Rep. **351**, 161 (2001).

[51] L. Van Hove, Z. Phys. C **21**, 93 (1983); M. Gyulassy, Nucl. Phys. **A400**, 31c (1983).

[52] S. J. Lindenbaum and R. S. Longacre, J. Phys. G **26**, 937 (2000).

[53] H. Heiselberg and A. D. Jackson, eprint nucl-th/9809013 (1998).

[54] I. N. Mishustin, Phys. Rev. Lett. **82**, 4779 (1999).

[55] S. Pratt, Phys. Rev. C **49**, 2722 (1994).

[56] M. Stephanov, K. Rajagopal, E. Shuryak, Phys. Rev. Lett. **81**, 4816 (1998).

[57] M. Stephanov, K. Rajagopal, E. Shuryak, Phys. Rev. D **60**, 114028 (1999).

[58] B. Müller, Nucl. Phys. **A702**, 281c (2002).

[59] G. Baym and H. Heiselberg, Phys. Lett. B **469**, 7 (1999).

[60] O. Scavenius, A. Dumitru and A. D. Jackson, Phys. Rev. Lett. **87**, 182302 (2001).

[61] S. A. Bass, P. Danielewicz and S. Pratt, Phys. Rev. Lett. **85**, 2689 (2000) [nucl-th/0005044];S. y. Jeon and S. Pratt, Phys. Rev. C **65**, 044902 (2002) [hep-ph/0110043].

[62] J.G. Reid (STAR Collaboration), Nucl. Phys. **A698**, 611c-614c (2002).

[63] R. L. Ray, (STAR Collaboration), "Correlations, Fluctuations and Flow Measurements from the STAR Experiment," in the proceedings of the 16th International Conference on Ultra-Relativistic Nucleus-Nucleus Collisions - *Quark Matter-2002*, to be published in Nucl. Phys. **A** (2003).

[64] T. A. Trainor, "Event-by-Event Analysis and the Central Limit Theorem," eprint hep-ph/0001148 (2000).

[65] E. Schnedermann, J. Sollfrank and U. Heinz, Phys. Rev. C **48**, 2462 (1993); B. Tomášik *et al.* nucl-th/9907096 (2001); Phys. Rev. C **65**, 031902(R) (2002).

[66] M. Gyulassy and M. Plümer, Phys. Lett. B **243**, 432 (1990); X. N. Wang and M. Gyulassy, Phys. Rev. Lett. **68**, 1480 (1992); M. Gyulassy and X. N. Wang, Nucl. Phys. **B420**, 583 (1994); R. Baier, D. Schiff and B. G. Zakharov, Ann. Rev. Nucl. Part. Sci. **50**, 37 (2000).

[67] C. Adler *et al.,* STAR Collaboration, "Disappearance of back-to-back high p_T hadron correlations in central Au+Au collisions at $\sqrt{s_{NN}} = 200$ GeV," submitted to Phys. Rev. Lett.

[68] L. Bettencourt, K. Rajagopal and J. Steele, Nucl. Phys. **A693**, 825 (2001).

[69] M. Bleicher *et al.,* Phys. Lett. B **435**, 9-12 (1998); M. Gaździcki and St. Mrówczyński, Z. Phys. C **54**, 127 (1992).

[70] G. Wilk and Z. Wlodarczyk, "Imprints of nonextensivity in multiparticle production," eprint hep-ph/0011189 (2000).

[71] A. Ishihara, Univ. of Texas at Austin (STAR Collaboration), Bull. Am. Phys. Soc. **46**, 29 (2001); contributed paper given at the Joint Fall 2001 Nuclear Physics Division Meeting of the APS and JPS.

[72] J.G. Reid, T.A. Trainor, Nucl. Inst. and Meth. **A457** (2001) 378-383.

[73] C. Adler *et al.,* STAR Collaboration, "Event-by-event $\langle p_T \rangle$ fluctuations in Au-Au collisions at $\sqrt{s_{NN}} = 130$ GeV," in progress.

[74] M. J. Tannenbaum, Phys. Lett. B **498**, 29 (2001).

[75] H. Appelshäuser *et al.* (NA49 Collaboration), Phys. Lett. B **459**, 679 (1999); H. Appelshäuser *et al.* (CERES Collaboration), Nucl. Phys. **A698**, 253c (2002); J. G. Reid (NA49 Collaboration), private communication.

[76] J. Whitmore, Phys. Rep. **27**, 187-273 (1976).

[77] B. Anderson, Cambridge Monogr. Part. Phys. Nucl. Phys. Cosmol. **7**, 1-471 (1997).

[78] C. Adler *et al.* (STAR Collaboration), Phys. Rev. C **66**, 034904 (2002).

[79] G. Roland (NA49 Collaboration), Nucl. Phys. **A638**, 91c (1998).

[80] S. E. Vance, M. Gyulassy and X. N. Wang, Phys. Lett. B **443**, 45 (1998); Nucl. Phys. **A638**, 395c (1998).

[81] D. Teaney, J. Lauret and E. V. Shuryak, eprint nucl-th/0110037 (2001).

[82] O. Barannikova, F. Wang, (STAR Collaboration), "Mid-rapidity $\pi^{\pm}$, $K^{\pm}$, and $\overline{p}$ yields and spectra in Au+Au collisions at RHIC from STAR," in the proceedings of the 16th International Conference on Ultra-Relativistic Nucleus-Nucleus Collisions - *Quark Matter-2002*, to be published in Nucl. Phys. **A** (2003).

[83] Qingjun Liu, Univ. of Washington, private communication.

[84] C. Adler *et al.* (STAR Collaboration), "Kaon production and kaon to pion ratio in Au+Au Collisions at $\sqrt{s_{NN}} = 130$ GeV," submitted to Phys. Rev. Lett. (2002); W. Deng, see STAR protected web are under: protected/strange/wdeng-/qm2001/support/readme.txt.

[85] T. Ludlam *et al.,* "STAR Future Physics and Detectors – Report of the Bar Harbor Workshop," (June 2002), see http://www.star.bnl.gov/STAR/meetings_l-/collab_l/future/summary.html.

[86] K. Adcox *et al.* (PHENIX Collaboration), Phys. Rev. C **66**, 024901 (2002).

[87] X. N. Wang and M. Gyulassy, Phys. Rev. D **44**, 3501 (1991).

[88] R. L. Ray and R. S. Longacre, eprint nucl-ex/0008009 (2000).

[89] Manuel Calderon de la Barca Sanchez, "Charged Hadron Spectra in Au+Au Collisions at $\sqrt{s_{NN}} = 130$ GeV," Ph.D. Thesis, Yale University (2001).

[90] C. Adler *et al.,* STAR Collaboration, Phys. Rev. Lett. **87**, 112303 (2001).

[91] C. Adler *et al.,* STAR Collaboration, Phys. Rev. Lett. **87**, 262302 (2001).

[92] T. Sakaguchi *et al.*, nucl-ex/0209030.

[93] J. L. Klay *et al.*, nucl-ex/0210026.

[94] D. Kharzeev and E. Levin, Phys. Lett. **B523**, 79 (2001).

[95] X. N. Wang and B. Muller, Nucl. Phys. **A566** (1994) 555c.

[96] E. Shuryak, Nucl. Phys. **A566** (1994) 559c.

[97] Z. Lin and M. Gyulassy, Nucl. Phys. **A590** (1995) 495c.

[98] H. Satz, Rept. Prog. Phys. **63** (2000) 1511.

[99] P. Braun-Munzinger, Quark Matter 2002 Proceedings, nucl-th/0209035.

[100] C. Adler *et al.*, STAR Collaboration, "Centrality Dependence of High p_T Hadron Suppression in Au+Au Collisions at $\sqrt{s_{NN}}$ = 130 GeV/nucleon", to appear in Phys. Rev. Lett.

[101] X.N. Wang, M. Gyulassy, Phys. Rev. Lett. **68** (1992) 1480.

[102] C. Adler *et al.*, STAR Collaboration, "Azimuthal anisotropy and correlations in the hard scattering regime at RHIC", nucl-ex/0206006.

[103] Y. L. Dokshitzer, D. Kharzeev, Phys. Lett. **B519** (2001) 199.

[104] K. Adcox *et al.*, PHENIX Collaboration, Phys. Rev. Lett. **88** (2002) 192303 (nucl-ex/0202002).

[105] C. Adler *et al.*, STAR Collaboration, "$K^*(892)^0$ production in relativistic heavy ion collisions at $\sqrt{s_{NN}}$ = 130 GeV," submitted to Phys. Rev. Lett. (2002).

[106] C. Adler *et al.*, STAR Collaboration, Nucl. Phys. **A698** (2002) 64c.

[107] M. C. Abreu *et al.*, NA50 Collaboration, Nucl. Phys. **A698** (2002) 127c

[108] L. W. Alvarez, Nobel Prize Lecture, 1968.

[109] J. Rafelski, Quark Matter 2002, Nantes, France.

[110] R. Rapp and J. Wambach, Adv. Nucl. Phys. **25** (2000) 1; R. Rapp, Phys. Rev. C **63** (2001) 054907.

[111] J. Letessier, *et al.*, nucl-th/0011048; G. Torrieri, J. Rafelski, Phys. Lett. B **509** (2001) 239.

[112] L.V. Bravina, *et al.*, hep-ph/0010172; D. Teaney, *et al.*, nucl-th/0110037.

[113] J. Rafelski and B. Mueller, Phys. Rev. Lett. **48** (1982) 1066; **56** (1986) 2334(E).

[114] J. Kapusta *et al.*, Phys. Rev. C **66** 014903 (2002).

[115] P. Fachini, STAR Collaboration, "ρ and $K^\star$ measurements from STAR", Quark Matter 2002; P. Braun-Munzinger, E. Shuryak, private communications.

[116] Y. J. Pei, Z. Phys. C **72**, 39 (1996), and references therein; P.V. Chliapnikov, Phys. Lett. B **470**, 263 (1999).

[117] D.E. Groom *et al.*, Eur. Phys. J. C **15**, 1 (2000).

[118] N. Xu and M. Kaneta, Nucl. Phys. A **698**, 306c (2002); F. Becattini, Z. Phys. C **69**, 485 (1996); F. Becattini and U. Heinz, Z. Phys. C **76** 269 (1997); P. Braun-Munzinger *et al.*, Phys. Lett. B **518** 41 (2001).

[119] B. Zhang *et al.*, Phys. Rev. C **61** 067901 (2000).

[120] M. Bleicher, J. Aichelin, Phys. Lett. B **530**, 81 (2002).

[121] C. Adler *et al.*, STAR Collaboration, "Midrapidity ϕ production in Au+Au collisions at $\sqrt{s_{NN}} = 130$ GeV," Phys. Rev. C **65**, 041901(R) (2002).

[122] X.N. Wang, Phys. Rev. C **58**, 2321 (1998); private communication.

[123] I. Vitev, M. Gyulassy, Quark Matter 2002, e-Print Archive: hep-ph/0208108.

[124] C. Adler *et al.*, STAR Collaboration, Phys. Rev. Lett. **89**, 092301 (2002).

[125] C. Adler *et al.*, STAR Collaboration, Phys. Rev. Lett. **87**, 082301(2001).

[126] B. Tomasik, "Simultaneous fits to spectra and HBT radii from RHIC experiments," Talk presented at the RHIC/INT Winter Workshop, Seattle, WA., January 2002.

[127] F. Retière for the STAR collaboration, nucl-ex/0111013

[128] D. Teaney, J. Lauret, E.V. Shuryak, nucl-th/0110037

[129] K. Adcox *et al.*, PHENIX Collaboration, submitted to Phys. Rev. Lett.,preprint nucl-ex/0201008.

[130] A. Enokizono, for the PHENIX collaboration, proceedings of the Quark Matter 2002 conference. nucl-ex/0209026.

[131] O. Barannikova, M. Kaneta, K. Schweda, and N. Xu, "Mid-rapidity proton and antiproton distributions from Au+Au collisions at $\sqrt{s_{NN}} = 130$ GeV,"Talk presented at the STAR Physics Analysis Meeting, Nov-Dec 2001.

[132] C. Adler *et al.*, STAR Collaboration, "Pion-kaon correlations In Au+Au collisions at $\sqrt{s_{NN}} = 130$ GeV," in progress.

[133] F. Retière for the STAR collaboration, proceedings of the Quark Matter 2002 conference.

[134] S.T. Butler and C.A. Pearson, Phys. Rev. **129**, 836 (1963).

[135] R. Scheibl and U. Heinz, Phys. Rev. C **59**, 1585 (1999).

[136] C. Adler *et al.*, STAR Collaboration, Phys. Rev. Lett. **87**, 262301 (2001).

[137] A. Polleri, J.P. Bondorf, and I.N. Mishustin, Phys. Lett. B **419**, 19 (1998).

[138] R. L. Jaffe, Phys. Rev. Lett. **38**, 195 (1977); **38**, 617(E) (1977).

[139] J. Schaffner-Bielich, Phys. Rev. Lett. 84, 4305 (2000); and private communications.

[140] Z.Y. Zhang *et al.*, Phys. Rev. C61, 065204 (2000).

[141] Y.W. Yu, Z.Y. Zhang and X.Q. Yuan, Commun. Theor. Phys., 31, 1 (1999).

[142] Q.B. Li, P.N. Shen, Z.Y. Zhang and Y.W. Yu, Nucl. Phys. A683, 487 (2001).

[143] Y.W. Yu et al., Phys. Rev. C, to be published (2002).

[144] S. Pal, C.M. Ko, and Z.Y. Zhang, nucl-th/0107070.

[145] M.C.S. Williams, Nucl. Phys. A 698, 464 (2002).

A Appendix – Simulation Codes used in Section 3.3

All calculations and simulations presented in Section 3.3 were done using a set of standalone computer codes which produce events, simulate the inefficiencies and performances of STAR (TPC plus MRPC-TOF), and compute physics analysis quantities. This fast simulation method is an expedient way to estimate the essential performance parameters and to facilitate evaluation of the TOF system with respect to multiple physics programs. This kind of analysis of "new physics" performance lies in between a "back-of-the-envelope" estimate and a full-blown GSTAR-Reconstruction-DST-Physics analysis. Considerable care was taken to insure that the relevant performances of STAR were reproduced. The general features of the codes are described here.

MEVSIM: – A Monte Carlo code for producing events from a user controlled momentum space distribution model with user determined particle types. MEVSIM [88] has been used extensively in STAR for the past several years.

FastDetecRespSim: – [Fast Detector Response Simulator] This code applies parametrized versions of measured STAR performances to the particles in the simulated events. Included are the acceptance and decay losses, track finding efficiencies, momentum vector smearing, two-track merging, and particle identification (PID) using dE/dx in the TPC gas, kink finding for charged kaons in the TPC [84], and the proposed MRPC-TOF with varying amounts and configurations of trays. In general these quantities are p_T and η dependent and also depend on particle type where specific parameters for pions, kaons, protons and antiprotons were used.

The acceptance, losses due to particle decay (mainly for kaons), and track finding efficiencies were combined into an overall efficiency function which was randomly sampled using the standard rejection method to determine if a given particle will be reconstructed. The sources of information used are from the year 2000 and 2001 data analyses and include: (1) Manuel Calderon de la Barca Sanchez's Ph.D. thesis section 8.2.1 and 8.2.2 [89], (2) QA plots for the year 2001 data, (3) results from the negative hadron spectra analysis [90], and (4) results from the antiproton spectra paper [91]. The overall efficiency was modeled as: (1) an exponential dependence on p_T representing acceptance and particle decay losses, (2) a quadratic dependence at low p_T becoming constant at higher p_T representing tracking efficiencies, and (3) constant at mid-pseudorapidity but falling off quadratically at larger $|\eta|$ beginning at $|\eta| = 1$. The parameters were determined for pions, kaons and protons. At mid-rapidity and larger p_T this overall track reconstruction efficiency was assumed to be 0.80, 0.74 and 0.82 for pions, kaons and protons, respectively.

The PID performance of the TPC based on dE/dx for pions, kaons and protons was obtained from Manuel Calderon de la Barca Sanchez's Ph.D. thesis [89] using Figures 10.2, 8.7 and 6.2 as well as results published in the antiproton spectra paper [91]. The function used here represents the *additional* loss in identified particles due to the tighter cuts which are applied to tracks selected for dE/dx PID analysis. The depen-

dence on p_T was again modeled as a quadratic at low momentum becoming constant above 0.5 GeV/c. The additional loss in identified particles varies from about 30% at 0.2 GeV/c to 4% above 0.5 GeV/c. The momentum ranges where TPC based dE/dx PID was applied are: (values are for $p_{T,min}$ and $P_{Total,max}$) (1) 0.0 - 0.75 GeV/c for pions, (2) 0.0 - 0.6 GeV/c for kaons, (3) 0.4 - 0.95 GeV/c for protons, and (4) 0.0 - 0.95 GeV/c for antiprotons. False particle identifications were not included.

The kaon identification performance based on reconstructed charge decays in the TPC was included and parameterized according to results presented by W. Deng [84]. The overall kink finding efficiency is about 1%.

Finally, the expected performance parameters of the proposed TOF detector with respect to acceptance, PID efficiency, and momentum range were used. Particle trajectory intercepts at the TOF average radius of 220 cm were computed and it was determined whether or not the particle hit an area covered by a TOF tray. For those that did the geometrical acceptance was assumed to be 90% and of those we assumed that 96% were successfully identified. This *additional* identified particle efficiency of 0.864 was randomly applied to those tracks which reach a TOF tray and which also survived the preceding acceptance, decay loss and track finding efficiency cuts. The momentum ranges where TOF based PID was applied are: (values are for $P_{Total,min}$ and $P_{Total,max}$) (1) 0.3 - 1.7 GeV/c for pions, (2) 0.3 - 1.7 GeV/c for kaons, and (3) 0.3 - 2.9 GeV/c for protons. False particle identifications were not included.

B Appendix – The STAR TOFp and pVPD Systems

A small-area TOF system was installed in STAR in the Spring of 2001. The STAR Time Of Flight Patch ("TOFp") [3] uses a standard CTB tray in which the two CTB slats have been replaced by 41 Bicron BC-420 plastic scintillator slats plus Hamamatsu R5946 mesh dynode PMT and Cockroft-Walton base assemblies. Also on-detector are eleven boards of custom high-performance FEE that include a fast discrimination of the PMT signals very close to the detectors. The TOFp detectors span roughly one unit of pseudorapidity and $1/60^{th}$ of the azimuth. Also part of the TOFp System are two smaller detectors called the pVPD's (pseudo Vertex Position Detector's), which are positioned very close to the beam pipe outside of STAR and provide the electronic start signals for the TOFp stops. The digitization is done on the platform in CAMAC. The goal is the measurement of the single-particle charged hadron spectra in a limited acceptance, but over many events. The system was operated for the first time during the 2001 RHIC run. The arrangement of the TOFp detectors and the two pVPD detectors with respect to the STAR TPC (shown in cutaway) and the RHIC beam pipe is shown in figure 53.

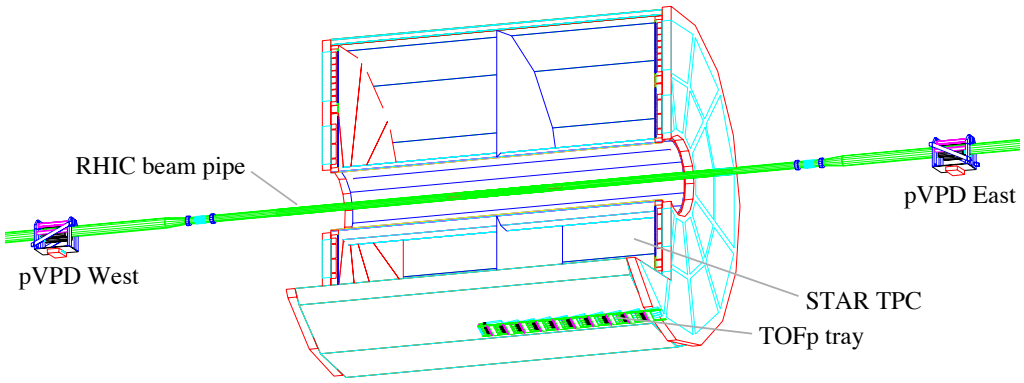

Figure 53: The arrangement of the TOFp detectors and the two pVPD detectors with respect to the STAR TPC (shown in cutaway) and the RHIC beam pipe.

While the technologies used in the TOFp system are not the same as those presently proposed for the full system, we include in this appendix comments related to the TOFp Systems for the following reasons:

- The TOFp system performed to expectations during the 2001 RHIC run, and provided particle identification for tracks in the TOFp acceptance up to the expected momenta. The TOFp performance is thus an experimental verification of the general expectations for the full system outlined in section 4.1.
- A considerable amount of custom software is needed for the full system to extrapolate TPC tracks and match them to the correct stop detector channels, to

calibrate the start and stop timing information, to perform the particle identification using on the calibrated information, and to evaluate the efficiencies involved via embedding simulations. The software performing these tasks for the TOFp data exists and is presently being optimized (see below for the present status). This TOFp software is directly applicable for the full system - while the technologies differ, both systems require TPC track extrapolation and matching to detector channels, and both systems exhibit similar-looking time-amplitude slewing and signal propagation velocities inside the detectors. The correction algorithms are thus effectively the same in both cases and only the parameters change. Thus, the offline software for the full system is effectively under development now, years ahead of the existence of the system itself. This means it will be possible to extract physics results from the system very quickly after the raw data is collected.

- The TOFp System was proposed, constructed, and operated by members of STAR that are also participants in the present proposal. Thus the present group has real experience operating a TOF detector system in the STAR environment, and performing TOF-based PID analyses using STAR data.

The "production" software used to perform the track-to-slat matching for the TOFp system is described in section B.1. The offline calibrations algorithms on both the start (pVPD) and stop (TOFp) sides, as well as the resulting PID performance in central Au+Au collisions at $\sqrt{s_{NN}}$=200 GeV during the 2001 RHIC run, are described in section B.2.

B.1 TOFp Production and Matching Software

The data flow of the TOFp detector is fully embedded in the STAR raw data production scheme. This ensures storage and handling of the TOFp data in a standardized environment requiring only a few TOFp-dedicated software modules. The production and analysis platform of STAR, StEvent, is built on top of the Root package. The Root package is an object-oriented data analysis framework widely used in the heavy ion and high-energy community. The StEvent classes inherit from Root classes which allows both batch processing and interactive use and assures the persistency of its inherited classes so they can be stored in Root files. The StEvent analysis modules are called Makers. The TOFp analysis software, therefore, consists of a few Makers with some additional utility classes.

In figure 54 the essential components of the offline production are depicted. The online production, *i.e.* the STAR data acquisition, wraps the TOFp data banks in raw data files. In the offline production, the StTofMaker calls the DAQ Reader to check for TOFp data banks. If available, this data is then copied and formatted into an StEvent-based TofCollection. Collections are set up on a per-event basis and are accessible by other Makers, *e.g.* the TofMaker can access track or trigger-detector collections. In the offline production the collections are persistent classes and as such can be stored in Root files. These files tend to be sizable and a

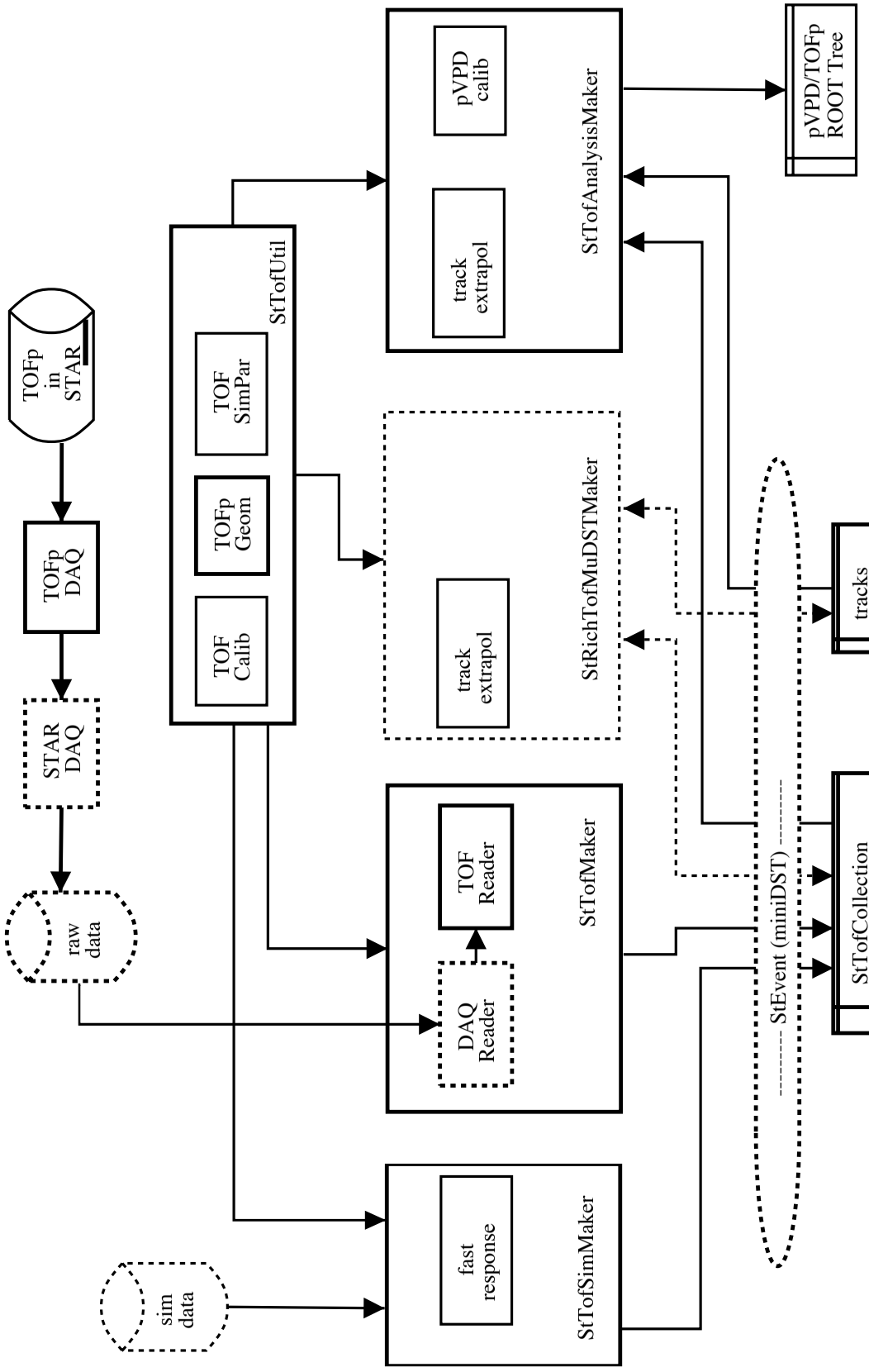

Figure 54: The components of the offline software for the STAR TOFp Systems.

Data Summary Tape (DST) Maker is used to pick out and store into smaller ROOT trees those variables that are relevant.

The first stage of the TOFp analysis focusses on the calibration of the detector. This requires both the raw TOFp data and the tracking information from the TPC. During this year's offline production, the TOFp maker only stored the raw ADC and TDC data in the TOFp collection. The TOFp detector has only limited geometrical acceptance so many of the TPC tracks do not extrapolate to one of its slats. Since the RICH detector is in similar situation and the detectors overlap in acceptance, efforts were joined in a miniDST Maker which filters out those tracks that are not close to these detectors, *i.e.* have no chance of extrapolating to either the TOFp or the RICH. Not only did this reduce the size of our data set considerably, it also sped up the analyses based on it. This TOFp miniDST contains all STAR global tracks that extrapolate into an area containing the TOFp detectors that is approximately two trays wide in azimuth ($\sim$12 degrees) and $\sim$250cm long.

The RICH/TOF mini-DSTs remain based on the StEvent model so prototype analysis makers can easily be fed back in future STAR-wide production runs. For the calibration analysis, the StTofAnalysisMaker builds a flat ROOT Tree summarizing only those slats that have tracks pointing to them (see next subsection). Besides the various TOFp makers a number of utility classes and functions have been written. Typically, they provide access to the STAR database, geometrical or timing calculations and calibration routines.

Matching Results

Time-of-Flight based particle ID relies on accurate tracking information: apart from the obvious timing information provided by the TOFp, momentum and path length are essential ingredients for calculating the mass hypotheses. In fact, tracking information is already vital in the early calibration stage where the timing dependencies of the various track parameters are investigated. This section describes the procedure by which tracks are extrapolated and matched to TOFp slats. The length of straight line TPC tracks from the center (Z=0) of the STAR barrel to the TOFp tray varies between L=2.2m on the $\eta\sim0$ side to L=3.2m at $\eta\sim1$. For low momentum tracks, the STAR magnetic field curves the paths of charged particles and the straight line tracks are the limit for high momentum charged particle tracks.

Identified global tracks are usually parameterized with a helix trajectory. Such a parameterization and knowledge of the STAR magnetic field (B=0.5 T maximum) allows the measurement of the track momenta, dip angles, and curvatures of the trajectories in the TPC. More sophisticated methods like the Kalman filter take energy losses along the flight paths into account. The typical momentum resolution of the TPC is about 1.3%. The track total path length, s, is given by,

$$s = \sqrt{s_T^2 + s_Z^2} \tag{7}$$

where the transverse and parallel components of the path length, respectively, are,

$$s_Z = Z_{hit} - Z_{PV} \qquad \text{and} \qquad s_T = (2R) arcsin(C/2R). \tag{8}$$

Here Z_{PV} and Z_{hit} are the STAR Z positions of the primary vertex and the hit in the TOFp slat, R is the track total radius of curvature from the helix fit, and C is the straight line distance in the bend plane from the primary vertex to the hit in the slat, *i.e.* $C = [(x_{hit} - x_{PV})^2 + (y_{hit} - y_{PV})^2]$.

A global track which extrapolates to any one the 41 TOFp slats is called a "match." For last year's analysis, no requirements were set for the tracks other than having a valid helix parameterization. In future analyses, cuts will be placed on *e.g.* the number of hits and/or fit points on the track (see also the Calibrations section below). Although it is expected that slats hit by more than one track can be analyzed, currently the calibration and analysis concentrates only on singly-hit slats. All other matches are ignored for now.

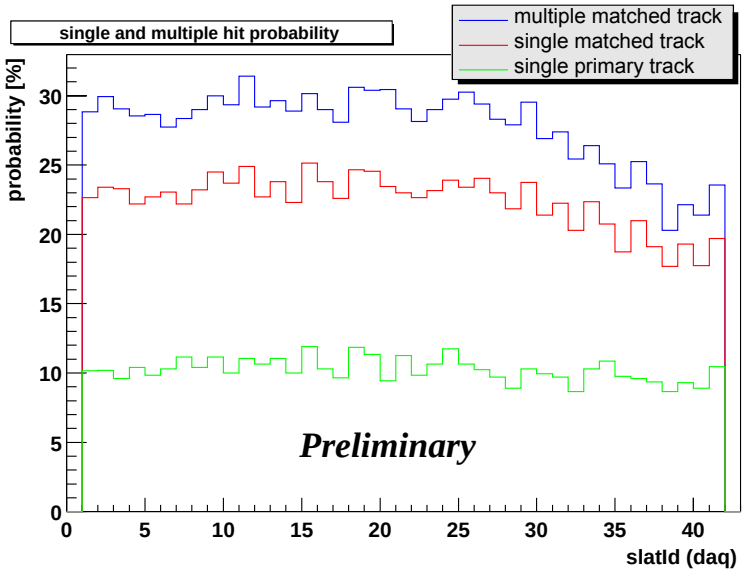

Figure 55: TPC to TOFp match probabilities per track from central Au+Au collisions.

In figure 55 the match probability in central Au+Au collisions for each of the slats is plotted. Low slat numbers start on the $\eta\sim0$ side and increase to the $\eta\sim1$ side of the tray. The (upper) blue histogram depicts the match probabilities when extrapolating all STAR global tracks in the TOFp/RICH miniDST (*i.e.* near the TOFp/RICH acceptance). The (middle) red histogram are those global track matches for which the slat matched to the track and no other tracks were matched to this slat in this event. The (lower) green histogram indicates the probability the global track matched to single-match TOFp slat is also a primary track. Primary tracks are those that originated from the event vertex while global tracks may point to secondary vertices away from the primary vertex. Our analyses are primarily aimed at charged hadron spectra so at present we are concentrating only on the primary tracks.

The matched candidates are stored in a ROOT tree together with the raw ADC and TDC value of the associated slat. Additional track information such as local hit position on the slat, angles of incidence on the slat and path length in the slat are stored as well.

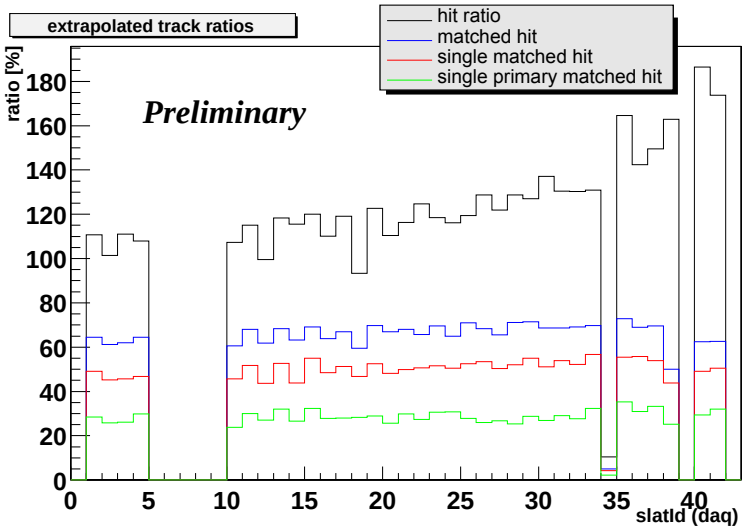

Figure 56: TPC to TOFp match ratios per track from central Au+Au collisions.

In figure 56 the hit ratios are plotted for each individual slat. The colored lines have the same meaning as Figure 55 with an additional requirement that the slat selected by the matching algorithm saw a charged particle hit (via a threshold cut on the ADC value). The (highest) black histogram indicates the ratio of the number of times a slat fired and the number of times at least one global track was matched to this slat. The (2^{nd} highest) blue histogram then includes the requirement that the slat was struck at least once via the ADC cut. The (3^{rd} highest) red and (lowest) green histograms are the ratios under the same conditions as in figure 55. For the global track matches (highest, black), the hit ratio is typically above 100% which means that a slat fired more often than a global track extrapolated to it. This ratio is very sensitive to the cut placed on the ADC value to locate hit slats. The other histograms show how the ratio decreases when the additional matching criteria are applied. Approximately 30% of the tracks in the TOFp/RICH miniDST are tracks that are primary and strike a singly-struck TOFp slat. The holes in the plot for slat numbers 5-8, and 9, 34 and 39 are the result of FEE board and dead HV cells, respectively.

B.2 TOFp Systems Calibrations and Performance

The production code described in the previous section produces a ROOT N-tuple containing the event, track, and TOFp/pVPD information for all "matches". The development of all the calibrations software needed to turn the raw TOFp/pVPD

information into time intervals, and then into particle identification information, is based on this N-tuple. This allows this development to be quickly and efficiently performed at Rice under local Linux and Mac OSX machines. The calibration code for the central full-energy Au+Au data from the 2001 run is complete. The TOFp System performed as expected in these data. Some details on the TOFp calibrations software and the observed performance of the system are described in this section.

pVPD Calibrations

The start detector for the TOFp System is the pVPD. The information needed from this detector is the corrected average of the times measured in those channels of the pVPD that fire in a given event. In the central Au+Au data from the 2001 run, all six channels of the pVPD fire in every event. The average of the six raw TDC values in each event is the crudest measure of the event start time, as it is smeared by the so-called "slewing" effect intrinsic to PMTs and MRPC detectors. The first calibration necessary is thus the correction of the pVPD start times for the slewing effect.

In order to avoid bias during this correction, we compare the TDC average of one East pVPD channel and one West pVPD channel to the average of the other four pVPD TDC channels. This difference of averages, referred to as "$\langle 2\rangle - \langle 4\rangle$", is centered at zero by definition but has a standard deviation that is increased by the fact that all six of the times used in this average depend on the respective six ADC values for these channels. An iterative technique was employed where two channels are selected, *e.g.* East 1 and West 1, and the difference of TDC averages $\langle 2\rangle - \langle 4\rangle$ is plotted versus the two ADC values for East 1 and West 1, respectively. This two-dimensional profile is then fit with a polynomial function of the two ADC values, and the fit parameters are used in later passes through the data to remove these correlations.

The next step of the iteration then involves the next pair of channels, *e.g.* East 2 and West 2. The difference of TDC averages, $\langle 2\rangle - \langle 4\rangle$, is plotted versus the ADC values for East 2 and West 2, respectively, where the $\langle 4\rangle$ average includes the corrected TDC values for East 1 and West 1 following the first iteration and the still uncorrected East 3 and West 3 TDC averages. This two-dimensional profile is then fit with a polynomial function of these two ADC values, and the fit parameters recorded for use in subsequent iterations. This process is continued in nine passes such that each East and West pair of pVPD TDCs is fit and corrected versus their respective pairs of ADC values three times.

The results from this process are shown in figure 57. The different point styles in this figure correspond to the different iterations performed. The black points are the raw data, indicating the resolution on the quantity $\langle 2\rangle - \langle 4\rangle$ with simply the raw data is approximately 2.6 TDC channels, or ∼130ps. The method has converged to the best possible resolution after the fourth iteration. After the procedure, the standard deviation of the quantity $\langle 2\rangle - \langle 4\rangle$ is reduced to approximately 0.9 TDC channels, or ∼45ps.

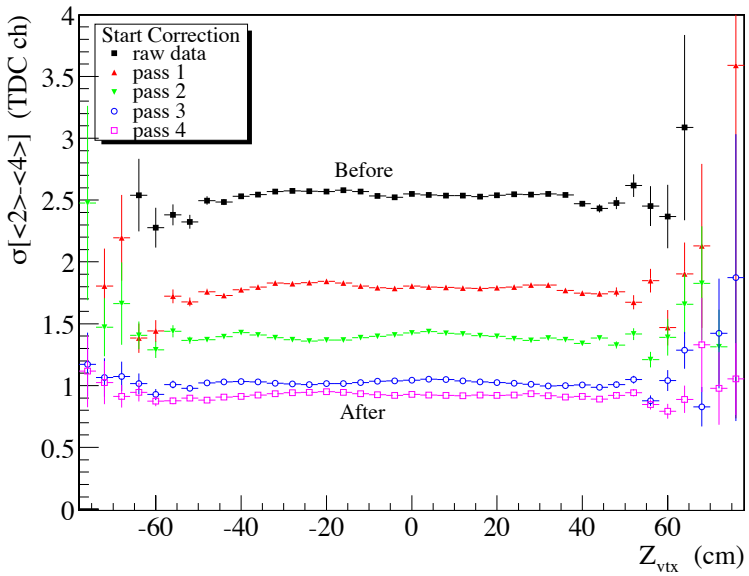

Figure 57: The standard deviation of the quantity $\langle 2\rangle - \langle 4\rangle$ in units of TDC channels (50ps/ch) versus the primary vertex location. The different point styles correspond to individual passes during the start correction procedure.

The start time needed by the TOFp system is the average of all six (slew-corrected) TDCs, *i.e.* "$\langle 6\rangle$". Assuming that all six pVPD PMTs have the same single-detector resolution, the standard deviation of the difference of averages $\langle 2\rangle - \langle 4\rangle$ is related to the standard deviation of the average of all six pVPD PMTs by a factor of $\sqrt{4/3}/\sqrt{6}$, or 0.47. The pVPD start time resolution in the central full-energy Au+Au events is thus $\sigma_{\langle 6\rangle}$=24 ps, and the equivalent single detector resolution is $\sigma_{\langle 1\rangle}$=58 ps. This start-timing performance is considerably better than necessary to do efficient time of flight analyses in the STAR geometry. The corrections one then needs for the stop side are now described.

TOFp Calibrations

The TOFp slats also slew causing a correlation between TOFp TDC and ADC values. Also, these slats are "single-ended," requiring the additional correction for the time taken for the scintillation light to propagate from the location of the hit inside the slat to the PMT photocathode. This distance is referred to as $Z_{\rm hit}$. This propagation time was measured on the bench using a Nitrogen laser on the TOFp slats to be linear with a slope of ∼65 ps/cm. In the case of the STAR detector, the TOFp geometry, and real events, however, these two corrections are hopelessly correlated with a large number of other variables requiring some care in the software used to correct for these effects. That is, in the case of TOFp in STAR, the slewing does not simply go like the function const/$\sqrt{\rm ADC}$ or const/ADC, and the scintillation

light propagation time is not simply const*Z_{hit}.

The ADC value in a TOFp slat, which is assumed to correlate directly to the pulse height that is directly related to the slewing, also depends on a number of other quantities. It depends on the momentum via Bethe-Bloch-like energy loss. Indeed the PID resolution from the ADC values in the 2cm-thick TOFp slats is not unlike that from TPC dE/dx. It depends on the location of the hit along the slat via the scintillation photon attenuation inside the wrapped scintillator. It depends on the length of the track inside the volume of the slat, as primary scintillation light is created all along this path. This length depends on the location of the slat in the TOFp tray (due to aspects of the angles of the slat positioning), the primary vertex location, and the track momentum components p_T (in the bend plane) and p_Z (in the non-bend-plane). The TDC value depends on the actual time of flight of the particle in STAR, the scintillation light propagation time, and the shift from the slewing.

Thus there are numerous correlations between the TDC values and the ADC and Z_{hit} values beyond those simply related to the slewing effect and the scintillation photon propagation time. We thus use an iterative technique here as well, where polynomials in ADC or Z_{hit} are fit to the data in several steps. The quantity that is minimized in this case is the difference between the experimental and expected $1/\beta$=cτ/s values for pions, where c is the speed of light and τ is the measured TDC value minus a global offset multiplied by the time-to-digital calibration of 50 ps/ch. The quantity s is the primary track total path length calculated using the reconstructed track helix parameters and the STAR and TOFp geometry. All calibrations are defined by optimizing the pions, and these corrections are then applied to all tracks in subsequent pass through the data.

A typical plot of corrected inverse velocity versus the track momentum is shown in figure 58. The solid lines are the values expected based on the momentum and the assumption of a mass of that for a pion (lowest line), Kaon, proton, and deuteron (highest line). Strong bands for pions, kaons, and protons are seen with the expected resolution. The insets depict the projections onto the inverse velocity axis for specific momentum regions near the required limits of TOFp's reach. The insets show that TOFp met the requirements - allowing TOF-based physics analyses in STAR for the first time.

Shown in figure 59 is the total TOFp+pVPD time resolution for 0.5-1.5 GeV/c pions versus the slat number. The slats with numbers 0-4 are in the first row inside the tray near $\eta\sim0$, while the slats with numbers $37-40$ are in the last row near $\eta\sim1$. The squares depict the resolution for all tracks passing the quality cuts listed in the figure. There is a slightly better time resolution for those matches that are not close to the PMT in a given slat. The circles depict the resolution with an additional cut that Z_{hit} is greater than 10 cm.

There are a few poorly-performing channels, and one FEE board (slats 5-8) that was off for this portion of RHIC Run-2. All of these have since been repaired. The average total time resolution of the TOFp+pVPD system over all slats was 87 ps. The average total time resolution over the best 25 slats was 79 ps.

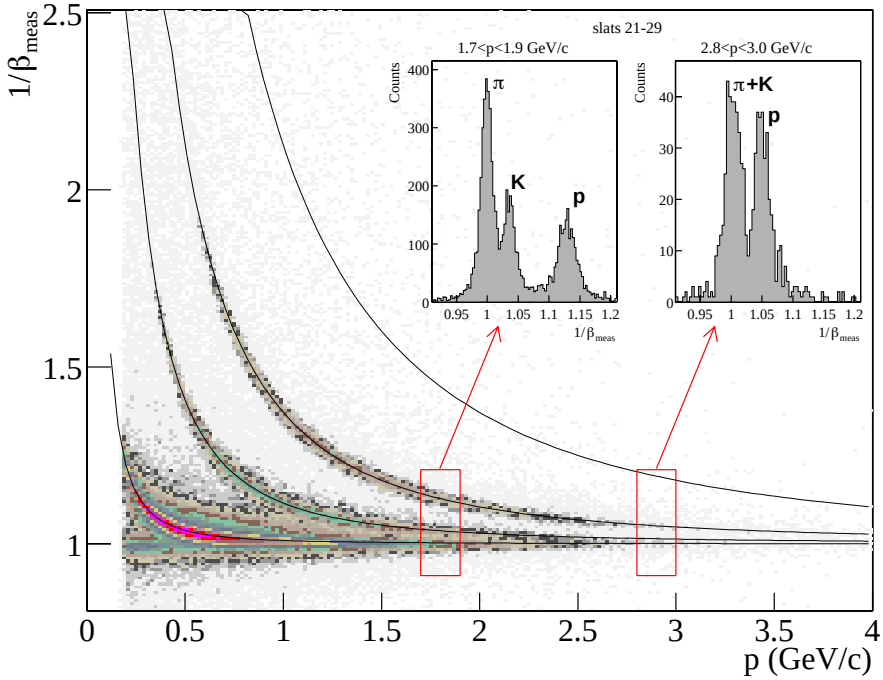

Figure 58: The corrected inverse velocity versus momentum from TOFp+pVPD for central Au+Au collisions from RHIC Run-2. The insets depict the projections onto the inverse velocity axis for specific momentum regions near the required limits of TOFp's reach. Prominent peaks for the various hadron species are observed in both insets.

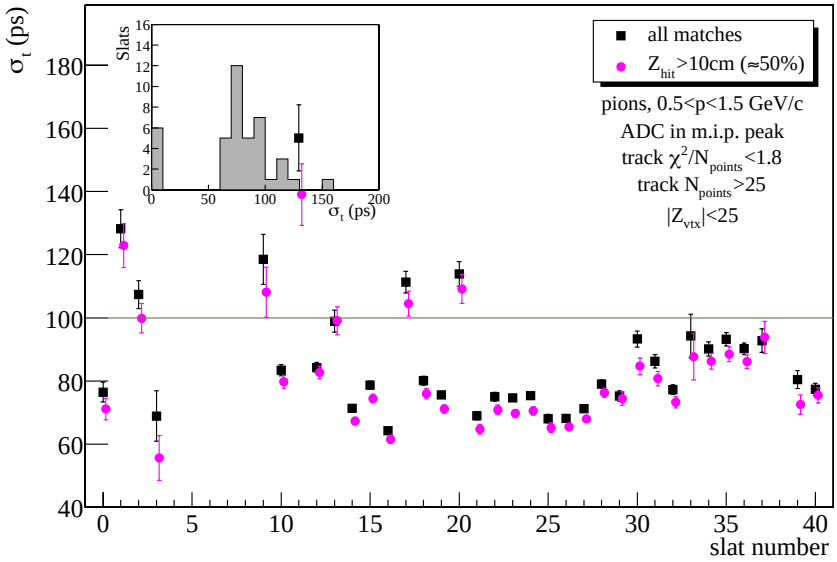

Figure 59: The total time resolution versus the TOFp slat number from the RHIC Run-2 Au+Au running. The inset depicts the histogram of these values. The average total time resolution over all(the best 25) slats was 87(79) ps.